Diplomarbeit

Simulation of auditory nerve fiber excitation with prostheses implanted in the scala vestibuli

zur Erlangung des akademischen Grades

Diplom-Ingenieur

im Rahmen des Studiums

Biomedical Engineering

ausgeführt von

Fred Bucek, BSc

51832477

am Institut für Analysis und Scientific Computing
der Fakultät für Mathematik und Geoinformation
der Technischen Universität Wien

unter der Betreuung von
Ao.Univ.-Prof.i.R. Privatdoz. Dipl.-Ing. Dr.sc.med. Dr.techn. Dr.rer.nat.
Frank Rattay
und
Projektass.(FWF) Dipl.-Ing. Dr.techn. Paul Werginz

Wien, 2023

Kurzfassung

Seit den 1970er-Jahren sind Cochlea-Implantate (CI) ein weitverbreitetes Mittel zur Wiederherstellung von verlorengegangener oder schlechter Hörfunktion. Dabei werden üblicherweise Elektroden in die Scala Tympani (ST) eingeführt, die in weiterer Folge die Hörnervenfaser (ANF) stimulieren. Im Falle einer blockierten oder verknöcherten ST wird es jedoch schwer bis gar unmöglich Elektroden einzuführen, weshalb alternative Orte zur Elektrodenpositionierung gesucht werden. Das Ziel dieser Arbeit ist es, die Unterschiede im Zuge der ANF-Erregung zwischen Elektroden, die in die ST eingeführt wurden, und Elektroden, die in der Scala Vestibuli (SV) platziert werden, welche den anderen großen Gang der Cochlea bildet, zu vergleichen. Vier Nervenfasern wurden dazu herangezogen und mit einem Model vom Typ Hodgkin-Huxley in Matlab R2021b simuliert. Anodische und kathodische Schwellwerte wurden für jede einzelne Faser berechnet und das dabei resultierende Verhalten der ST- und SV-Elektroden miteinander verglichen. Die Fasern wurden außerdem auch durch das Entfernen der Dendriten als degenerierte Fasern simuliert. Es hat sich gezeigt, dass mit Elektroden in der SV niedrigere Schwellwerte zur Erregung nicht-degenerierter Fasern nötig sind. Bei degenerierten Fasern sind höhere Stromamplituden notwendig, insbesondere für Elektroden in der SV. Als beste Elektrodenposition wurde die mid-dendritische Position identifiziert. Obwohl noch weitere Forschung zum Festigen dieser Ergebnisse von Nöten ist, hat sich gezeigt, dass die Platzierung von Stimulationselektroden in der SV eine adäquate Alternative ist.

Abstract

Since the 1970s, the cochlear implant (CI) is a widespread device to restore bad or missing hearing function. For this, electrodes which stimulate the auditory nerve fiber (ANF) are usually inserted in the scala tympani (ST). However, in case of an obstructed or ossified ST, electrode insertion becomes impeded or even impossible. Therefore, alternative locations for insertions are needed. The aim of this thesis is to compare the ANF excitation behavior between electrodes that are inserted in the scala vestibuli (SV), the other large cochlear duct, and ST-positioned electrodes. Four nerve fibers were analyzed by defining a model of the Hodgkin-Huxley type and conducting a simulation in Matlab R2021b. Anodic and cathodic threshold values were computed for each fiber and the performance of ST- and SV-positioned electrodes was compared. Moreover, the fibers were also simulated as degenerated fibers by cutting-off the dendrite. The outcomes of this thesis show lower threshold values for SV-positioned electrodes in non-degenerated fibers. In degenerated fibers higher currents are needed for excitation, especially for electrodes in the SV. This thesis also suggests mid-dendritic electrode position as the best electrode location. Although further research is needed, it can be stated that the SV is an adequate alternative for electrode insertion.

Acknowledgements

First of all, I would like to heartily thank Dr. Rattay for supervising this thesis and his expertise, which has always helped me to progress. Then, I would also like to thank Dr. Werginz for supervising, but especially for his support when I got stuck with programming. I also want to show my gratitude to Dr. Wenger and Dr. Fellner for inspiring discussions. Finally, I would like to thank my family and friends for their support.

Contents

Acronyms

ANF	auditory nerve fiber
AP	action potential
BE	Backward Euler
CI	cochlear implant
CN	cranial nerve
FE	Forward Euler
NoR	node of Ranvier
ODE	ordinary differential equation
SM	scala media
ST	scala tympani
SV	scala vestibuli

1 Introduction

This chapter introduces the reader into the topic and the problem analyzed in this thesis before a more detailed description of the basics is given in chapter 2.

1.1 Motivation

Electrical nerve stimulation is, compared to the roots of the broad fields of neurosciences, a rather young discipline. First neuroscientific hypotheses and assumptions about nerve structure, causes of neurological disorders, and the perception of emotions date back to ancient Greece. (Crivellato and Ribatti, 2007) Experiments and the medical use of electrical currents are also reported to be 2000 years old. In contrast, the early steps of electrical nerve stimulation were made in the 18th century. (Rattay, 1990) One of the first pioneers was Luigi Galvani who stimulated nerves and muscles using a bimetallic rod, written down in his *De viribus electricitas in motu musculari commentaries* (1791). Further research and work by different authors followed, but it took until 1952 to set the fundament for nowadays electrical nerve stimulation. In 1952, Alan Lloyd Hodgkin and Andrew Field Huxley published their ingenious work discovering the mechanisms of nerve fiber excitability. (Hodgkin and Huxley, 1952b) Since then, the field of neuroscience developed fast. New disciplines evolved, new applications were discovered, and other applications of electrical nerve stimulation were improved: cardiac pacemakers, electrical stimulation for the restoration of lost or damaged body functions, stimulation devices for anal or urinary incontinence, or prostheses for people with vision or auditory impairments can be stated here exemplarily. (Rattay, 1990) All these applications are often summarized by the term of functional electrical stimulation (FES). FES is the application of electrical current to excitable tissue, such as nerves or muscles, to support or restore a damaged or lost body function. (Rattay, 1990; Peckham and Knutson, 2005) FES in combination with a sensory organ, like the ears, makes up a field of special interest of FES due to the complex functioning of the ears themselves and the direct impact on the quality of life in case of bad or lost auditive perception. To overcome such losses, researchers use FES, often in terms of cochlear implants

(CI), to restore auditive perception. CIs were first introduced to the market around the 1970s. A CI is a biomedical device which is implanted in case of deafness or of severe hearing loss caused by the destruction of sensory hair cells. The idea is to bridge these damaged or missing structures and to excite the neurons of the auditory nerve directly by the use of electrical currents. (Eshraghi et al., 2012; Lenarz, 2017)

A scheme of a CI is depicted in Figure 1.1 showing the main parts of a CI such as the external speech processor, the internal implant, and the electrode array (see also chapter 2.2.3). The electrodes are inserted into the cochlea and excite the auditory nerve. To create optimal stimulation conditions, the position of the electrodes is crucial, which is the main focus of this thesis.

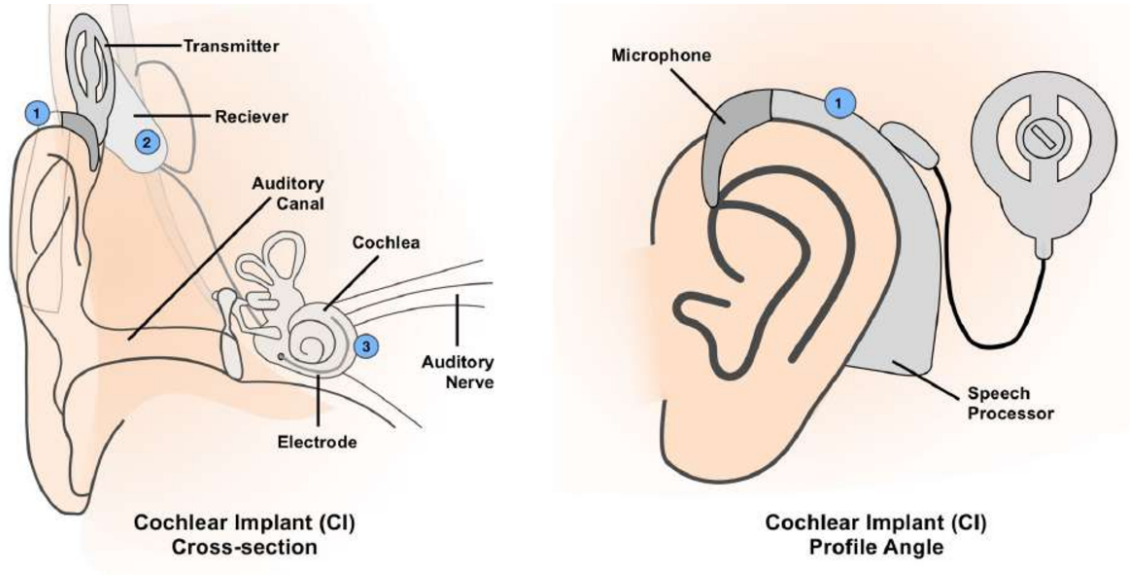

Figure 1.1: Depiction of a typical cochlear implant. Left: Cross-sectional view of a CI with 1) being the external speech processor, 2) the internal implant and 3) shows the electrode arrays inside the cochlea. Right: Profile view of the CI. (Gorman and Flatla, 2017)

1.2 State-of-the-art Location for Electrodes

The cochlea consists of three fluid-filled ducts, which enable different possibilities for electrode placement inside the cochlea. The cochlea ducts are: the scala tympani (ST), which is the descending spiral, the scala vestibuli (SV), also described as the ascending spiral, and the scala media (SM), known as the central cochlear duct, (see also chapter 2.1.1). The ST and SV are filled with perilymph - a fluid similar to cerebrospinal fluid-, whereas the SM is filled with endolymph, which is a potassium rich fluid. (Hans et al., 1999; Daniels et al., 1996) However, the ST and the SV are usually the only ducts considered for electrode insertion, *inter alia* due to space requirements of the electrodes and accessibility reasons.

The state-of-the-art approach is to insert the electrodes into the ST. (Gulya and Steenerson, 1996; O'Connell et al., 2016; Lenarz, 2017) There are mainly two reasons why the ST is the state-of-the-art location for electrode placement. First of all, the ST is easier accessible than the SV, since the electrodes can be inserted into the ST through the round window (House, 1982; Hoffmann et al., 2022) or via cochleostomy (Gantz et al., 1988; Richard et al., 2012), whereas the SV is only accessible by drilling a hole for electrode insertion (Steenerson et al., 1990; Tokat et al., 2022; Holzmeister et al., 2022). Secondly, the ST is attributed to have higher speech perception and hearing preservation. (O'Connell et al., 2016)

1.3 Problem

However, in case of cochlear obstruction or ossification the insertion of the electrodes into the ST is impossible or at least impeded, especially deep insertion is not possible leading to poor stimulation of the low-frequency auditory nerve fibers (ANF)s following limited speech understanding. (Lin et al., 2006; Kiefer et al., 2000; Rinia et al., 2006) There are various conditions which can be the reason for partial or total obstruction respectively obliteration of the cochlea, but the most common ones are meningitis, tumors, fractures or infections. (Lin et al., 2006; Berrettini et al., 2002) Around 15% of people who need a CI and 80% of CI candidates, who became deaf due to meningitis, are affected by an obstructed cochlea, which is why an alternative for electrode insertion is required. (Berrettini et al., 2002)

Different studies show that insertion into the SV is a valid alternative for ST implantation. (Trudel et al., 2018; Lin et al., 2006; Kiefer et al., 2000; Lin, 2009; Berrettini et al., 2002) Some studies even report better performance in patients where the electrodes were inserted into the SV. Better performance considering sentence recognition in a noisy environment was reported by (Trudel et al., 2018) and better word recognition performance was the result of the clinical study by (Pasanisi et al., 2002). However, there are also studies reporting insertion trauma when inserting the electrodes into the SV leading to the possible rupture of the Reissner's membrane and having impact on the Organ of Corti following destruction of residual hearing. (Adunka et al., 2005) Sometimes it is assumed that there is not enough space to insert electrodes into the SV close to the fiber, because it is thought that the Reissner's membrane impedes close-fiber-insertion, which is why the implantation is often dispensed with. (see also (Gulya and Steenerson, 1996)) This assumption; however, is often based on the anatomy of animals, but, as (Raufer et al., 2020) show by using the example of a guinea pig, there is a difference between the position and course of the Reissner's membrane in animals and humans, which allows electrode insertion close to the fiber in humans (see also Figure 1.2). (Gulya and Steenerson, 1996) support this approach by showing that the SV has sufficient anatomic dimension for insertion of a whole electrode array.

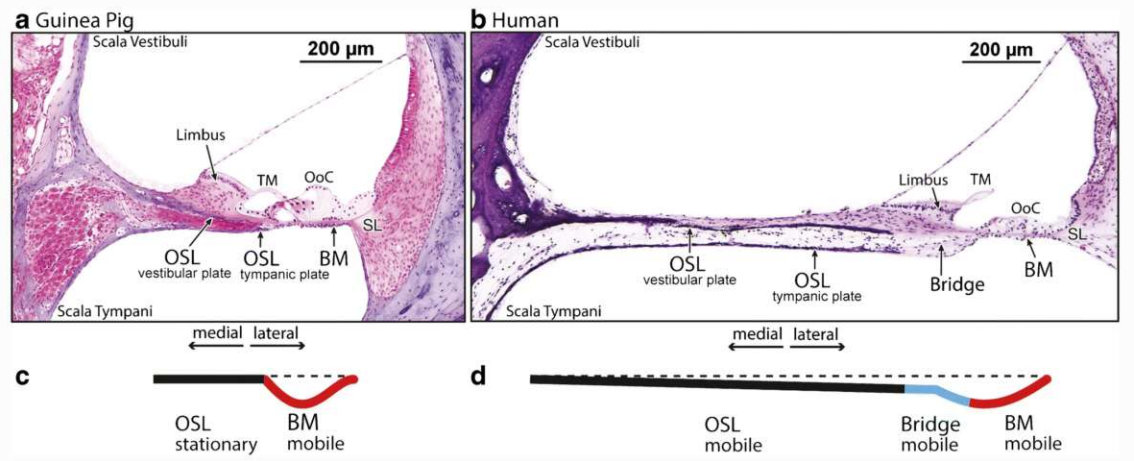

Figure 1.2: Comparison between the SV of a guinea pig and the SV of a human showing their difference between the position and course of the Reissner's membrane. (Raufer et al., 2020)

To get a better understanding of the differences in ANF excitation and spiking behavior between electrode placement in the ST compared to SV electrode placement, it would be useful to have human single ANF recordings. However, due to ethical reasons, only single ANF recordings in animals exist, which are not directly translatable to humans. (Rattay et al., 2001b) Computer simulations are a well-established alternative in such cases, but no paper focusing on this question was found after literature research (National Library of Medicine, Google Scholar, Science Direct). Up to now, little is known about these possible differences. To change this and to gain further knowledge this thesis was written.

1.4 Aim

The aim of this thesis is to analyze differences in ANF excitation behavior when the electrodes are located in the ST compared to electrodes located in the SV. As approach a computer simulation using a Hodgkin-Huxley type model was conducted.

2 Fundamentals

In this chapter, the anatomical and physiological as well as the technical basics useful for understanding this thesis are explained.

2.1 Anatomical and Physiological Background

2.1.1 Anatomy of the Ear

The ear is the organ of the human body responsible for the perception of sounds and tones in the range of 20 Hz to 16 kHz. It is subdivided into three sections: into the outer, middle, and inner ear. In Figure 2.1 the most important parts of the human ear are depicted. The outer ear consists of the pinna, which is also called auricula and mainly consists of elastic cartilage, of the outer auditory canal, and of the eardrum (membrana tympani), which forms the boarder to the middle ear. The main parts of the middle ear are the tympanic cavity, which includes the auditory ossicles (malleus, incus, and stapes), the tuba auditiva, and many smaller cavities covered with mucosa. The most prominent part of the inner ear is the cochlea, which is an osseous spiral with two and three quarter turns (Hans et al., 1999; Daniels et al., 1996) around its main axis, known as the modiolus. In a cross section of the cochlea, three different scalae can be distinguished: the scala tympani (ST), the scala vestibuli (SV), and the scala media (SM). The ST and SV are filled with perilymph, a fluid similiar to cerebrospinal fluid (Daniels et al., 1996), and range from the round window respectively from the oval window to the helicotrema, where the ST and SV merge. The SM is filled with endolymph, a potassium rich fluid, and is located between the ST and SV. The lamina basilaris builds the border to the ST, whereas the Reissner's membrane is the wall to the SV. The lamina basilaris includes the organ of corti which contains the inner and outer hair cells, the receptor cells for hearing. The tectorial membrane lies above the hair cell bundles and mainly consist of extracellular matrix. To actually hear sounds, the hair cells are connected synaptically with neurons whose axons travel as *Nervus vestibulocohlearis*, which is the eighth cranial nerve (CN), to the brain stem. (Faller and Schünke, 2016)

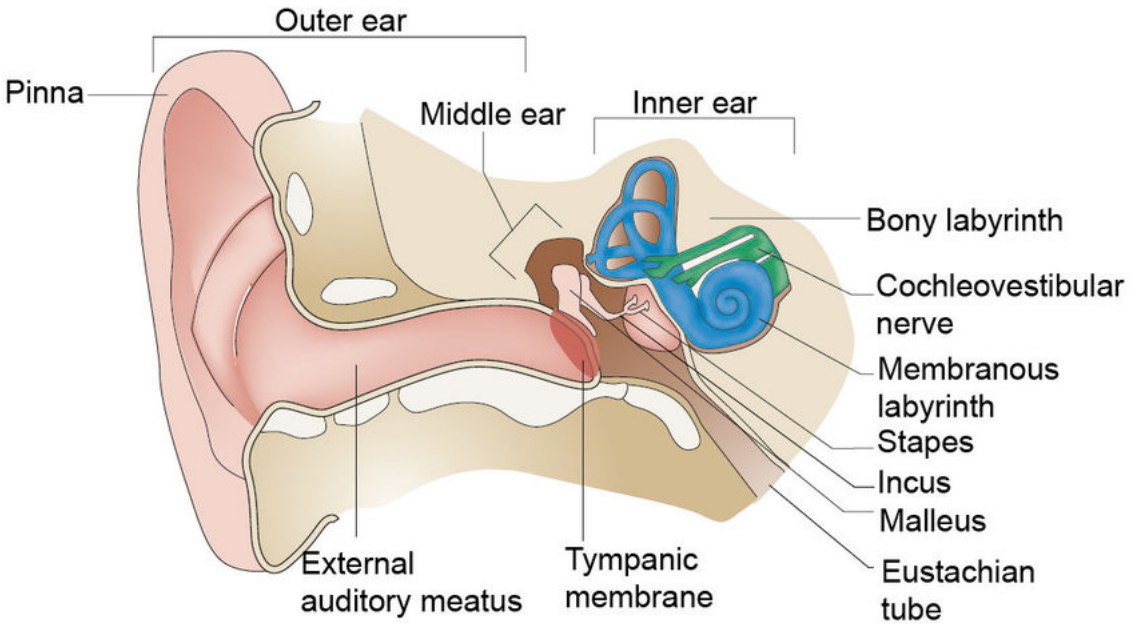

Figure 2.1: Schematic drawing of the anatomy of the ear. The main parts of the ear, i.a. the outer, middle and inner ear, are labelled. (Adapted from (Kelley, 2006))

In more detail, the hearing process works as follows: Acoustic waves are caught by the pinna and travel through the outer auditory canal to the ear drum, which starts to oscillate. The auditory ossicles transmit these oscillations through the oval window to the inner ear. The stapes finally converts the oscillations of the ear drum into oscillations of the fluid filled SV. The pressure waves propagate along the SV to the helicotrema and propagate back along the ST. Due to the opposite fluid movements, the fluid inside the SM starts to oscillate leading to the excitation of the hair cells and propagation of an electrical signal to the brain stem. Worth to mention is that the lamina basilaris is wider at the tip of the cochlea than at the base. This is why low-frequency sounds are perceived at the tip of the cochlea and high-frequency sounds at the base of the cochlea. (Faller and Schünke, 2016)

2.1.2 Structure of Neurons

The main task of nerve cells, also called neurons, is to transmit information. (Azarfar et al., 2018) To fulfill this task, neurons have - compared to other cells in the human body - a special structure. A neuron consists of a cell body, called soma, and at least of one of the two types of neurites. A neurite that transmits information away from the soma is called axon, a neurite transmitting information in the other direction is called dendrite. For the sake of completeness, it should be mentioned that cell organelles like mitochondria, nucleus, or lysosomes are also contained in a neuron. (Ashley and Lui, 2023) Figure 2.2 shows the structure of a typical neuron.

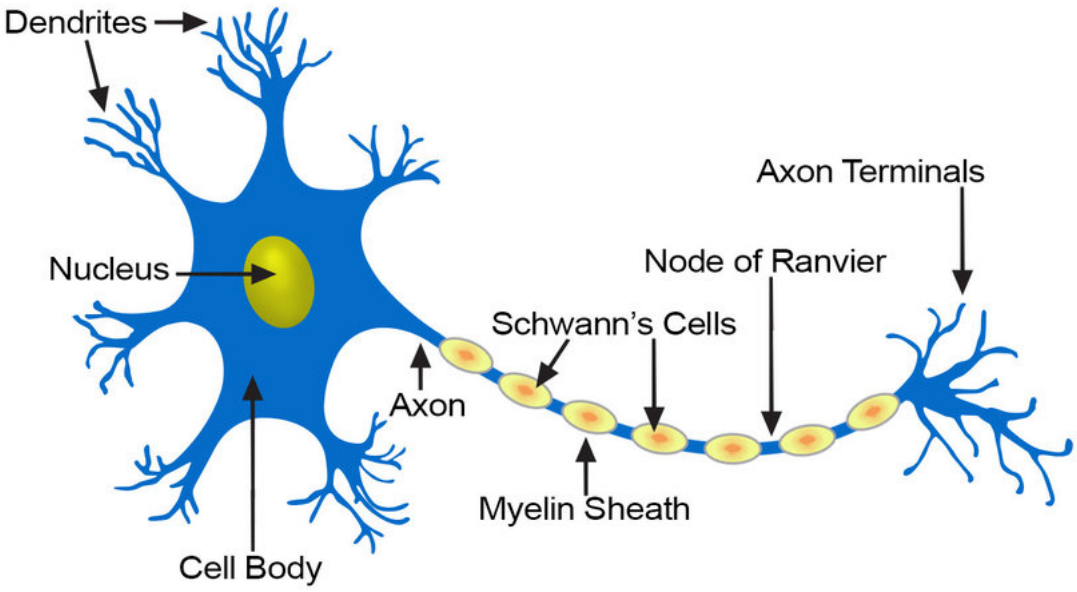

Figure 2.2: Schematic functional drawing of a neuron. Depicted are the dendrites, representing the input region of the neuron, the soma, labelled as cell body, and the axon, representing the output region of the cell. This axon is myelinated, since myelin sheaths cover it. Due to the myelinated axon the signal travels much faster, which is known as saltatory conduction. (Adapted from (Sochacki, 2020))

Some axons are covered with myelin which increases the conduction velocity of the information transmitted. Myelin is formed by Schwann cells which are wrapped around the axon and squeeze out their cytoplasm leaving a layer of myelin around the axon at the end. (Rattay, 1990; Ashley and Lui, 2023) As shown in Figure 2.2, there is not a continuous strand of myelin along the axon, but myelin covers the axon in sections with small gaps in between, called the nodes of Ranvier (NoR). The axons that are covered with myelin are called myelinated fiber, the ones without myelin sheaths are called non-myelinated fibers. The main difference is, as already mentioned, the conduction velocity of the signal. Unmyelinated fibers feature a continuous propagation of the signal along the fiber, whereas in myelinated fibers the signal jumps from one NoR to the next one. This type of conduction is called saltatory conduction. The conduction velocity in myelinated fibers is higher than in non-myelinated fibers. Generally spoken, the conduction velocity depends on the diameter of the fiber (see equations 1 and 2). (Rattay, 1990)

$$v_{myelinated} = 4.5 \cdot d \tag{1}$$

$$v_{unmyelinated} = 1.1 \cdot \sqrt{d} \tag{2}$$

It should be stated that for myelinated fibers with a diameter greater than 11 µm the proportionality factor in equation 1 changes to 6. (Rattay, 1990)

2.1.3 Composition of the Cell Membrane

The cell membrane separates the inside of the cell, the intracellular space, from the outside of the cell, the extracellular space. There are different dissolved substances, such as salts, as well as different ionic concentrations on both sides of the membrane. In Table 2.1, the different ionic concentrations of the most relevant ions are shown. These concentration differences are responsible for a potential gradient between extra- and intracellular space, called the resting membrane potential (see chapter 2.1.4) . Thus, the cell membrane plays a major role in the context of excitation of the cell. (Faller and Schünke, 2016)

The cell membrane consists of a phospholipid bilayer, which means that there are two layers of lipid molecules arranged in a way that their hydrophobic tails face the inside of the cell membrane, whereas the hydrophilic heads form the inside and outside edge of the membrane. The membrane acts as a barrier and prevents polar and also bigger molecules from passing through by simple diffusion. (Guidelli, 2020) However, the cell membrane is penetrated by proteins which enable the transport of specific types of substances, e.g. ions. These kind of proteins are called integral membrane proteins, but there are also proteins that do not penetrate the membrane, but are just located on the surface of the membrane, known as peripheral proteins respectively globular proteins. It is worth to mention that the outside of the cell membrane is coated with a thin layer of carbohydrates, called glycocalyx, which is important for the specific immune defense, since through the glycocalyx, cells are able to recognize other cells as body's own or foreign. (Faller and Schünke, 2016)

Table 2.1: List of the different ionic concentrations in the intracellular and extracellular space. (Faller and Schünke, 2016)

Ion	**Concentration [mM]**	
	Intracellular	**Extracellular**
K^+	139	4
Na^+	12	145
Cl^-	4	116
Organic Anions	138	34

Figure 2.3 shows a schematic drawing of the cell membrane visualizing the integral proteins which ultimately form ion channels. Ion channels can be subdivided into voltage-gated ion channels and ligand-gated channels. The main difference between these two types of channels is the mechanism upon which they open. Voltage-gated channels open upon changes in the membrane potential, while ligand-gated channels open when a neurotransmitter or hormone binds to the channel. Ion channels are selective which means that there are specific ion channels for specific ions and the channel only opens for that specific ion. (Barker et al., 2017)

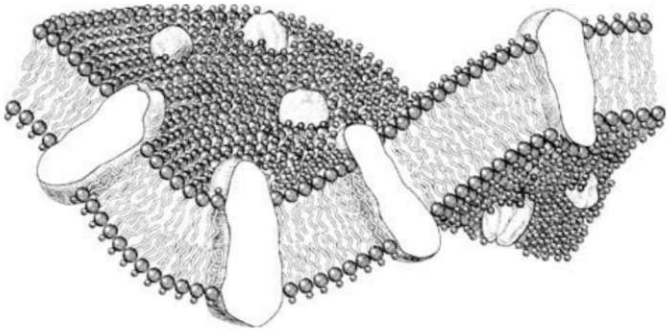

Figure 2.3: Schematic drawing of the overall structure of the cell membrane. The phospholipid bilayer can be seen as well as the integral membrane proteins. Note that is figure does not show the other types of proteins such as surface proteins. (Adapted from (Pfützner, 2011))

Based on the ion specificity the following ion channels can be differentiated: Na^+,K^+, Ca^{2+}, and Cl^- channels. The most relevant ones for excitable, neuronal cells are Na^+,K^+, and Ca^{2+} channels, which are often summed up by calling them tetrametric cation channels. Ion channels are not only relevant for exciting the cell, but are also involved in diseases. Potassium channels, or to be more precise mutations or alterations of their genetic representation, can be linked to many diseases of the heart, kidneys, or of the nervous system. (Tillman and Cascio, 2003; Guidelli, 2020)

Most of the ion channels are closed while the cell is at its resting potential, but there are also leakage currents which means that a few ions diffuse through the membrane; however, this current is rather small. For a decisive transport of ions through the membrane, a special pump is needed, called the Na-K-pump. This pump depicts one of the most important active transport processes in a cell. An active transport process is characterized by the use of energy. The Na-K-pump consists mainly of an enzyme called the Na-K-ATPase, which hydrolyses ATP and works against the electrochemical gradient, and exchanges three sodium ions against two potassium ions. The three sodium ions are transported out of the cell, while the two potassium ions are flowing into the cell. (Nakao and Gadsby, 1986; Armstrong, 2003; Faller and Schünke, 2016)

The ion concentration on both sides of the membrane as well as the knowledge about the existence of ion channels is crucial for understanding the development of an action potential (AP) and neural stimulation (see chapter 2.1.4 and 2.3).

2.1.4 Development and Propagation of Action Potentials

The information transmitted by neurons in the nervous system is coded in a frequency-modulated electrical signal, called action potential (AP). In case of the ANF, the acoustic stimulus, e.g. a pure tone or sound wave, must be converted first by the hair cells before an AP is generated at a later point. The hair cells have a complex conversion mechanism and structure, which is shown in Figure 2.4. At the tips of the hair cells, mechanically-sensitive potassium channels are located, which are connected to tip-links, which are in turn again connected to the neighboring stereocilium. When a mechanical stimulus, in this case a sound wave, now hits the tips of the hair cells, the stereocilia deflect leading to the opening of the connected potassium channels. The resulting potassium influx will depolarize the cell, which triggers the opening of voltage-gated calcium channels. As a result, glutamate, a neurotransmitter, is released leading to the excitation of the peripheral ends of the *Nervus vestibulocochlearis*. (Swenson, 2017; Hopkins, 2015)

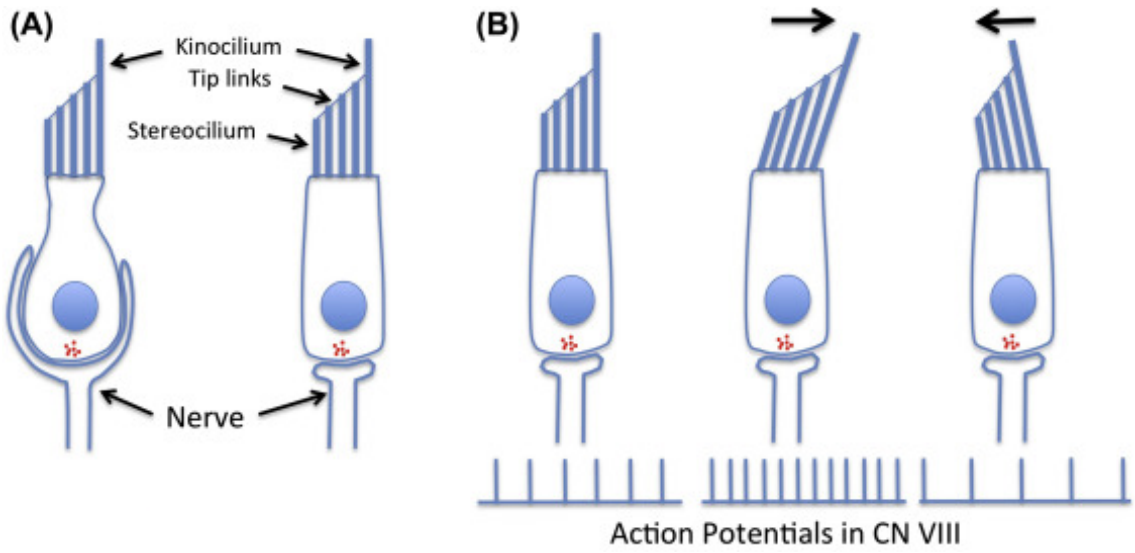

Figure 2.4: Schematic drawing of the structure of the hair cells. A) shows the main parts of a hair cell. B) Left: Hair cell fibers with spontaneous activity, otherwise no AP would result. B) Middle and right: Periodically moving stereocilia of many hair cells give in sum the shown AP in the cranial nerve (CN). (Adapted from (Swenson, 2017))

As shown in Figure 2.2, a neuron can have many dendrites transmitting signals to the soma. To ensure that the cumulated signal will be further conducted in form of an AP, its amplitude has to be above a certain threshold value. For a better understanding of this process, it should be explained that the nerve cell has a certain resting potential, which results from different ionic concentrations on both sides of the membrane. The ions, which are mainly involved, are Na^+, K^+, and Cl^-. To define this resting potential, the Nernst equation comes in handy (see equation 3).

$$E_m = \frac{R \cdot T}{n \cdot F} \cdot \ln \frac{c_2}{c_1} \tag{3}$$

It describes the voltage across the cell membrane, when only one single type of ion is involved. In contrast to that, the Goldman equation is valid for more than one ion type (see equation 4). (Rattay, 1990)

$$E_m = \frac{R \cdot T}{F} \cdot \ln \frac{P_K \cdot [K]_o + P_{Na} \cdot [Na]_o + P_{Cl} \cdot [Cl]_i}{P_K \cdot [K]_i + P_{Na} \cdot [Na]_i + P_{Cl} \cdot [Cl]_o} \tag{4}$$

P is the permeability of the corresponding ion. To indicate the concentration of an ion, the notation of the type $[K]$ (for potassium) is used, where the lower case letter i and o clarify, whether the outside or the inside concentration of the cell is meant. R is the gas constant ($\mathrm{R} = 8.314\,41\ \mathrm{J/(mol \cdot K)}$), T stands for the absolute temperature, and F is the Faraday constant ($\mathrm{F} = 96485.33\ \mathrm{C/mol}$).

Using equation 4, the resting membrane potential of a typical nerve cell is calculated to be in the range of -65 mV. To trigger an AP, the sum of all signals coming from the different input branches of the neuron must lie above a value between -50 mV and -40 mV. (Raghavan et al., 2019) An AP follows the all-or-none-principle, which means that an AP is only elicited upon reaching the threshold value. Every rise of the potential below the threshold value will not trigger an AP. (Adrian, 1914) An AP always obeys the same procedure, which is also why it always looks the same and has no amplitude attenuation during propagation. (Debanne et al., 2011) In more detail, the AP develops as follows (see Figure 2.5):

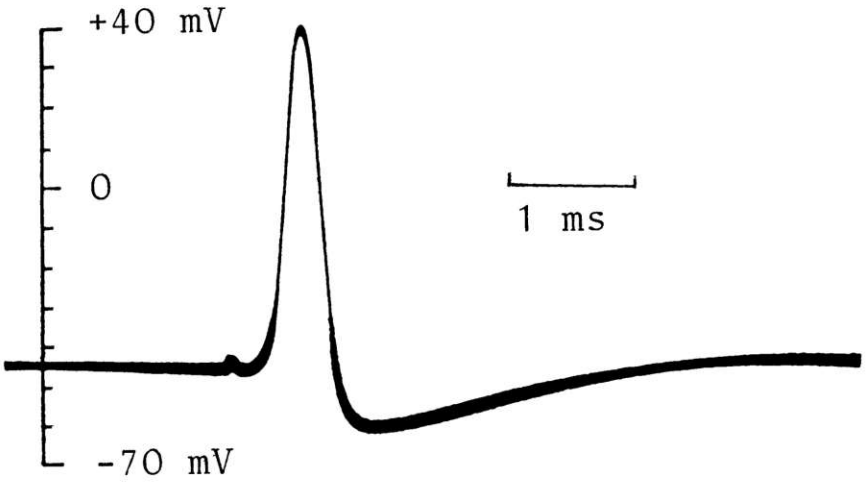

Figure 2.5: Recorded AP from a giant squid axon. The phases described in the text are transferable: The first significant rise of the membrane potential is the depolarization phase of the cell. The potential decrease is the repolarization followed by hyperpolarization before the resting membrane potential is reached again. (Adapted from (Hodgkin and Huxley, 1945))

Upon reaching the threshold value, voltage-gated sodium-channels open leading to a rapid influx of sodium ions, which depolarizes the cell (Yu and Catterall, 2003), i.e. raises the membrane potential to positive values (approximately 30 - 40 mV). After a certain time, the sodium channels close again, while voltage-gated potassium channels open resulting in an outflow of potassium ions. The membrane voltage decreases again, which is called repolarization. After repolarization, hyperpolarization follows which drives the membrane potential even below the resting membrane potential before the resting state is reached again. The sodium channels stay inactivated for some time, which means that during this phase no new AP can be elicited, known as the refractory period. (Chen and Lui, 2022; Raghavan et al., 2019) The AP travels along the axon and will finally arrive at the brain stem, where the auditory information transmitted is processed.

2.2 Technical Background

2.2.1 Basic Concepts of Electrical Engineering

As mentioned in chapter 2.1.4, an acoustic signal is converted into an electrical signal for auditive perception. Furthermore, as shown in chapter 2.3, for neural stimulation it is advantageous to have basic knowledge about current, voltage, and electrical networks in general. Thus, these concepts are covered in the next paragraphs, but it should also be mentioned that a detailed explanation would go beyond the scope of this thesis.

When there is movement of electrical charge in some way, it is called an electrical current, which is why electrical current can be seen as the transport rate of electrical charge. The SI-unit of electrical current is Ampere ($1\,\mathrm{A} = 1\,\frac{\mathrm{C}}{\mathrm{s}}$). Voltage is generally defined over the path-integral of the electrical field and can also be seen as charge-related work. But, there is also a particular case: In electrostatics and quasi-electrostatic the voltage can also be defined as potential difference. The SI-unit of the voltage is Volt ($1\,\mathrm{V} = 1\,\frac{\mathrm{J}}{\mathrm{C}} = 1\,\frac{\mathrm{kg}\cdot\mathrm{m}^2}{\mathrm{A}\cdot\mathrm{s}^3}$). The quotient of voltage and current is called electrical resistance with the unit Ohm ($1\,\Omega$) following Ohm's law. Ohm's law, the probable most fundamental law in electrical engineering, is expressed in equation 5 and states that voltage and current are proportional to each other with the proportionality factor R being the resistance. Thus, one can say that this law is the basis for the definition of the resistance. Resistors, at which Ohm's law holds true, are called ohmic. The reciprocal of the resistance is the conductance with the unit ($1\,\mathrm{S}$). (Prechtl, 1994).

$$U = R \cdot I \tag{5}$$

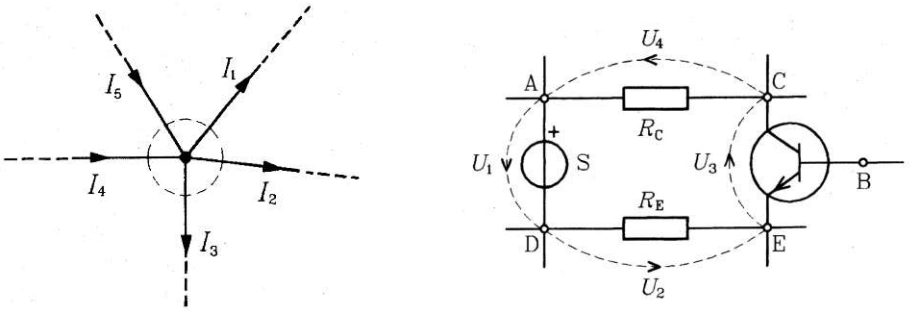

(a) First law of Kirchhoff. (b) Second law of Kirchhoff.

Figure 2.6: Schematic drawing of two electrical networks to show (a) the first and (b) the second law of Kirchhoff. In (a) a common node of different currents is shown. (b) shows a circuit loop where different voltage drops are marked. (Adapted from (Prechtl, 1994))

For the analysis of electrical networks, it is useful to know the two laws of Kirchhoff. The first law states that the sum of all currents in a node is zero. In Figure 2.6(a), a node is drawn, where different currents flow together. In mathematical terms, with the help of Figure 2.6(a), the first law of Kirchhoff can be written as (Prechtl, 1994):

$$I_1 + I_2 + I_3 - I_4 - I_5 = 0 \tag{6}$$

The second law of Kirchhoff is concerned with voltages and states that the sum of all voltages in a closed circuit loop is zero. In Figure 2.6(b), a circuit is drawn where the second law of Kirchhoff is used. The functionality of the single electrical components must not be known for the application of the law. In equation 7, the second law of Kirchhoff was applied for Figure 2.6(b). (Prechtl, 1994)

$$U_1 + U_2 + U_3 + U_4 = 0 \tag{7}$$

2.2.2 Equivalent Circuit of a Patch of Membrane

For simulation of nerve fiber excitation, not only an understanding of the anatomical and physiological matter, but also of the technical description is useful (also see chapter 3.1). As mentioned in chapter 2.1.3, the cell membrane plays a major role in the excitation process of the cell, which is also possible to describe in technical terms. The cell membrane, as shown in Figure 2.3, can electrically be described in form of an equivalent circuit. The equivalent circuit can be of different complexity, but the underlying components are a resistor and a capacitor in parallel connection. The equivalent circuit can also be extended to account for dielectric dispersion phenomena for example. (Merla et al., 2012) For this thesis, two approaches of different

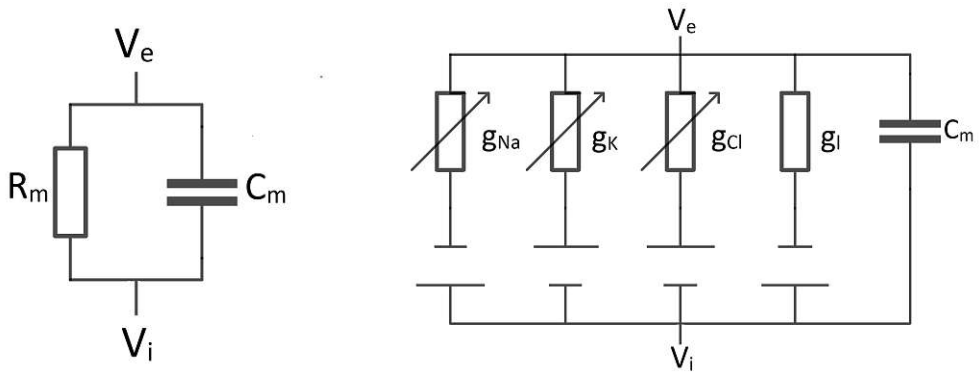

(a) Passive membrane. (b) Active membrane.

Figure 2.7: Equivalent circuits for a patch of membrane. In a) the equivalent circuit for a passive patch of membrane is shown, whereas b) shows the active patch of membrane. a) is a RC-circuit with constant values. In b) the conductances are dependent on the transmembrane voltage and describe the different ion channels. The individual voltages coming from different ionic concentrations in the intra-and extracellular space are each modelled by a battery in series to the conductance. As shown, the sodium and leakage channel lead to an inward current, while the potassium and the chloride channel produce a current flowing out of the cell. Although b) depicts sodium, potassium, chloride, and a leakage conductance, this thesis will exclude the role of chloride channels to be in accordance with the later described Hodgkin-Huxley model. (Adapted from (Rattay, 1990))

complexity will be discussed. Both approaches refer to a patch of membrane in accordance with the patch-clamp experiments of Neher and Sakmann. (see (Neher and Sakmann, 1976)) The first approach is a passive membrane model, which can be used to describe the internodes, which are the myelinated parts of an axon (Figure 2.2). In those parts, no voltage-gated channels are present, which means that the resistance of the circuit is independent from the voltage across the membrane and the circuit reduces to a simple RC-circuit. Figure 2.7(a) shows this passive model, whereas Figure 2.7(b) depicts the active circuit. (Merla et al., 2012)

The equivalent circuit of the passive membrane approach can analytically be solved to get the membrane voltage V_m. The membrane voltage is defined as $V_m = V_i - V_e$ and based on the first law of Kirchhoff (see equation 6), it follows that the overall membrane current splits up into an ohmic and a capacitive part (current through the resistor and current through the capacitor). Thus, one can write $I_m = I_{ohm} + I_{cap}$. Based on the second law of Kirchhoff (see equation 7), it follows that the voltage drop across the R_m equals V_m. Setting up those equations and inserting Ohm's law (see equation 5), it can be written:

$$I_m = \frac{V_m(t)}{R_m} + C_m \cdot \frac{dV_m(t)}{dt} \tag{8}$$

When a current stimulus is applied, which satisfies the condition $I_{stim(t)} + I_m = 0$ equation 8 can further be simplified (see equation 9).

$$\frac{dV_m(t)}{dt} = [-I_{stim}(t) - \frac{V_m(t)}{R_m}] \cdot \frac{1}{C_m} \tag{9}$$

Finally, one can insert the condition $V_m = V_i - V_e$ and gets equation 10, which can be solved for an initial value being $V_m(t) = V_{rest}$, where V_{rest} is equal to -65 mV.

$$\frac{d(V_i(t) - V_e(t))}{dt} = [-I_{stim}(t) - \frac{V_i(t) - V_e(t)}{R_m}] \cdot \frac{1}{C_m} \tag{10}$$

The second approach is shown in Figure 2.7(b) representing the equivalent circuit for an active patch of membrane, which usually is a NoR. In this case, conventionally conductances, so the reciprocals of the resistances, are used. Each conductance is dependent on the voltage V_m. Again, the electrical network can be analyzed using the laws of Kirchhoff (see equation 6 and 7) and for the conductances, it follows with the inclusion of the individual voltages (Nernst potentials) of the corresponding ion:

$$G_{Na}(t) = \frac{I_{Na}(t)}{V_m(t) - V_{Na}} \tag{11}$$

$$G_K(t) = \frac{I_K(t)}{V_m(t) - V_K} \tag{12}$$

As mentioned before, only the sodium and potassium channels are of interest for this thesis. As shown in Figure 2.7(b), the leakage conductance is independent from V_m, which is why I_L can be written as (see equation 13):

$$I_L = [V_m(t) - V_L] \cdot \frac{1}{R_m} \tag{13}$$

Now it is again possible to insert the condition $V_m = V_i - V_e$ and the differential equation for the transmembrane voltage V_m looks as follows:

$$\begin{aligned} \frac{d(V_i(t) - V_e(t))}{dt} = [&-I_{stim}(t) - G_{Na}(t) \cdot (V_m(t) - V_{Na}) \\ &- G_K(t) \cdot (V_m(t) - V_K) - G_L \cdot (V_m(t) - V_L)] \cdot \frac{1}{C_m} \end{aligned} \tag{14}$$

As one can see, in equation 14 every term represents a current which goes hand in hand with the view of the excitation process of being a charge transport of different ions through the membrane. This differential equation can also be seen as pre-stage for the Hodgkin-Huxley model (see chapter 2.3). (Rattay, 1990).

2.2.3 Cochlear Implants

A CI is a biomedical device which is implanted to treat deafness or severe hearing loss caused by the destruction of sensory hair cells. (Eshraghi et al., 2012; Lenarz, 2017). The basic idea behind a CI is to bridge those damaged parts and to stimulate the ANF directly via electrodes inserted into the cochlea. The actual stimulation of the ANF is the result of a series of steps happening before. At first, the sound is picked up by a microphone, which is connected to the so-called external speech processor, which encodes the acoustic signal into a digital signal. This digital signal is then further converted into a radiofrequency signal (RF) signal, which is sent to an internal processor, which is implanted under the skin. The transmission happens via inductively coupled coils with one coil being the sender and the other one being the receiver. In a next step, the signal gets decoded and is then converted into an electrical signal, a current, which is sent to the electrodes, which finally stimulate the ANF. Figure 2.8 shows a schematic drawing of an implanted CI and the approximate position of the electrodes in the cochlea. (Mistrík et al., 2017)

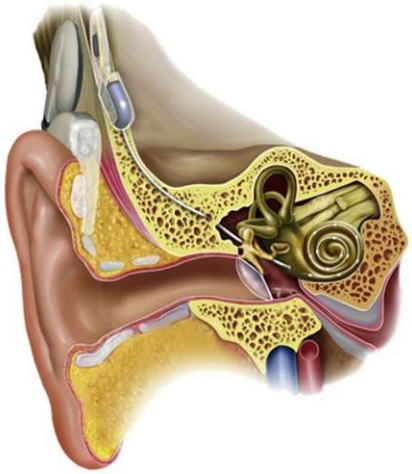

Figure 2.8: Depiction of an implanted CI. Behind the ear there is the external processor which picks up sounds by a microphone. The sound is then converted into a digital signal, is again converted into a radiofrequency (RF) signal which is transduced via inductive coupling to an internal receiver. The signal is then decoded into an electrical signal and the electric current pulses stimulate the ANF. (Adapted from (Mistrík et al., 2017))

.

The indications for the implantation of a CI are continuously modified, but the current indications are bilateral postlingual deafness, bilateral sensorineural hearing loss, bilateral profound hearing loss for high-frequencies while maintaining low ones, and asymmetric hearing loss with severe tinnitus in the deaf ears which cannot be treated in an other way. (Szyfter et al., 2019) For those cases, implantation should be a standard routine, but there are also cases, where the ST, the state-of-the-art location for electrode insertion, may be ossified or obstructed, which impedes implantation (see also chapters 1.2 and 1.3). This is not the only aspect of a CI

which is in need of further research. Although CIs are used for more than 50 years now, there is still ongoing research to improve the sound processing and perception of speech and especially of music. (also see (Gfeller and Lansing, 1991; Gfeller et al., 2006)) The underlying problem is the electrode-nerve interface, since up to now only a single digit number of channels is available, leading to less accurate speech and music perception. (Lenarz, 2017) A key factor for the quality of stimulation and in further steps for the perception of sounds is the electrode position, especially the insertion depth. A insertion depth of 360° is pursued to reach as many spiral ganglion cells as possible, which is the ganglion where the somata of the eighth cranial nerve are located. (Carricondo and Romero-Gómez, 2019) But the insertion depth is not the only limiting factor, also the design of the electrodes itself is of importance as well as other aspects such as pulse shape for example, where alternatives to the standard rectangular pulses are under investigation. (see also (Navntoft et al., 2021) This thesis also aims to contribute by analyzing differences between ST and SV stimulation.

2.3 Stimulation of Nerve Fibers

2.3.1 Hodgkin-Huxley Model

In 1952 Alan Lloyd Hodgkin and Andrew Fielding Huxley introduced a mathematical model to describe the generation of an AP (see chapter 2.1.4) respectively the voltage-current relation at the membrane of a squid axon, where they originally conducted their experiments. (Rattay, 1990) The model built holds true even after more than 50 years. (see (Hodgkin and Huxley, 1952b)) The model is based on the idea to describe the cell membrane in electrical terms, as shown in Figure 2.7(b). Again, it should be noted that to be in accordance with the model from Hodgkin-Huxley, only sodium, potassium, and leakage currents are of relevance. By convention, which is also indicated in equation 9, the occurring currents I_{stim} and I_{ion} have different impacts on the cell, since a positive I_{stim} will depolarize the cell, i.e. making the membrane voltage more positive, and a positive I_{ion} will hyperpolarize the cell, making V_m more negative. Another declaration concerning the membrane voltage should also be mentioned here. For the further calculation of the Hodgkin-Huxley model, one can either choose the membrane voltage or the reduced membrane voltage. The difference is that for the reduced membrane voltage, the term of the resting membrane voltage ($V_{rest} = -65$ mV) is also taken into account:

$$V_m = V_i - V_e - V_{rest} \tag{15}$$

Often it is more convenient, to use the reduced membrane voltage. Coming back

to the actual Hodgkin-Huxley model with the equivalent electrical circuit shown in 2.7(b). The overall ionic current is the sum of the sodium, potassium, and leakage current (Note: The chloride channel is ignored). Mathematically, one can write:

$$I_{ion} = G_{Na} \cdot (V_m - V_{Na}) + G_K \cdot (V_m - V_K) + G_L \cdot (V_m - V_L) \tag{16}$$

Special attention should be given to the conductances G_{Na} and G_K, not only because they are voltage-dependent which can be traced back to the physiology of the cell membrane (see chapter 2.1.3), but also because the corresponding ion channels can theoretically be seen as a construct containing a certain number of gates, which control the ion flow through the channel. A gate can either be in a permissive or non-permissive state, according to the linguistic convention used by (Nelson and Rinzel, 1998). For the channel to be open and for ions to pass through the channel, all gates of that channel must be in the permissive state. In case that one or more gates are in the non-permissive state, no ions can flow, which finally means that the channel is closed. This behavior is included in the Hodgkin-Huxley model by assuming that the probability of a gate to be in a permissive or a non-permissive state depends on V_m. (Nelson and Rinzel, 1998) For a better understanding of this complex gating mechanism, a variable y being a function of voltage and time can be defined. y defines a gating process and describes the gating behavior of a large number of channels of a specific type in a statistical manner. The variable y is a probability lying between 0 or 1, where 1 means that all gates are in a permissive state and 0 means that all gates are in a non-permissive state. Mathematically it can be expressed as the following: (Rattay, 1990)

$$\frac{dy}{dt} = \alpha \cdot (1 - y) - \beta y \tag{17}$$

In equation 17, α and β are rate constants dependent on the voltage V_m. α resembles the transition rate from the non-permissive to the permissive state, while β gives information about the transition rate from the permissive to the non-permissive state. Before the Hodgkin-Huxley model is complete, the dummy-variable y must be replaced by the actual gating variables m, n, and h, where, generally spoken, each gating variable corresponds to an ion channel. Hodgkin-Huxley stated that the sodium channel contains three identical, rapidly-responding activation gates, which are called the m-gates, and of a single, slower responding inactivation gate, which is the h-gate. In contrast, the potassium channel only involves 4 individual activation gates, known as the n-gates, but no inactivation gate. In mathematical terms, one can write (Nelson and Rinzel, 1998; Rattay, 1990)

$$G_{Na} = g_{Na} m^3 h \qquad G_K = g_K n^4 \tag{18}$$

with g_{Na} and g_K being the conductance of the corresponding ion. m to the power

of 3 and n to the power of 4 result, because of the number of gates and the fact that all gates have to be in the permissive state for the channel to be open. For the Hodgkin-Huxley model to be complete, equations 16-18 must be put together, resulting in the following four differential equations, known as the Hodgkin-Huxley model:

$$\frac{dV_m}{dt} = [-g_{Na}m^3h(V - V_{Na}) - g_K n^4(V - V_K) - g_L(V - V_L) + i_{st}]/c \tag{19}$$

$$\frac{dm}{dt} = [-(\alpha_m + \beta_m) \cdot m + \alpha_m] \cdot k \tag{20}$$

$$\frac{dn}{dt} = [-(\alpha_n + \beta_n) \cdot n + \alpha_n] \cdot k \tag{21}$$

$$\frac{dh}{dt} = [-(\alpha_h + \beta_h) \cdot h + \alpha_h] \cdot k \tag{22}$$

with the rate constants α and β being

$$\alpha_m = \frac{2.5 - 0.1 \cdot V}{e^{2.5-0.1 \cdot V} - 1} \qquad \beta_m = 4 \cdot e^{-\frac{V}{18}} \tag{23}$$

$$\alpha_n = \frac{1 - 0.1 \cdot V}{10 \cdot (e^{1-0.1 \cdot V} - 1)} \qquad \beta_n = 0.125 \cdot e^{-\frac{V}{80}} \tag{24}$$

$$\alpha_h = 0.07 \cdot e^{-\frac{V}{20}} \qquad \beta_h = \frac{1}{e^{3-0.1 \cdot V} + 1} \tag{25}$$

To be independent from geometrical parameters, it should be mentioned that every calculation is thought to be for 1 cm^2 of membrane, which means that currents become current densities, for example. That is why lower case letters are used in the equations. As already mentioned, the experiments were originally conducted in giant squid axons, which is why the original temperature during the experiments was $T = 6.3$°C. Thus, to apply this model to humans the temperature must be raised, which is why the factor k was added to the equations of the gating variables in the model. The factor k is given as (Rattay, 1990)

$$k = 3^{0.1 \cdot T - 0.63} \tag{26}$$

with T being the temperature in degree Celsius. The temperature greatly influences the shape and amplitude of the propagating AP, which is why the temperature must be taken into account during modelling. Hodgkin-Huxley found out that the gating processes react with the same sensitivity to temperature steps. Although the model still holds true for higher temperatures, the propagation of the AP is impeded due to the reduced amplitude and duration of the AP. This reduction in strength and the resulting failure of AP propagation starts to occur at temperatures above 31°C, which is termed *heat block*. (Rattay, 1990; Hodgkin and Katz, 1949)

2.3.2 Extracellular Stimulation and Activating Function

To study the electric behavior of neuronal membranes, Hodgkin-Huxley inserted electrodes into a giant squid axon, which was chosen because of its thickness of up to 1 mm, and measured the injected current while the time course of the voltage was given. There was no current flow along the axis and the whole membrane worked under the same condition, because of *isopotentials* inside and outside of the cell. (Rattay, 1990) The proportionality between conductance and current was the main result of these so-called voltage-clamp experiments by Hodgkin-Huxley, which then further contributed to the famous Hodgkin-Huxley model (see chapter 2.3.1). (Hodgkin and Huxley, 1952a) However, since electrodes were inserted into the axon, only intracellular stimulation had been analyzed. To study extracellular stimulation, i.e. when the electrode is placed in the extracellular space outside of the cell, the model has to be expanded. A current of an extracellular electrode generates a gradient of extracellular potential which may trigger an AP. (Schoen and Fromherz, 2007) The extracellular potential of a spherical electrode, which is located in a distance r to the axon, can be calculated using equation 27 (Rattay, 1990).

$$V_e = \frac{\rho_e I_{el}}{4\pi r} \tag{27}$$

ρ_e gives the specific resistance of the extracellular medium, which is about 300 Ωcm. I_{el} is the applied electrode current, and r gives the distance to the axon, which can be calculated using the Pythagorean theorem:

$$r = \sqrt{x^2 + z^2} \tag{28}$$

where x and z are Cartesian coordinates. Now, the extracellular potential can be calculated for every point along the axon, since the V_e is only dependent on the distance from the fiber. Usually, the fiber is segmented into so-called compartments to have a discretization in space. The compartments must be so small to approximate the behavior of each compartment by *isopotentials* inside and outside of the cell, which means that each compartment can be approximated by a mean voltage and current value. The number of compartments can vary from one, meaning that the whole cell is modelled with just one compartment, to more than 100 compartments, which is called a multi-compartment model. The Hodgkin-Huxley model can then be applied for every single compartment. (Rattay et al., 2018)

For the analysis of the situation when a spherical electrode is placed in a certain distance away from the fiber and used to stimulate the fiber, the Hodgkin-Huxley model, as already mentioned, must be expanded respectively merged with the information given by equation 27. The reduced membrane voltage can then be calculated as:

$$\frac{dV_n}{dt} = [-I_{ion,n} + \frac{V_{n-1} - V_n}{R_{n-1}/2 + R_n/2} + \frac{V_{n+1} - V_n}{R_{n+1}/2 + R_n/2} + \frac{V_{e,n-1} - V_{e,n}}{R_{n-1}/2 + R_n/2} + \frac{V_{e,n+1} - V_{e,n}}{R_{n+1}/2 + R_n/2}] \cdot \frac{1}{C_n} \tag{29}$$

where I_{ion} can be calculated by the four Hodgkin-Huxley equations 19 - 22, V_n is the reduced membrane voltage, V_e is the extracellular potential, where the index n stands for the n-th compartment. The parameter R is the axial resistance of the compartment and C is the membrane capacitance. The axial resistance R is a parameter dependent on the axial resistivity ρ_i, which is the resistivity of the axoplasm, i.e. the cytoplasm of the neuron, and on the geometry of the compartment. Often, the geometry of a compartment is modelled by a cylinder, for example the dendrites and axon. Then, equation 30 can be used:

$$R = \rho_i \cdot \frac{l}{r^2\pi} \tag{30}$$

where l is the length of the compartment and r is the radius of the cylindric compartment. Worth to mention is that for the calculation of the axial resistance of the soma, which is often modelled as a sphere, another approach must be chosen, since the axial resistance to the neighbor compartments depend on the compartment diameter. (Rattay et al., 2003) Thus, the following equation 31 can be used

$$\frac{R_{soma,j}}{2} = \frac{\rho_i}{2r\pi} \cdot \ln(\frac{r_{soma} + z_j}{r_{soma} - z_j}) \tag{31}$$

where j indicates the j-th process of the soma and $z_j = \sqrt{r_{soma}^2 - (d_{process,j}/2)^2}$. The membrane capacitance can be calculated as the product of compartment surface area and the corresponding compartment capacity. To determine the surface area, only the geometry of the compartment, i.e. surface of a cylinder, must be known. However, for the surface area of the soma, again a more complicated calculation must be done, as equation 32 shows:

$$A_{soma} = 4r_{soma}^2\pi - \sum(2r_{soma}\pi h_j) \tag{32}$$

with $h_j = r_{soma} - z_j$ where z_j was already mentioned above. (Rattay et al., 2003) With that, every parameter of equation 29 is defined. But it is useful to take a closer look at the last terms of equation 29, because that is known as the activating function, found by (Rattay, 1986). The activating function can thus be written as:

$$f_n = [\frac{V_{e,n-1} - V_{e,n}}{R_{n-1}/2 + R_n/2} + \frac{V_{e,n+1} - V_{e,n}}{R_{n+1}/2 + R_n/2}] \cdot \frac{1}{C_n} \tag{33}$$

The activating function gives information about the impact of an externally applied electrical field on a nerve fiber and has the physical dimension $[V/s]$ or $[mV/ms]$. The activating function is proportional to the second derivative of the extracellular potential and is a quite convenient tool, because it provides information about the excitation of the nerve fiber without knowing channel dynamics. A positive value of f_n indicates that a region gets depolarized and a negative value of f_n means that the region gets hyperpolarized. In other words, if the cell is in the resting state the activating function represents the slope of the membrane potential at the very first moment after a stimulus is applied. (Rattay, 1986)

2.3.3 Euler-Method

It is not always possible to have an exact, respectively an analytical, solution for an ordinary differential equation (ODE). Therefore, numerical solution methods, like the Euler-Method, must be used. It can be distinguished between the Forward Euler (FE) and the Backward Euler (BE) method. (Johnson and Chartier, 2017; Biswas et al., 2013)

The FE is an explicit method and has the form:

$$y_{n+1} = y_n + f(y_n, t_n) \cdot h \tag{34}$$

where h stands for the time discretization. The BE is an implicit method and has the form:

$$y_{n+1} = y_n + f(y_{n+1}, t_{n+1}) \cdot h \tag{35}$$

Both methods induce an error per step of $O(h^2)$ and have a global error of $O(h)$ (first order methods), but differ in terms of stability and computational complexity. The FE can become instable from a certain step size on, whereas BE stays stable for every step size. However, BE is more complicated to solve, because an implicit equation or even an implicit system of equations has to be solved, which can become complex if multiple ODEs are coupled. Since the Hodgkin-Huxley model consists of four ODEs (equation 19-22), with stiff ODEs for the gating variables (equation 20-22) and no analytical solution, a numerical method has to be used. For this thesis, the BE method was chosen for stability reasons.

3 Materials and Methods

As mentioned in chapter 1.4, the aim of this thesis is to analyze differences in ANF excitation behavior between ST- and SV-placed electrodes. For this, a computer simulation of an already established, but now modified model was conducted using different software tools. This chapter should give insights into the development of the model and the simulation.

3.1 Definition of the Model

The model of this thesis is based on the model proposed by (Rattay et al., 2001b). It resembles the standard human cochlear neuron and consists of a peripheral axon (=dendrite), a soma, and a central axon. However, the starting point of the model used in this thesis is the first figure of (Rattay et al., 2001a), shown in Figure 3.1. It is a microphotograph of the mid-modiolar section of a human cochlea. The first step then was to draw 4 nerve fibers as a dendrite-soma-axon combination, such as in (Rattay et al., 2001b), anatomically as accurate as possible into this microphotograph. The electrode positions were also drawn into the microphotograph. For the sake of clarity, a detailed explanation of this process is given in the following sections.

3.1.1 Defining the Fibers

As mentioned above, four nerve fibers, consisting of a dendrite, a soma, and an axon, were drawn into Figure 3.1 by approximating each fiber by three lines (=2 lines for dendrite, 1 line for axon), one circle (=soma), and an arc (for the dendrite). The final paths of the fibers are shown in Figure 3.2. The fibers' sections can further be subdivided into the unmyelinated terminal, peripheral nodes and internodes, the presomatic region, the soma, the postsomatic region, and into the central nodes and internodes. The compartments were accordingly chosen. It was tried to define four fibers in the same way, but due to the aspiration of anatomical correctness, it was

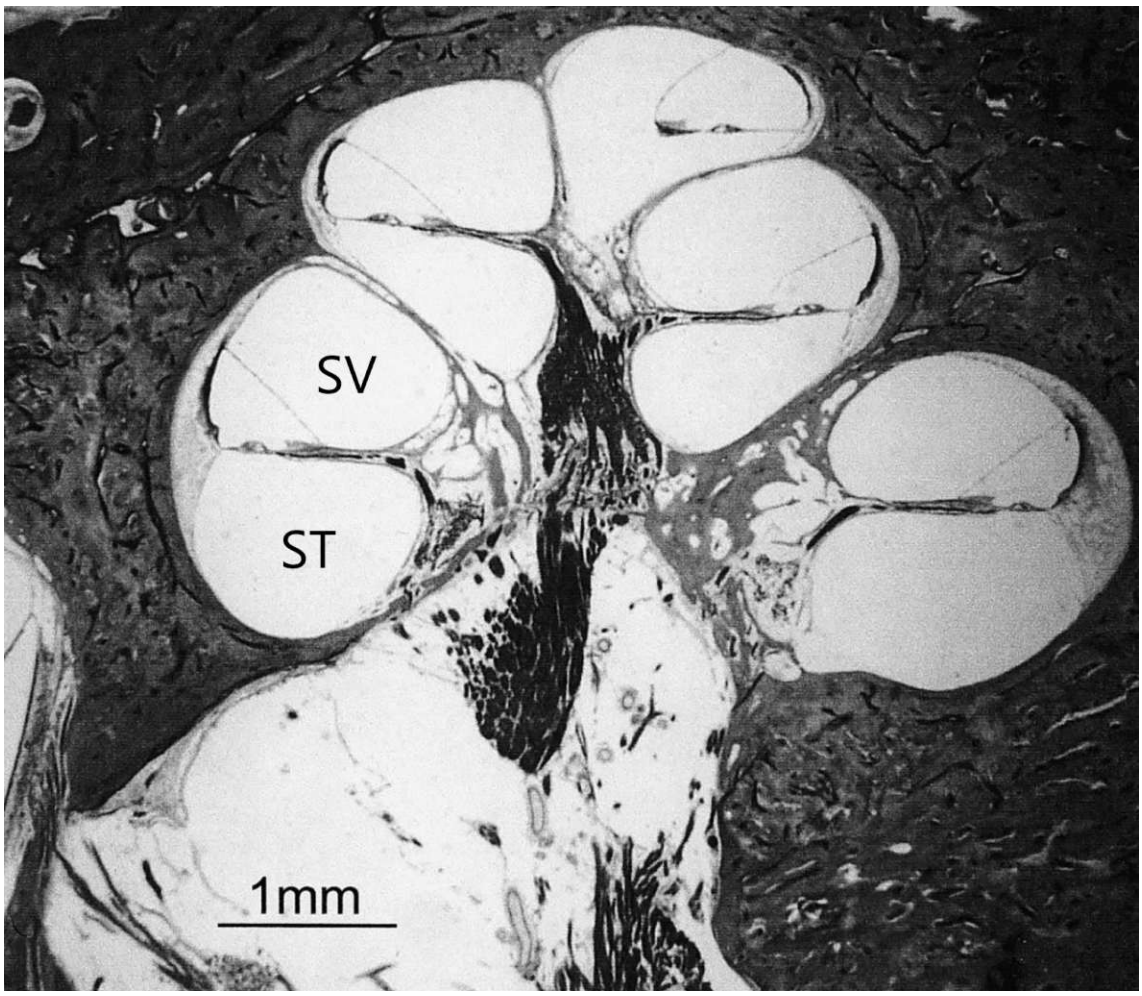

Figure 3.1: Mid-modiolar section of a human cochlea. This microphotograph is the basis for the definition of the fiber paths and electrode positions in this thesis.The ST and SV are labelled for better understanding. (Adapted from (Rattay et al., 2001a))

not possible. Generally, the fibers were defined as follows (exceptions for certain fibers are stated at the end of the paragraph): The dendrites of the fibers consist of a 10 μm long unmyelinated terminal end, of five internodes where each has a length of 250 μm, five NoR each with a length of 2.5 μm, one internode with a length of 210 μm, and one presomatic region, which has a length of 100 μm. The terminal end, the NoR and the internodes were each modeled with just one compartment, whereas the presomatic region was divided into three compartments of equal length. The soma of each fiber was defined as a sphere with a diameter of 20 μm, which is different from (Rattay et al., 2001b), where the diameter of the soma was 30 μm. The diameter was reduced due to one result of the study of (Potrusil et al., 2012), where a mean value for the diameter of the soma was detected to be 19 μm, indicating that the initial soma diameter of 30 μm was too large. The axons consist of a 5 μm long postsomatic region and as many NoR (2.5 μm in length) and internodes (500 μm

in length) as needed to have an AP spreading away from the soma upon excitation. The diameter of the axon was defined as 2 μm, which is double the diameter of the dendrite.

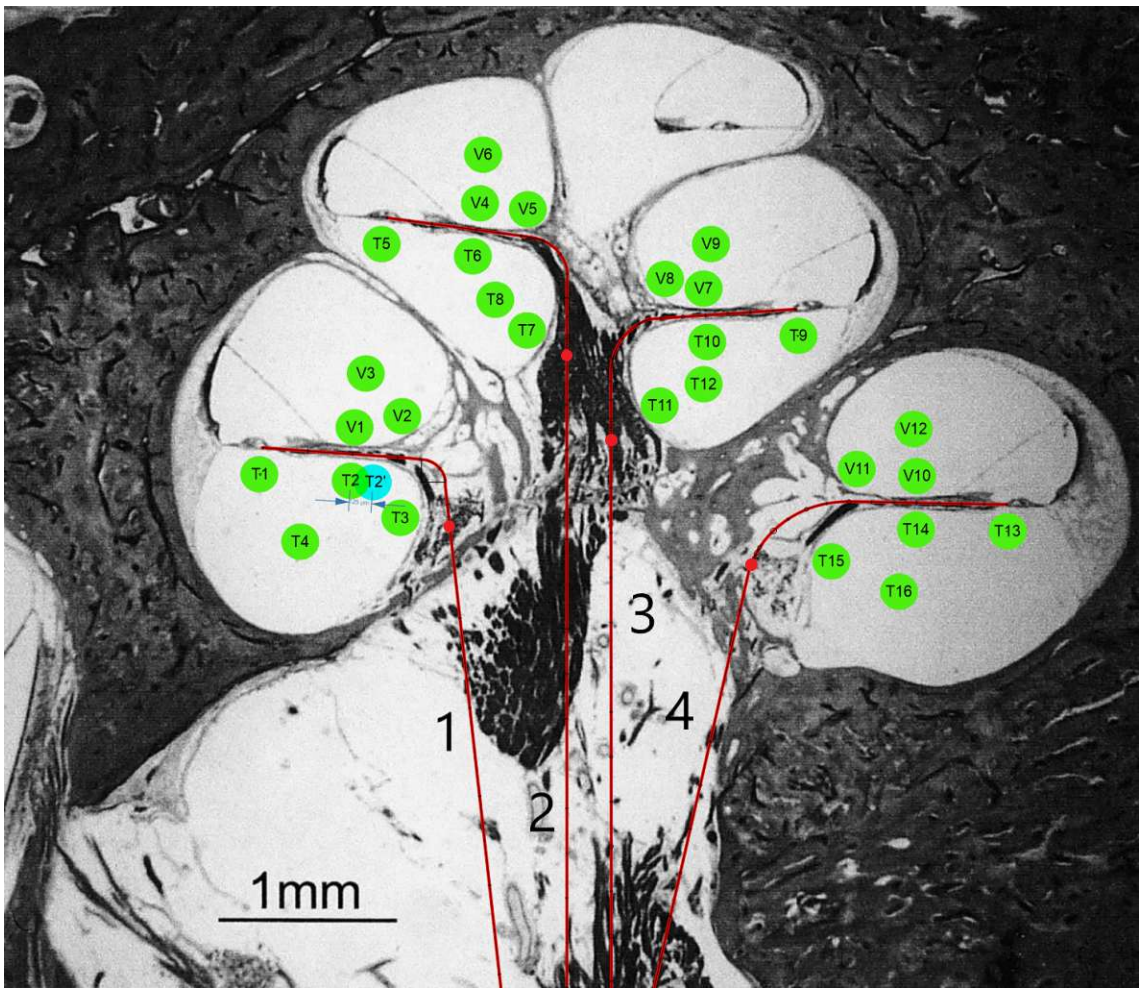

Figure 3.2: Same figure as Figure 3.1, but here the nerve fiber paths (red) as well as the electrode positions (green) are included. The fibers are numbered from left to right. Note that the somata are not drawn to scale for visual purposes. (Adapted from (Rattay et al., 2001a))

Fiber 2 and 3 (see Figure 3.2) correspond to the already given description, but Fiber 1 and Fiber 4 are different in some aspects. Fiber 1 is shorter than Fiber 2 and 3 to prevent a too low position of the soma of Fiber 1. Thus, Fiber 1 has one internode and NoR less, meaning that the dendrite of Fiber 1 consists of a 10 μm long unmyelinated terminal end, of four internodes (250 μm in length), four NoR (2.5 μm in length), one internode with a length of 210 μm, and one 100 μm long presomatic region. Fiber 4 is also shorter. Due to the lateral anatomical position, the pathway of Fiber 4 would be too steep when modeling the dendrite with two lines and one arc. Thus, to compensate for that, the dendrite was only approximated by one line and one arc and one internode was therefore shortened. Thereby, the

dendrite of Fiber 4 consists of one unmyelinated terminal (10 μm in length), four internodes (250 μm in length), five NoR (2.5 μm in length),one internode with 231.7 μm in length, one internode (210 μm in length), and one presomatic region (100 μm). The soma and axon of Fiber 1 and Fiber 4 were left unchanged. For a better overview of the fiber definition, the geometric parameters are listed in Table 3.1.

Table 3.1: Geometric Parameters of Fiber 1-4. Listed are the lengths (l) and the diameters (d) of each section of the fiber. I-1, I-2,..., I-6 stands for the peripheral internodes. They are listed individually since their dimensions change from fiber to fiber. Note that not every dendritic NoR is shown, since they always have the same dimensions, but they vary in number. Similar to that, only the dimensions of the central internodes (I-C) and NoR are shown and not their quantity.

	Fiber 1		**Fiber 2**		**Fiber 3**		**Fiber 4**	
Region	**l [µm]**	**d [µm]**	**l [µm]**	**d [µm]**	**l [µm]**	**d [µm]**	**l [µm]**	**d [µm]**
terminal	10	1	10	1	10	1	10	1
I-1	250	1	250	1	250	1	250	1
I-2	250	1	250	1	250	1	250	1
I-3	250	1	250	1	250	1	250	1
I-4	250	1	250	1	250	1	250	1
I-5	210	1	250	1	250	1	231.7	1
I-6	-	-	210	1	210	1	210	1
NoR	2.5	1	2.5	1	2.5	1	2.5	1
presomatic	100	1	100	1	100	1	100	1
soma	-	20	-	20	-	20	-	20
postsomatic	5	2	5	2	5	2	5	2
I-C	500	2	500	2	500	2	500	2
NoR	2.5	2	2.5	2	2.5	2	2.5	2

3.1.2 Electrode Positioning

For extracellular ANF stimulation electrodes are needed. Figure 3.2 shows the different electrode positions used for this thesis to analyze the differences in ANF excitation between ST and SV electrode placement. As already mentioned in chapter 2.1.1 and shown in Figure 3.1, there are two possible ducts to place electrodes, i.e. the ST and the SV. Beside the fact that the SM is not used as location for electrode insertion (Lenarz, 2017; Gulya and Steenerson, 1996), the anatomical dimensions of the SM are too small for electrode placement. Moreover, the risk of rupture of the Reissner's membrane may be too high when trying to surgically access the

SM. As one can see in Figure 3.1, there is potentially more space in the ST than in the SV for electrode placement, since the space in the SV is limited due to the Reissner's membrane. Therefore, only three electrodes per turn were inserted in the SV, while four electrodes per turn were placed in the ST (also see Figure 3.2). In total 29 electrodes were placed in the cochlea, each was drawn with a diameter of 200 μm, although for calculation of the extracellular potential (equation 27) the electrodes were assumed to be point sources. The electrode positions were chosen as follows. For the ST, one electrode (T1) was placed close to the terminal end of the fiber. The orthogonal distance between the electrode and the compartment center of the terminal end was 150 μm, The second electrode (T2) of the ST was placed orthogonally to the second NoR, again in a distance of 150 μm. The third electrode (T3), was placed as close to the soma as possible. For that, a circle with the center being the center of the soma was drawn. The point of intersection between this circle and the ST was the location for T3. The position of the fourth electrode (T4) was found by drawing the biggest possible inscribed circle in the ST. The center of the inscribed circle was the location for T4. The electrodes located in the other turns of the ST were found identically, meaning that T1, T5, T9, and T13 correspond to each other; T2, T6, T10, and T14 have equal positions; also T3, T7, T11, and T15 share the equivalent positions; and last but not least the positions of T4, T8, T12, and T16 were also found in the same way. The electrode positions of the SV were found with the same pattern, except that the electrode at the terminal end of the fiber is excluded, since the Reissner's membrane impedes electrode placement there. Thus, V1, V4, V7, and V10 are the electrodes, which were placed in an orthogonal distance of 150 μm to the compartment center of the second NoR. V2, V5, V8, and V11 are the electrodes closest to the soma and V3, V6, V9, and V12 are the electrodes placed in the center of the biggest inscribed circle of the SV.

To eventually gain more details about the ANF stimulation process, one electrode (T2') was placed additionally at one point in the ST. T2' can be thought of moving T2 by 125 μm medially, meaning that T2' is 150 μm away from the compartment center of the third peripheral internode. For the sake of completeness and clarity, it should again be mentioned that the electrodes were approximated by point sources for the simulation, meaning that equation 27 holds true.

3.1.3 Parameters of the Model

Up to now, the geometric definition of the fibers and the position of the electrodes were covered, but the electric properties needed for simulating the ANF excitation process (also see chapter 2.3.1) must be mentioned as well. Table 3.2 shows the electric parameters and properties used for the simulation.

Table 3.2: List of the electric parameters. The parameters of each section were defined identically for Fiber 1-4. Depicted are the capacitance (c), the conductance (g) and the number of myelin layers for each section. HH stands for Hodgkin-Huxley dynamics with the following channel conductances: g_{Na}=120 mS/cm^2, g_K=36 mS/cm^2, g_L=0.3 mS/cm^2. The index HH_{10} stands for a tenfold Hodgkin-Huxley channel dynamic, meaning that the conductances were multiplied by a factor of 10 for the simulation of the active compartments. (Rattay et al., 2001b; Rattay, 1990)

	region	**c** $[\mu F/cm^2]$	**g** $[mS/cm^2]$	**myelin layers [ ]**
peripheral	terminal	1	HH_{10}	0
	internodes	0.025	0.025	40
	NoR	1	HH_{10}	0
	presomatic	1	HH_{10}	0
soma	soma	0.33	HH	3
central	postsomatic	1	HH_{10}	0
	internodes	0.0125	0.0125	80
	NoR	1	HH_{10}	0

On the one hand, the conductance in Table 3.2 is modelled by Hodgkin-Huxley channel dynamics, meaning that the conductances for the different ion channels are defined as: g_{Na}=120 mS/cm^2, g_K=36 mS/cm^2, g_L=0.3 mS/cm^2. The index 10 in HH_{10} indicates a faster channel dynamic for the simulation of active compartments, which is done by multiplying each conductance by a factor of 10. (Rattay et al., 2001b) On the other hand, the passive compartments were modelled with a constant conductance value depending on the number of myelin layers. The same thing holds true for the capacitance, since the capacitance is dependend on the number of myelin layers. N layers of myelin act as N capacitors in series leading to the fact that the capacitance becomes the N-th part of the capacitance of a single layer (Rattay et al., 2001b). Besides electric parameters of the fibers, also electric parameters of the intracellular and extracellular space must be defined, in each case a homogeneous medium was assumed. The resistivity of the axoplasm is commonly defined as $\rho_i = 50 - 200\ \Omega cm$ and the resistivity of the extracellular fluid is usually $\rho_e = 300\ \Omega cm$. (Rattay, 1990) For the simulation a value of $\rho_i = 50\ \Omega cm$ was chosen.

Now that all parameters were defined, a schematic drawing of the situation simulated is shown (see Figure 3.3). An electrode is located in a certain distance ($r = 150\ \mu m$) from the fiber, where the dendrite, the soma, and a small segment from the central axon are depicted in the figure, and stimulates it. Based on Figure 2.7 it is also possible to create an equivalent circuit for Figure 3.3, which builds the base for the whole simulation. Figure 3.4, which was taken from (Rattay et al., 2001b) but modified, shows the equivalent circuit for Figure 3.3, respectively to be more precise for four compartments of Figure 3.3, i.e. the presomatic region, the soma, the postsomatic region, and the first central internode. For a better understanding, it is advised to compare Figure 3.4 with equation 29 and equations 19-22. The

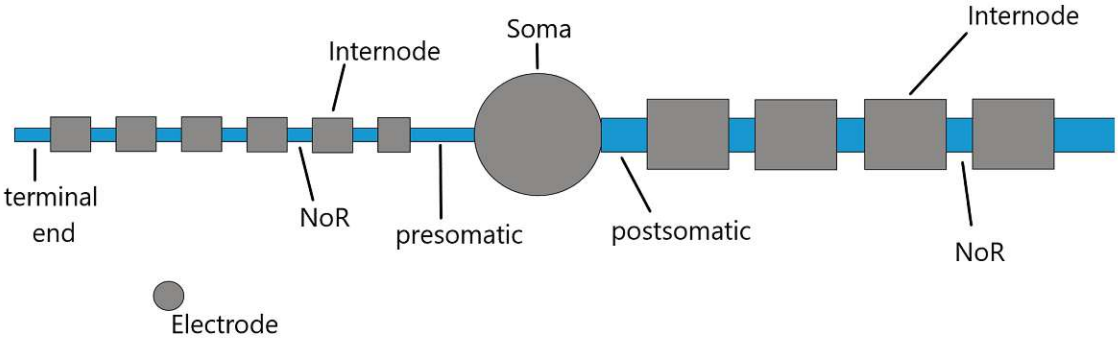

Figure 3.3: Schematic drawing of the situation simulated. Note that the drawing is not to scale. An electrode is located in a certain distance from the fiber and stimulates it. The fiber consists of the dendrite, the soma, and the central axon, including the postsomatic region, central NoR and central internodes.

$n-1$ and $n+1$ terms of equation 29 become more descriptive due to Figure 3.4 and represent the axial currents which flow from compartment n to the neighboring compartments $n-1$ and $n+1$.

To sum up, the simulation is mainly based on the equivalent circuit shown in Figure 3.4 and on the Hodgkin-Huxley equations 19-22. To solve the system of ordinary differential equations, the BE method (see chapter 2.3.3) was used and implemented in the code, which was written in Matlab (see chapter 3.2) and is shown in the Appendix.

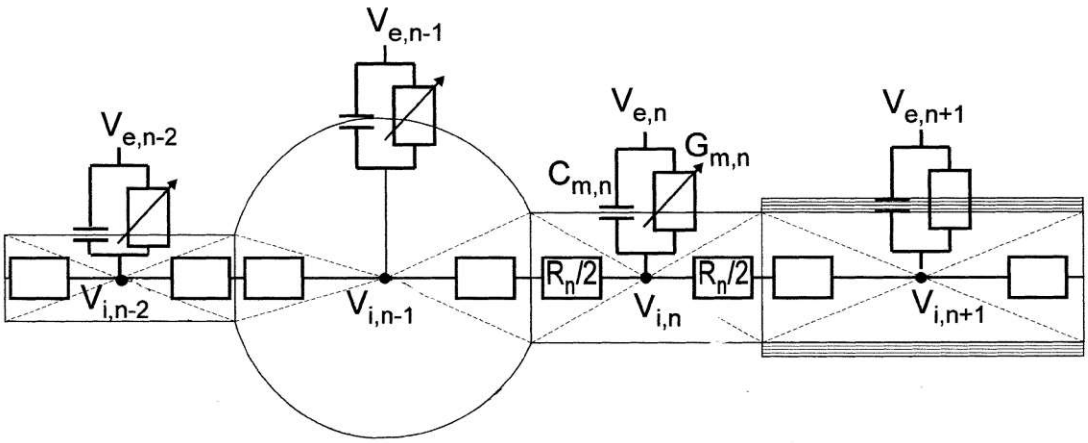

Figure 3.4: Equivalent circuit for the presomatic region, the soma, the postsomatic region, and the first central internode. The membrane of each compartment is simulated by a parallel circuit of a resistance and a capacitor. The axial resistances are also shown.(Modified from (Rattay et al., 2001b)

3.2 Software Packages Used

For this thesis two different software packages were used. To define, draw, and get the coordinates of the paths of the different nerve fibers and electrodes *CorelDraw Graphics Suite 2021* (Corel Corporation, Ottawa, ON, Canada) was used. The model was calculated, respectively implemented in MATLAB *R2021b* (The MathWorks, Inc., Natick, MA, USA).

3.3 Workflow

To give the reader a better overview of this thesis, this chapter summarizes the workflow. The first step was to define the fiber paths and the eletrode locations in a microphotograph. To get the coordinates of the compartment centers of the fibers and the center coordinates of the electrodes, the microphotograph was overlaid with a cartesian coordinate system. The coordinate system was scaled in 10 μm steps in vertical and horizontal direction. A smaller step size was tried to achieve, but was not possible, due to limitations - concerning clear arrangement- of the software used. It should be mentioned that the coordinates had to be converted to compensate for the initial scale of the microphotograph itself. Then, the coordinates were imported into Matlab. The code written is shown in the Appendix. The code works as follows: At first the geometric and electrical parameters were defined and then the Hodgkin-Huxley equations were solved using the BE method. Every simulation was possible to conduct with any of the seven electrodes per fiber, since it was possible to switch between the electrodes. Also, it was possible to simulate a degenerated nerve fiber, because in the code the possibility to cut-off the dendrite was implemented. To find the anodic and cathodic thresholds, (see chapter 4) a function (see Appendix) was written, which is based on a binary search algorithm. The current amplitude was doubled and halved until the value, where an AP was first elicited was found. For this, the AP had to be defined. If the membrane voltage was greater than -40 mV (Raghavan et al., 2019), it was called an AP. Finally, the results were depicted graphically and analyzed.

4 Results

This chapter covers the results of this thesis, which are the outcome of the simulation. Before the results of each fiber, which are the comparison between the ST and SV behavior for a physiological fiber and the equivalent comparison for a pathophysiological (degenerated) fiber, are stated, the electric field generated by an electrode is presented.

4.1 Electric Field

The electric field generated by a stimulating electrode is exemplarily shown in Figure 4.1 for electrode T4. A current pulse of 1 mA was applied for 0.1 ms. The electric field is depicted via equipotential lines and the values of the activating function are also inserted in Figure 4.1, which is depicted on the next page.

4.2 Fiber 1

The following chapters 4.2 - 4.5 are subdivided into the excitation of a physiological fiber and the excitation of a degenerated fiber.

4.2.1 Physiological Fiber

The threshold values for anodic and cathodic extracellular stimulation for the electrodes located in the ST and SV are shown in Table 4.1. The pulse duration was set to 0.1 ms each time. As mentioned in chapter 3.1.2, the electrode positions in the ST and SV correspond to each other, with electrode T1 at the beginning of the fiber being the exception of this rule. Thus, the corresponding electrodes are listed next to each other in Table 4.1.

Compartment	f [mV/ms]
terminal	1358.76
I-1	-1379.22
NoR-1	-4330.34
I-2	-1308.04
NoR-2	-1316.63
I-3	48.49
NoR-3	829.28
I-4	934.62
NoR-4	4418.76
I-5	195.47
Pre-1	-40.86
Pre-2	-19.54
Pre-3	-12.44
Soma	-34.5
Post	-679.4
I-1	-975.98
NoR-1	-503.96
I-2	215.42
NoR-2	786.04
I-3	290.26
NoR-3	586.55
I-4	183.83
NoR-4	352.85
I-5	110.3
NoR-5	240.56

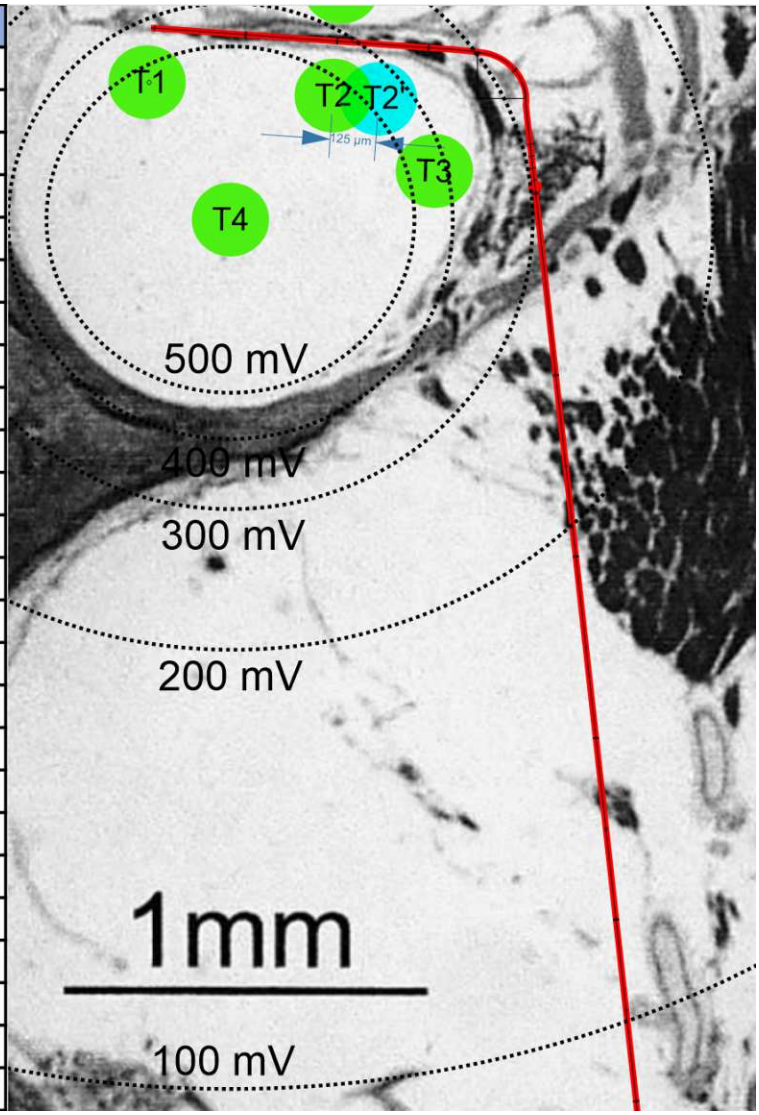

Figure 4.1: The electric field generated by electrode T4 is shown. The equipotential lines are drawn for 500 mV, 400 mV, 300 mV, 200 mV, and 100 mV. The table inserted shows the values of the activating function in [mV/ms] for each compartment in the figure detail. A current pulse of 1 mA for 0.1 ms was applied to electrode T4.

Table 4.1: The threshold values for anodic and cathodic stimulation are listed for each electrode. The pulse duration was set to 0.1 ms. The corresponding electrodes of the ST and the SV are listed next to each other. Electrode T2' is electrode T2, but moved by 125 μm to medial.

Fiber 1	Scala Tympani		Fiber 1	Scala Vestibuli	
Electrode	Anodic Threshold [µA]	Cathodic Threshold [µA]	Electrode	Anodic Threshold [µA]	Cathodic Threshold [µA]
T1	74.71	-22.5	-	-	-
T2	44.7	-23.1	V1	45.15	-22.8
T3	84.56	-163.52	V2	78.61	-43.5
T4	492.19	-259.98	V3	190.97	-147.31
T2'	46.65	-37.2	-	-	-

In Figure 4.2, the propagating AP along the fiber is shown for each electrode of Fiber 1. In each case, the anodic threshold value from Table 4.1 was used. Again, the corresponding electrodes of the ST and SV are plotted next to each other. However, due to space limitations, electrode T2' of the ST was plotted in the same line as T1. Each plot shows the propagating AP along the same Fiber 1, but the electrode activated was different. The x-axis gives the time in [ms], and the y-axis represents the compartments of the fiber, i.e. each horzontal line per plot represents a compartment. The pulse is also indicated in each plot.

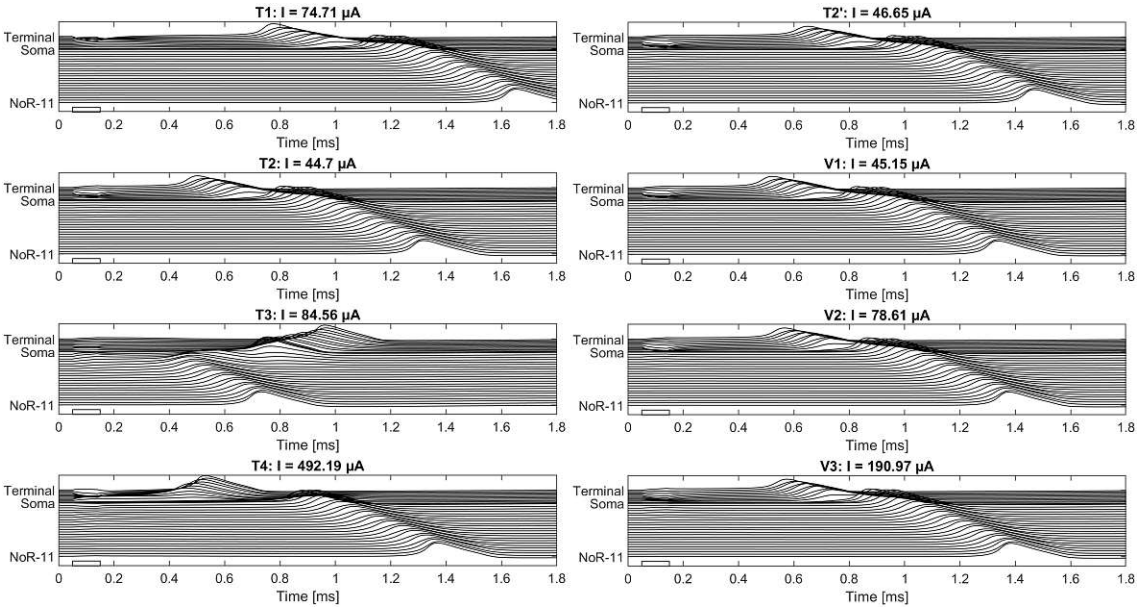

Figure 4.2: Anodic threshold stimulation of Fiber 1. Each electrode current was chosen according to Table 4.1. The pulse duration was set to 0.1 ms. The propagating APs along the fiber are shown for each electrode. Every line in each subplot corresponds to a compartment of the fiber.

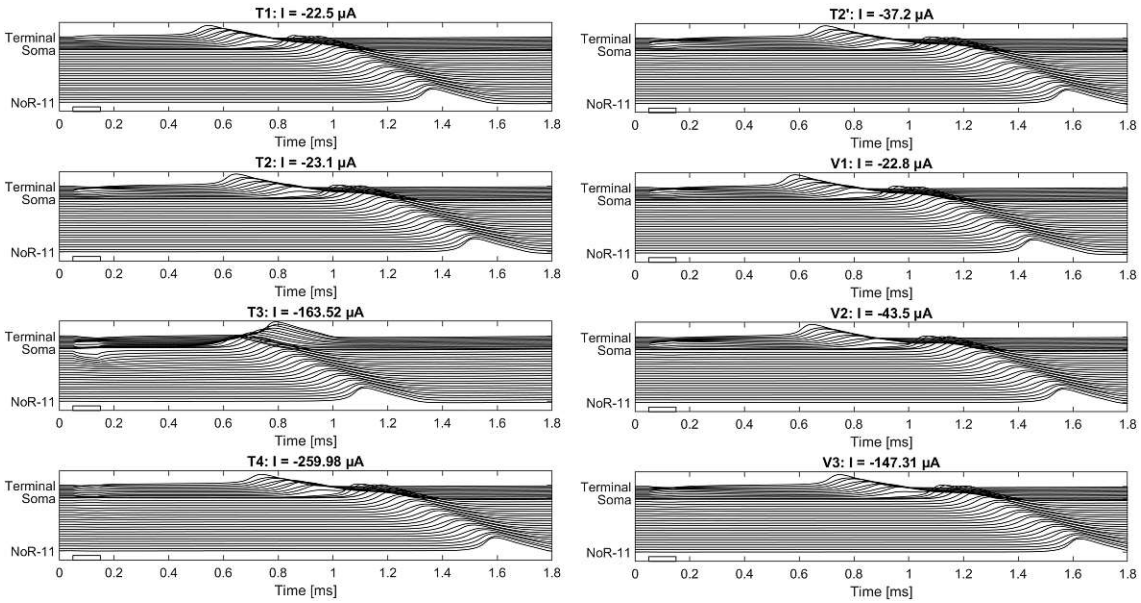

Figure 4.3: Cathodic threshold stimulation of Fiber 1. The electrode current was chosen according to Table 4.1. The pulse duration was 0.1 ms. Each line of every subplot corresponds to a compartment of Fiber 1.

Figure 4.3 shows the cathodic threshold stimulation of Fiber 1. The threshold values were taken from Table 4.1. The extracellular potential was also analyzed, which is shown in Figure 4.4. For consistency reasons, the current amplitude was set to the threshold values of the anodic stimulation.

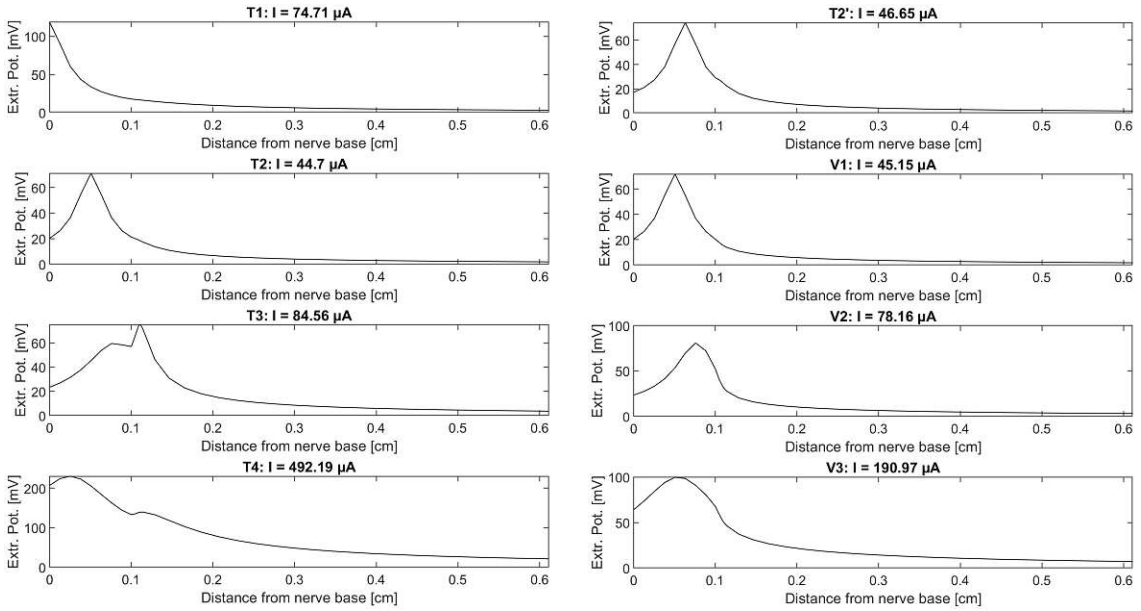

Figure 4.4: Extracellular potential of Fiber 1. The current was chosen according to the anodic threshold values of Table 4.1. The nerve base is the compartment center of the terminal end. The shortest distance from the other compartment centers to that one was measured (=x-axis).

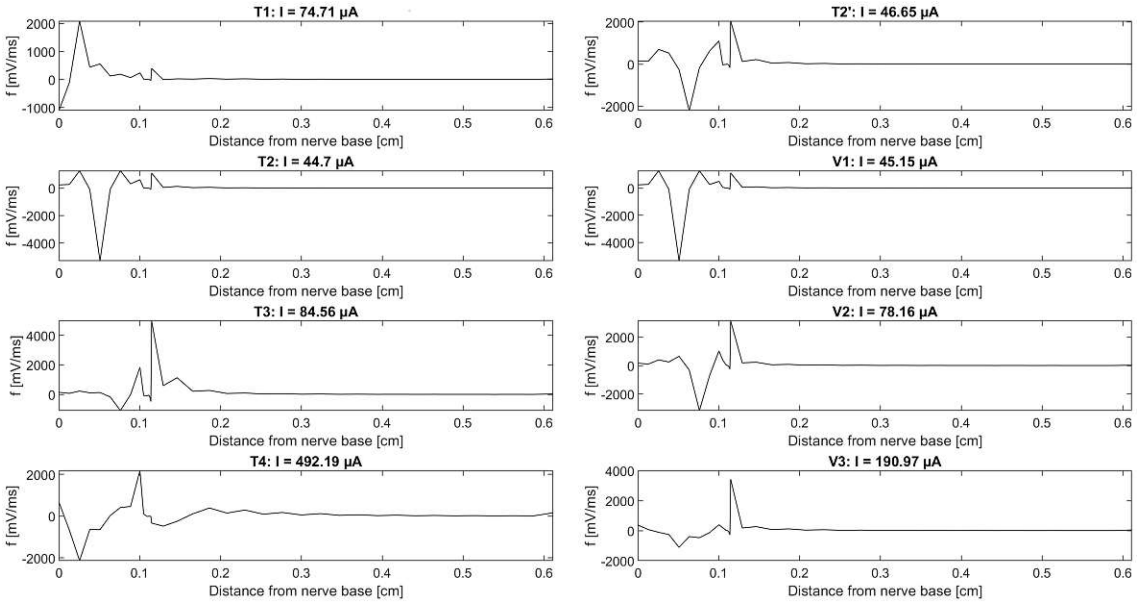

Figure 4.5: Activating function (f) for each electrode of Fiber 1 for anodic stimulation. The shortest distance from the other compartment centers to that one was measured (=x-axis).

The activating function f, which is the second derivative of Figure 4.4, is shown in Figure 4.5. The extracellular potential and the activating function were also computed for cathodic stimulation. Figure 4.6 shows the extracellular potential for cathodic stimulation of Fiber 1.

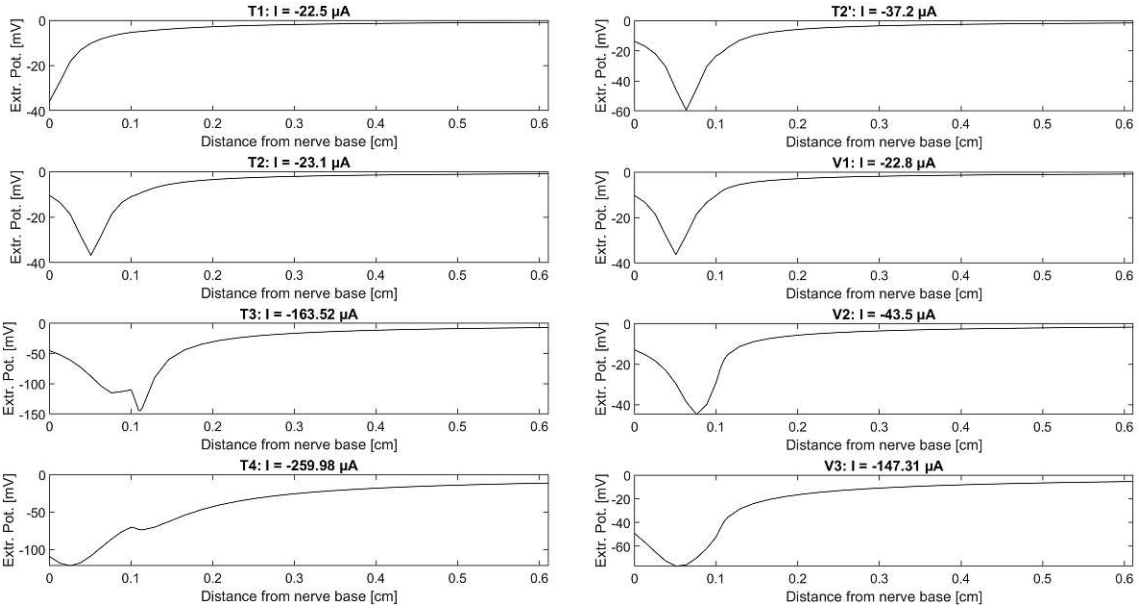

Figure 4.6: Extracellular potential upon cathodic stimulation of Fiber 1. The shortest distance from the other compartment centers to that one was measured (=x-axis).

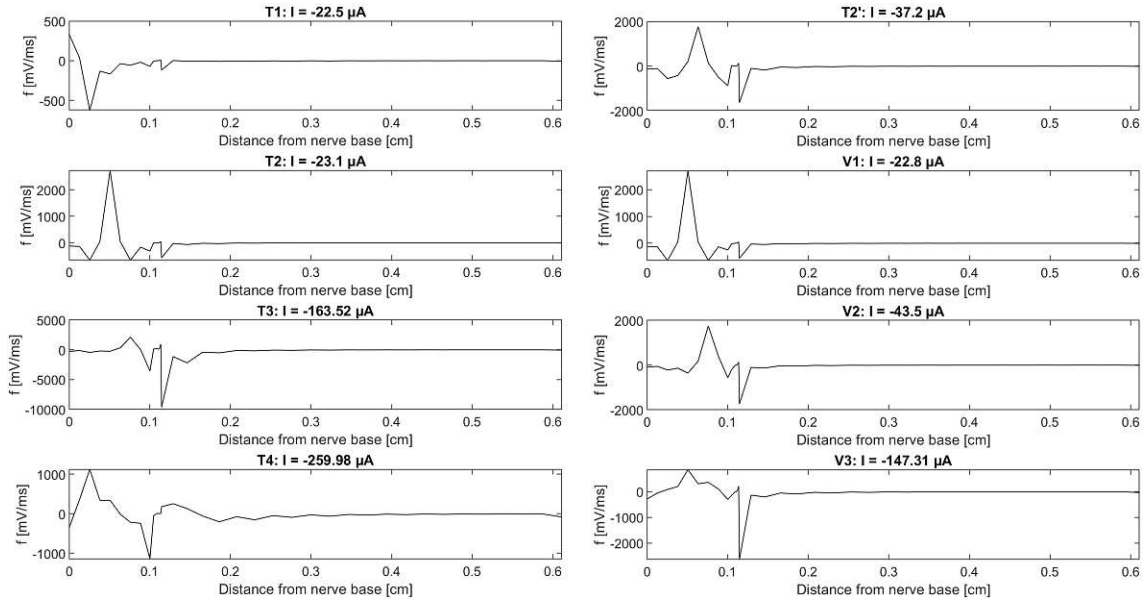

Figure 4.7: Activating function upon cathodic stimulation of Fiber 1. It is the second derivative of Figure 4.6.

Figure 4.7 shows the activating function for cathodic stimulation of Fiber 1. Up to now, all plots presented refer to a physiological fiber, but it is also possible to generate these plots for a degenerated fiber (see chapter 4.2.2).

4.2.2 Degenerated Fiber

As mentioned in chapter 3.3, the degenerated fiber was simulated by cutting off the dendrite, but the electrode positions and the workflow of the simulation were left unchanged. The computations conducted for the physiological fiber were also done for the degenerated fiber and are presented in this section of the thesis, respectively in the subsections of the other three fibers. In Table 4.2 the anodic and cathodic thresholds for Fiber 1 are listed. Due to stimulation artefacts coming from the higher current amplitudes, the level for defining an AP was raised from -40 mV (see chapter 3.3) to 20 mV. The program for finding the thresholds is attached in the Appendix.

Table 4.2: Threshold values for anodic and cathodic stimulation of the degenerated Fiber 1. The pulse duration was set to 0.1 ms. The corresponding electrodes of the ST and the SV are listed next to each other. Electrode T2' is electrode T2, but moved by 125 μm to medial.

Fiber 1	Scala Tympani		Fiber 1	Scala Vestibuli	
Electrode	Anodic Threshold [µA]	Cathodic Threshold [µA]	Electrode	Anodic Threshold [µA]	Cathodic Threshold [µA]
T1	1053.86	-1156.77	-	-	-
T2	307.03	-425.59	V1	406.64	-554.11
T3	87.31	-147.76	V2	297.33	-435.34
T4	731.47	-916.29	V3	585.76	-761.78
T2'	205.17	-307.48	-	-	-

Figure 4.8 shows the propagating AP for anodic threshold stimulation of the degenerated Fiber 1. Again, each line per plot represents one compartment of the fiber; however, in contrast to the physiological fiber the first compartment is now the soma of the fiber. The current values were taken from Table 4.2 and the pulse duration was again set to 0.1 ms.

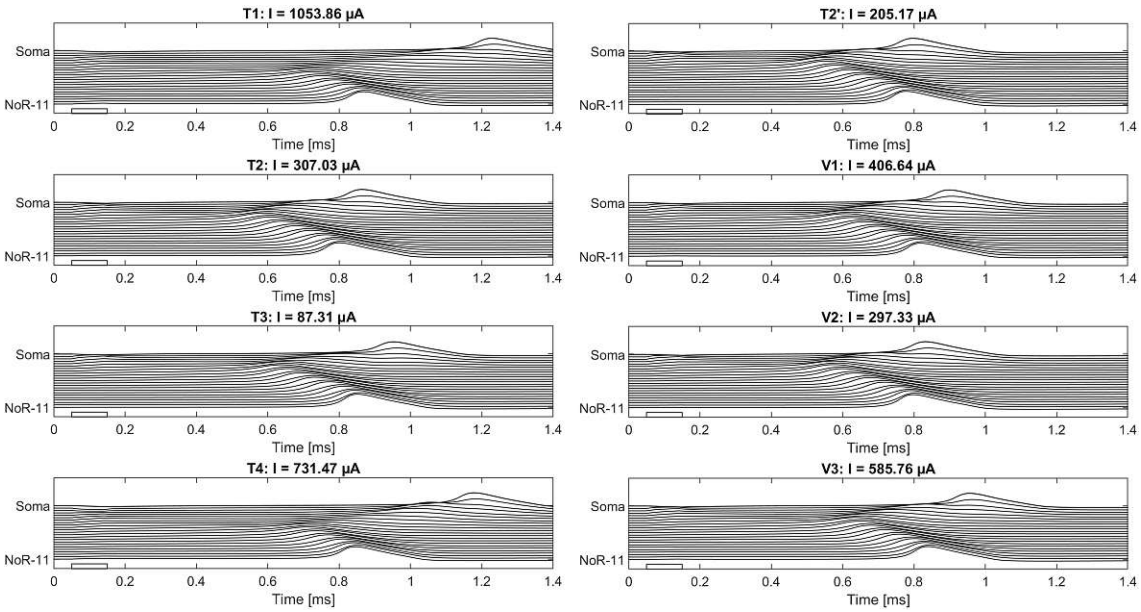

Figure 4.8: Anodic threshold stimulation for the degenerated Fiber 1, which was simulated by cutting-off the dendrite. The propagating APs along the fiber are shown. The threshold values were taken from Table 4.2.

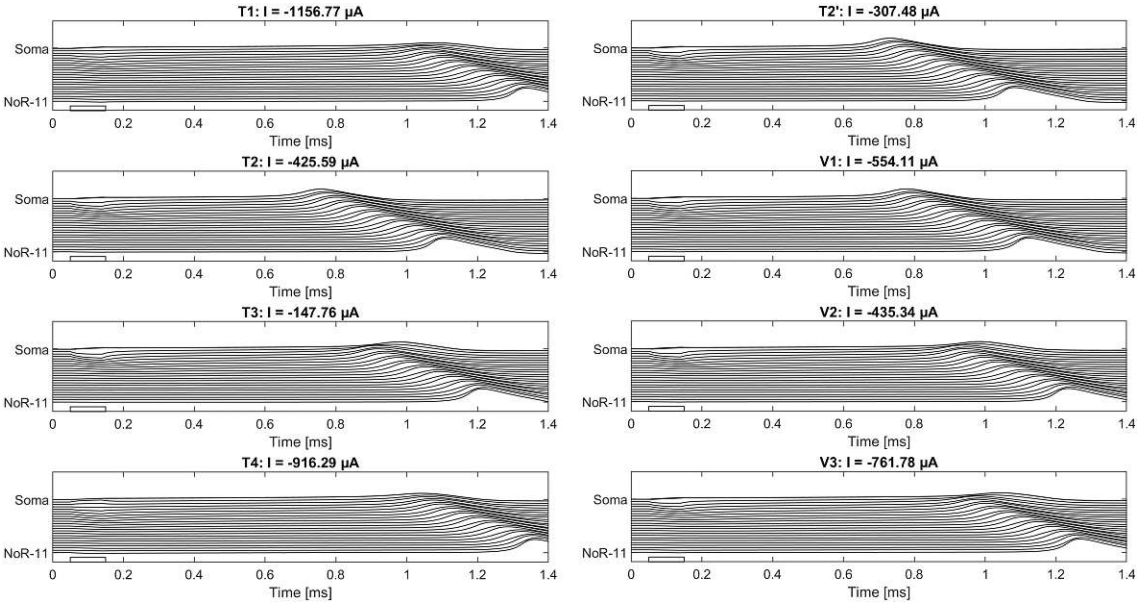

Figure 4.9: Cathodic threshold stimulation for the degenerated Fiber 1. Electrodes T1-T4, V1-V3, and T2' stimulated the Fiber 1, each resulting AP is propagating along the fiber shown in the corresponding subplot.

The results of stimulating the degenerated Fiber 1 with a cathodic current pulse are depicted in the subplots of Figure 4.9. The extracellular potential and the activating function were also computed for the anodic as well as for the cathodic case. Figure 4.10 shows the extracellular potential for anodic threshold stimulation.

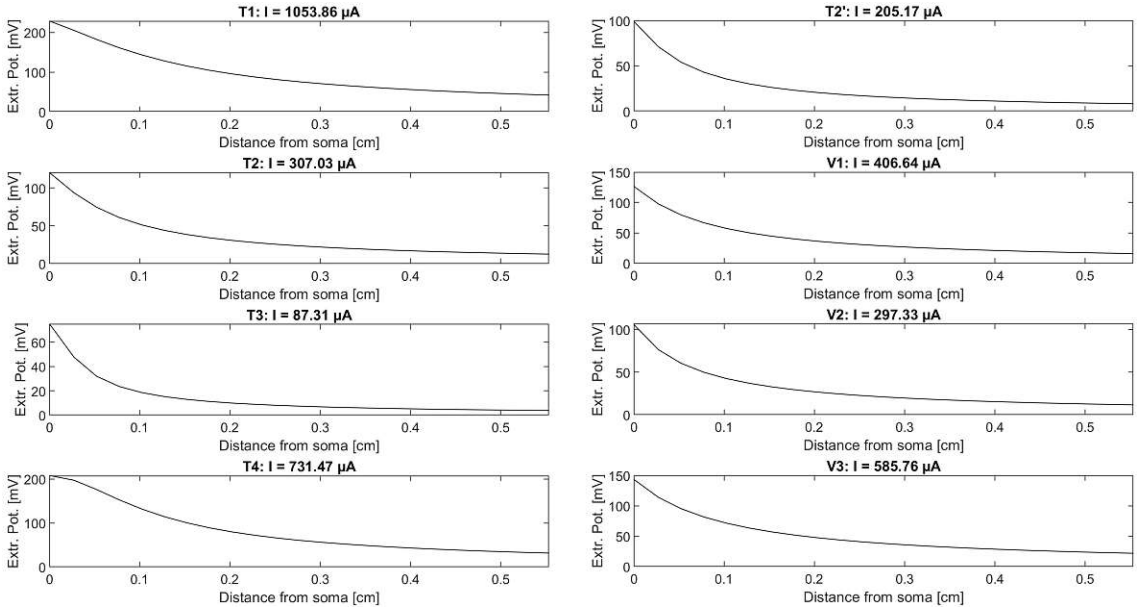

Figure 4.10: Extracellular potential for anodic threshold stimulation of the degenerated Fiber 1. Each subplot shows the extracellular potential resulting from a different electrode.

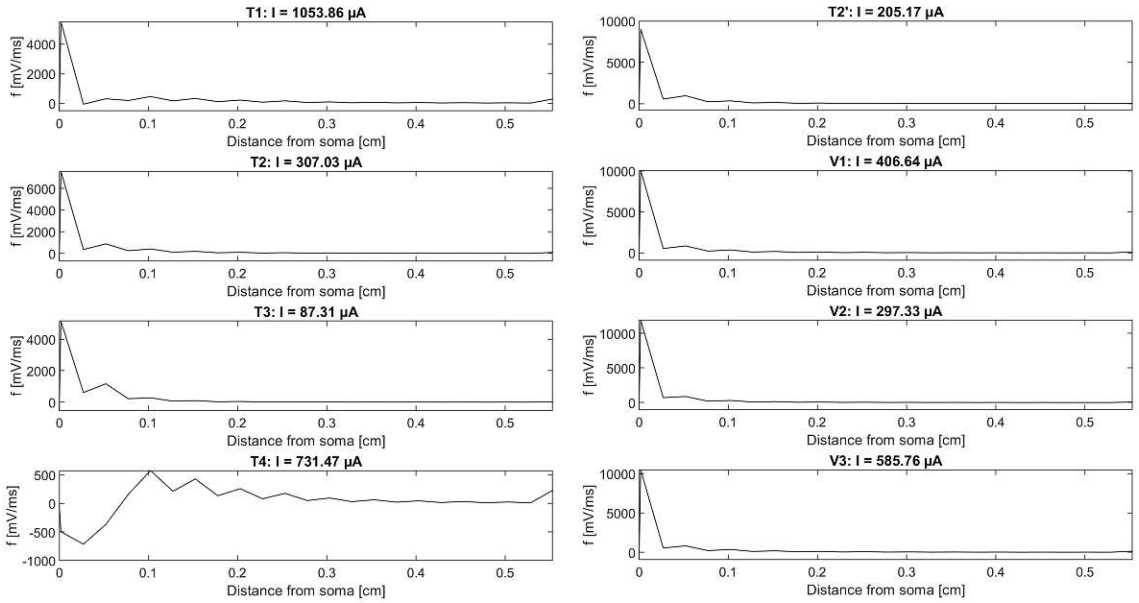

Figure 4.11: Activating function for anodic threshold stimulation of the degenerated Fiber 1. It can be seen as the second derivative of Figure 4.10.

Figure 4.11 depicts the activating function resulting from anodic threshold stimulation of Fiber 1. The extracellular potential and the activating function were also calculated for cathodic threshold stimulation. Figure 4.12 shows the extracellular potential and Figure 4.13 the activating function.

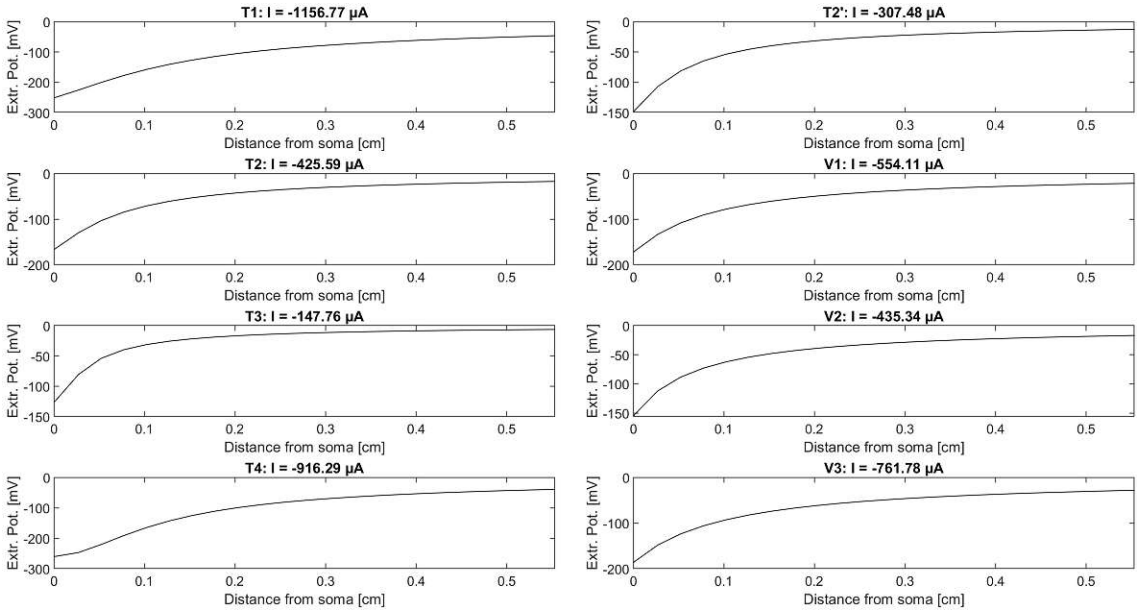

Figure 4.12: Extracellular potential resulting from cathodic threshold stimulation of the degenerated Fiber 1. Each subplot shows the extracellular potential resulting from a different electrode.

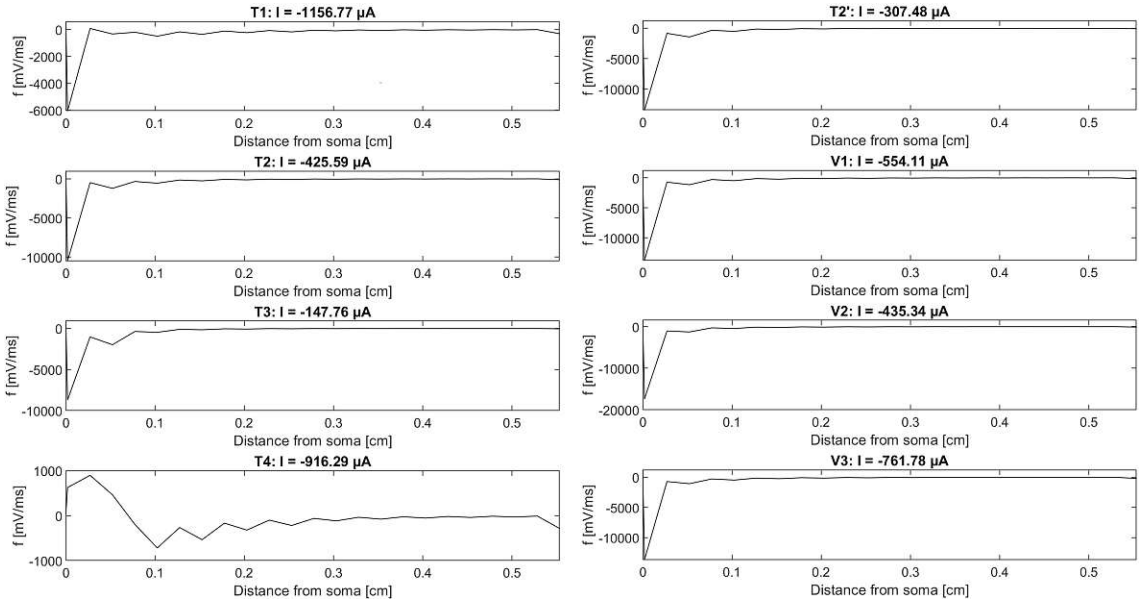

Figure 4.13: Activating function of degenerated Fiber 1 upon cathodic threshold stimulation. Each subplot represents a different electrode of Fiber 1.

4.3 Fiber 2

4.3.1 Physiological Fiber

The computations done for Fiber 1 were also conducted for Fiber 2. The threshold values for anodic and cathodic stimulation are shown in Table 4.3. Each line in the table represents the corresponding electrodes of the ST and SV.

Table 4.3: Threshold values for anodic and cathodic stimulation of Fiber 2. The pulse duration was set to 0.1 ms. The corresponding electrodes of the ST and the SV are listed next to each other.

Fiber 2	Scala Tympani		Fiber 2	Scala Vestibuli	
Electrode	Anodic Threshold [µA]	Cathodic Threshold [µA]	Electrode	Anodic Threshold [µA]	Cathodic Threshold [µA]
T5	71.11	-22.5	-	-	-
T6	44.25	-23.1	V4	44.7	-22.8
T7	70.4	-87.31	V5	56.56	-22.8
T8	114.31	-167.87	V6	182.27	-132.01

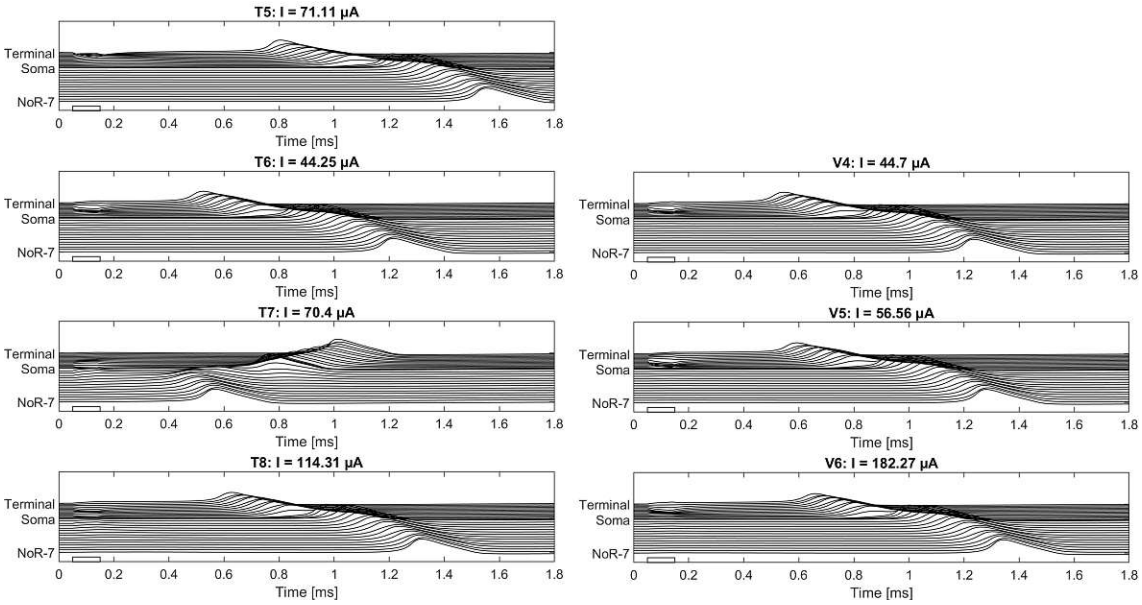

Figure 4.14: Propagation of APs elicited by anodic stimulation of the different electrodes. The threshold values were taken from Table 4.3 and the pulse duration was set to 0.1 ms.

Figure 4.14 shows the APs, elicited by the anodic stimulation of different electrodes, propagating along Fiber 2. The pulse duration was set to 0.1 ms. In contrast, Figure 4.15 shows the cathodic case of the same situation.

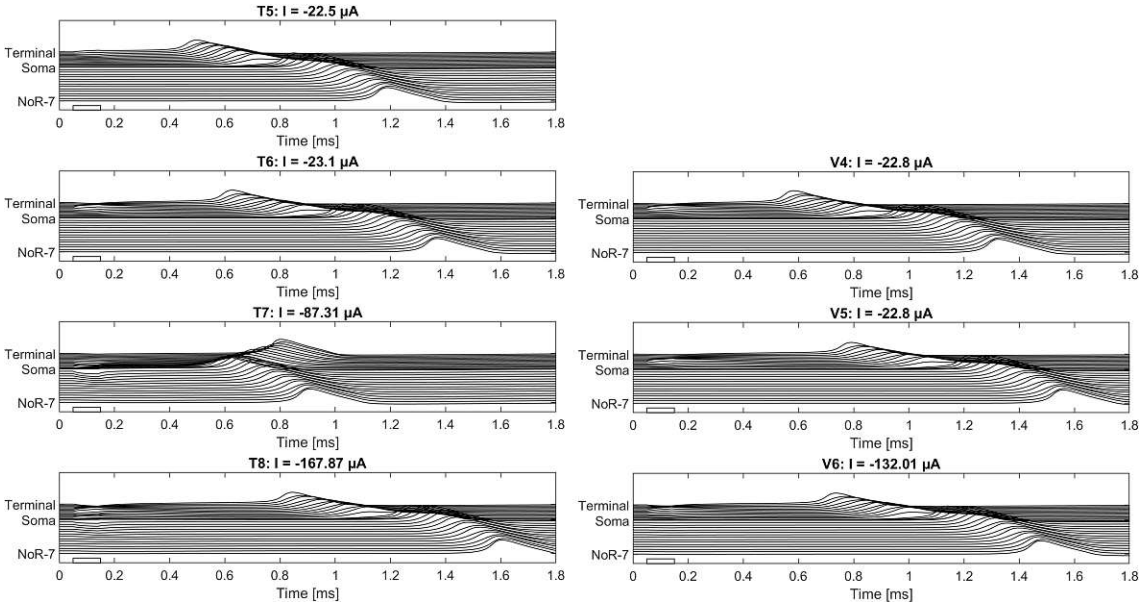

Figure 4.15: Each subplot shows the propagation of an AP upon cathodic stimulation with the stated electrode. Each line in each subplot corresponds to a compartment of the fiber. The stimulus (dur: 0.1 ms) is also indicated in each subplot.

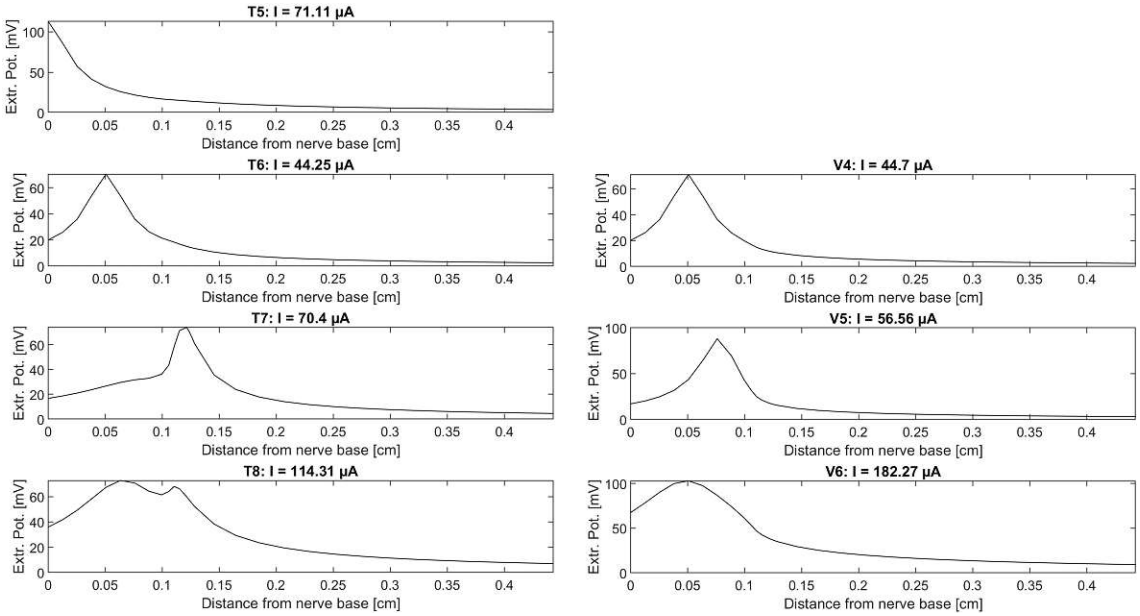

Figure 4.16: Extracellular potential during anodic stimulation of Fiber 2 with different electrodes, shown in the subplots. The x-axis gives the shortest distance in [cm] from the terminal end.

It is again possible to take a look at the extracellular potential and the activating function. Figure 4.16 shows the extracellular potential for the anodic case, while Figure 4.17 depicts the activating function.

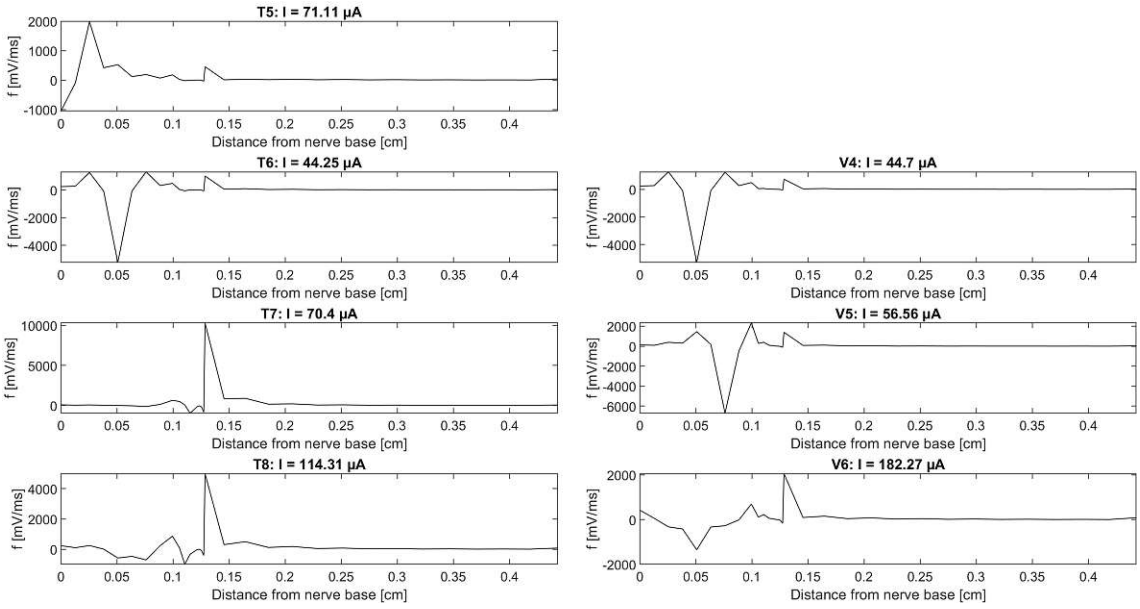

Figure 4.17: Activating function representing the second derivative of Figure 4.16. In each subplot another electrode is active resulting in different stimulation behavior.

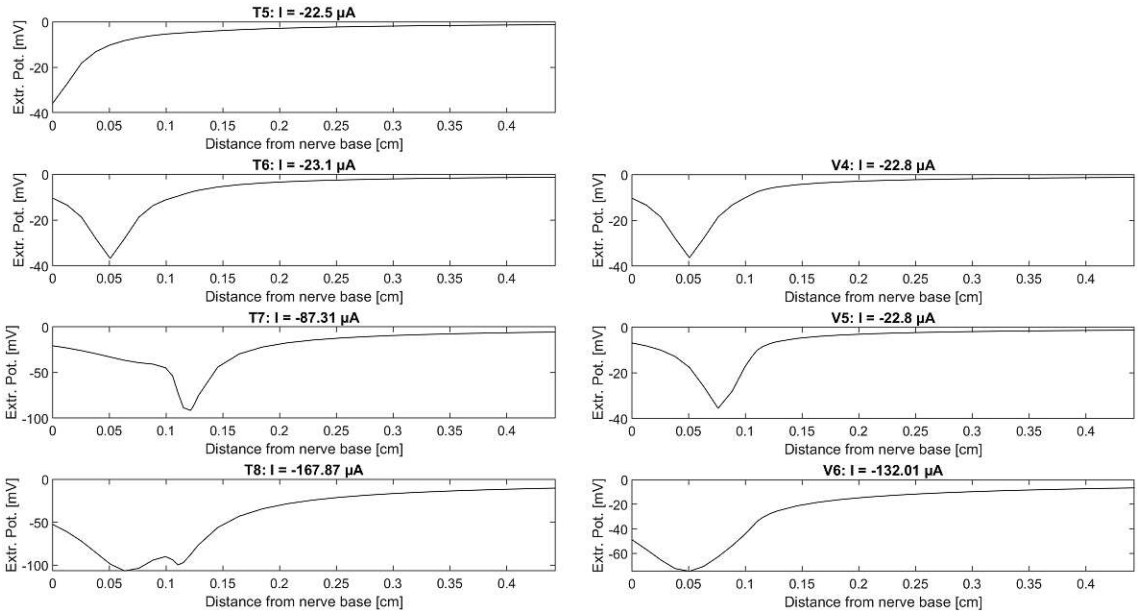

Figure 4.18: Extracellular potential generated by the electrodes T5-T8 and V4-V6 by cathodic stimulation. Again, the x-axis gives the shortest distance from the terminal end of the dendrite.

Figure 4.18 and Figure 4.19 show the extracellular potential and the activating function for cathodic stimulation of Fiber 2. Each subplot corresponds to another electrode that is active. Also, such as in the other figures, the left side of the figures corresponds to the ST and the right side to the SV.

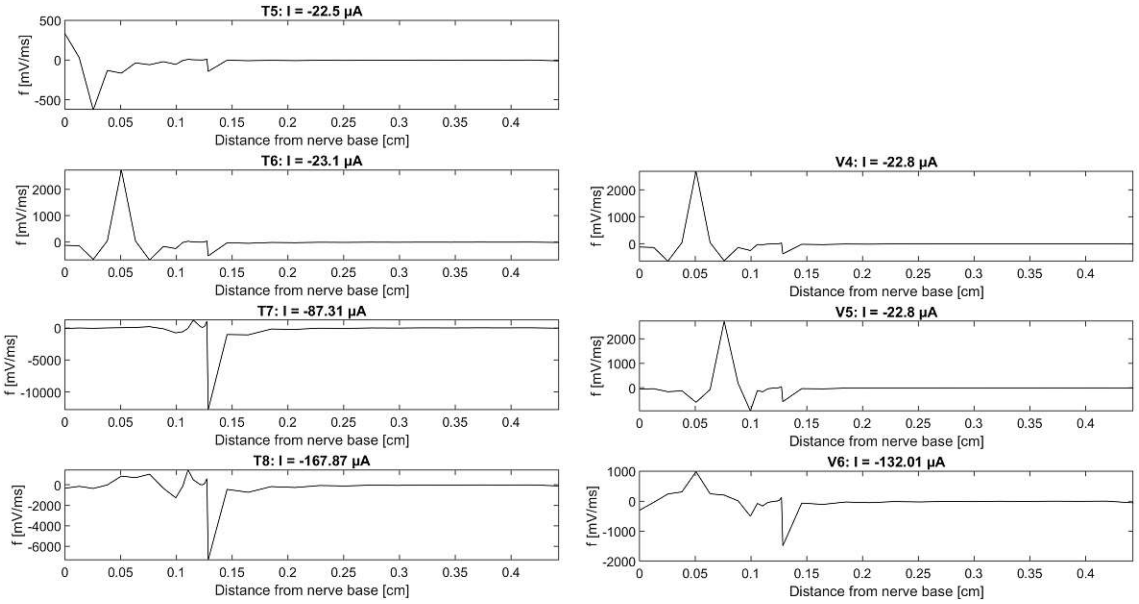

Figure 4.19: Activating function upon cathodic stimulation of Fiber 2 by different electrodes, given in the subplots. It can be seen as the second derivative of Figure 4.18.

4.3.2 Degenerated Fiber

Fiber 2 was also simulated as degenerated fiber. Thus, the dendrite was cut off and only the soma-axon combination was considered. In Table 4.4 the threshold values for anodic and cathodic stimulation are listed.

Table 4.4: Threshold values for anodic and cathodic stimulation of the degenerated Fiber 2. The pulse duration was set to 0.1 ms. The corresponding electrodes of the ST and the SV are listed next to each other.

Fiber 2	Scala Tympani		Fiber 2	Scala Vestibuli	
Electrode	Anodic Threshold [µA]	Cathodic Threshold [µA]	Electrode	Anodic Threshold [µA]	Cathodic Threshold [µA]
T5	798.98	-1249.62	-	-	-
T6	403.99	-568.11	V4	578.46	-792.83
T7	76.07	-133.06	V5	438.19	-621.51
T8	212.87	-321.63	V6	795.23	-1085.36

For anodic threshold stimulation of the degenrated Fiber 2, the AP propagation for each electrode is depicted in Figure 4.20.

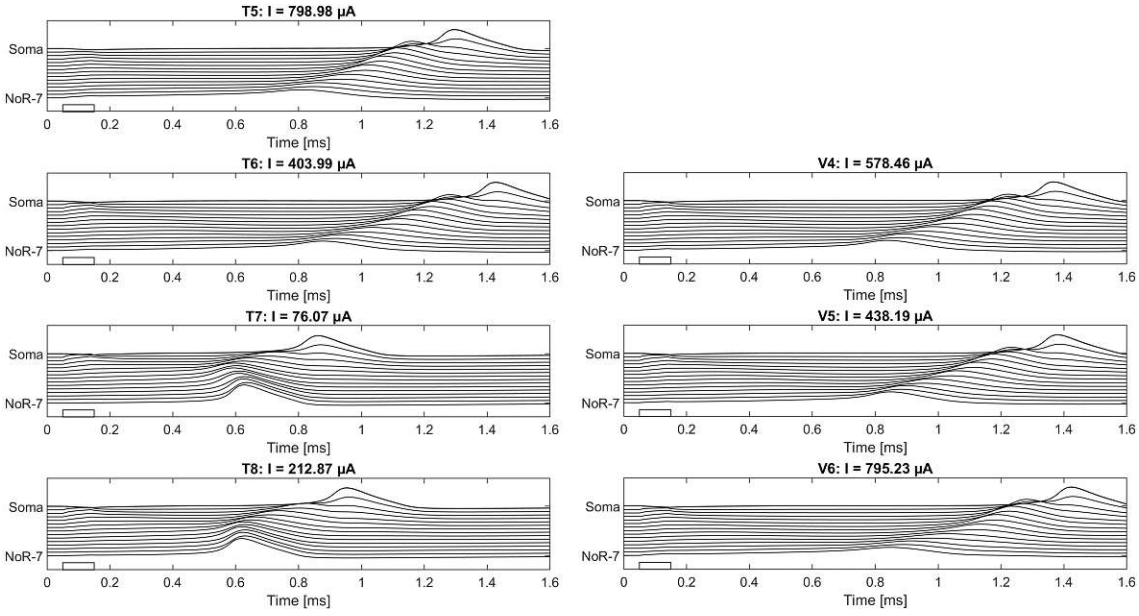

Figure 4.20: Anodic threshold stimulation for the degenerated Fiber 2. Threshold values were taken from Table 4.4. Each compartment is represented by one line in each subplot.

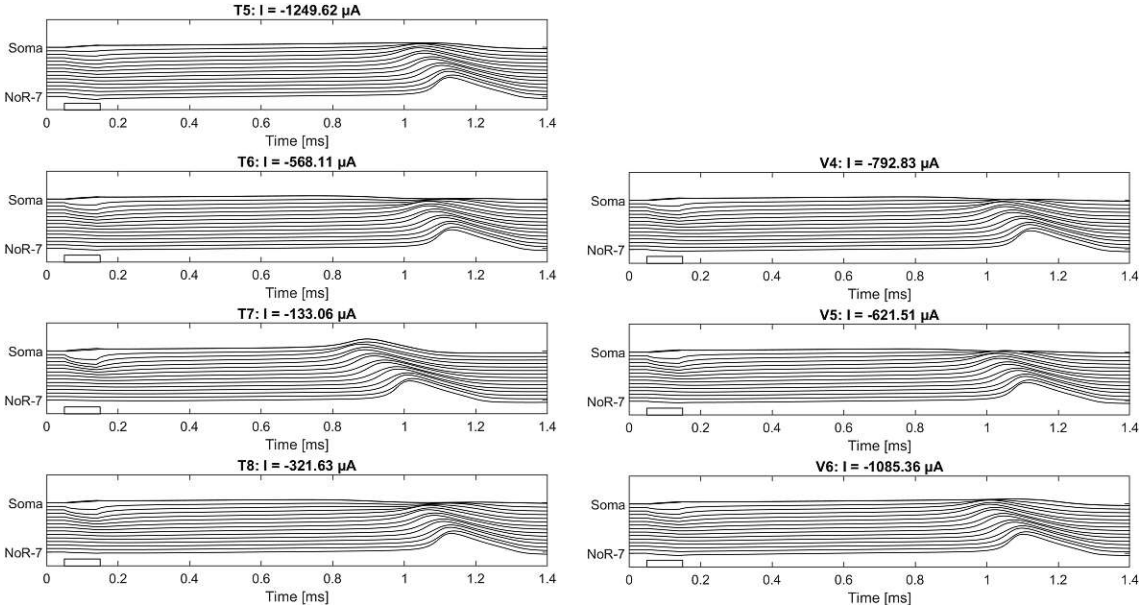

Figure 4.21: Cathodic threshold stimulation of degenerated Fiber 2. Threshold values were taken from Table 4.4. Each compartment is represented by one line in each subplot.

Figure 4.21 illustrates the propagation of the APs for cathodic stimulation of the degenerated Fiber 2. The extracellular potential and activating function for anodic and cathodic stimulation were analyzed as well. Figure 4.22 shows the extracellular potential for anodic threshold stimulation of the degenerated Fiber 2.

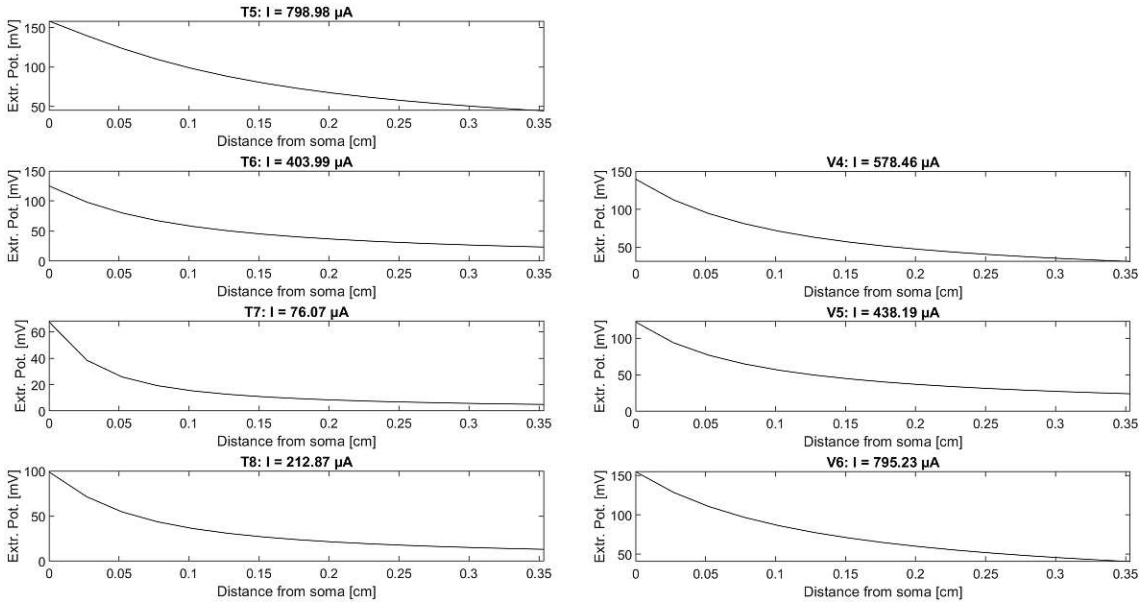

Figure 4.22: Extracellular potential upon anodic stimulation of the degenerated Fiber 2. The x-axis shows the shortest distance away from the soma.

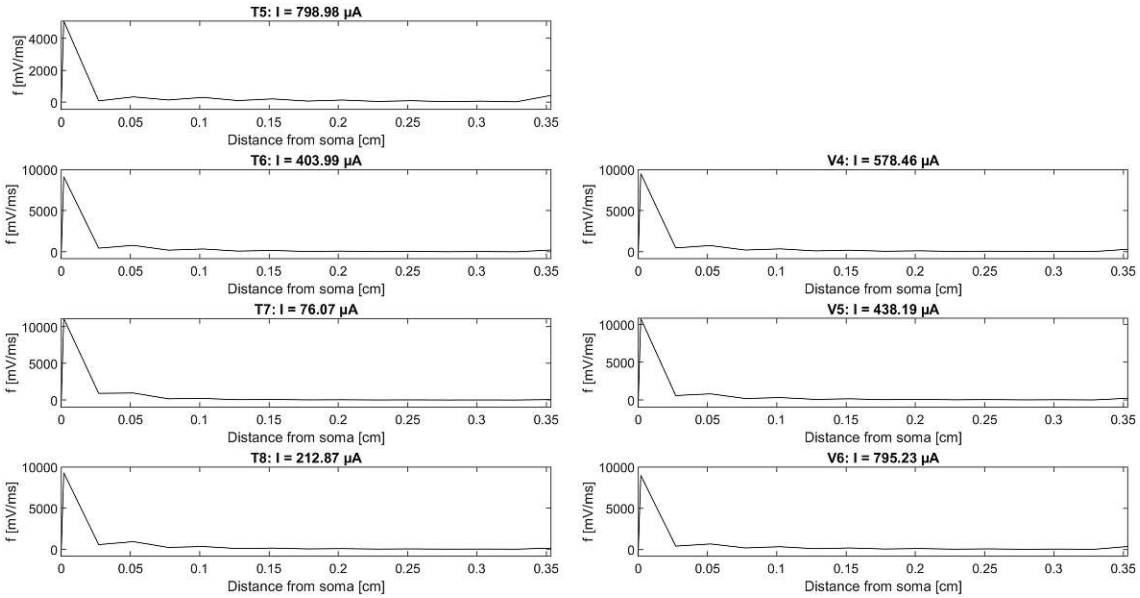

Figure 4.23: Activating function of degenerated Fiber 2 upon anodic threshold stimulation. It can be thought of as the second derivative of Figure 4.22.

The activating function for the anodic stimulation of the degenerated Fiber 2 is shown in Figure 4.23. The extracellular potential and activating function for cathodic stimulation of the degenerated Fiber 2 are shown in Figure 4.24 and Figure 4.25.

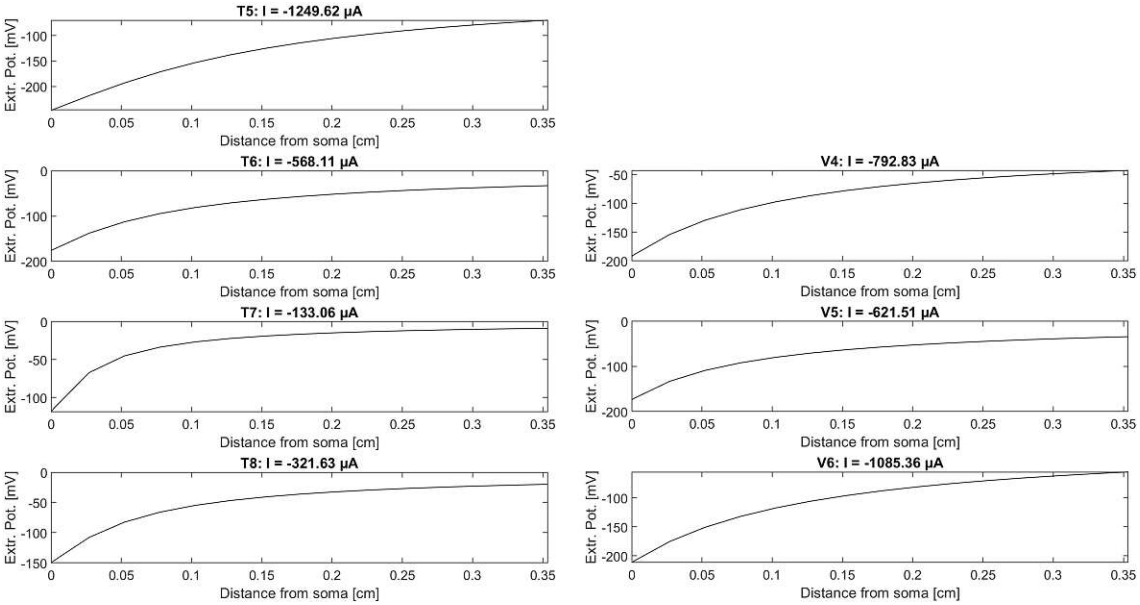

Figure 4.24: Extracellular potential upon cathodic stimulation of Fiber 2, which was simulated as degenerated by cutting-off the dendrite. Each subplot shows the extracellular potential for another electrode.

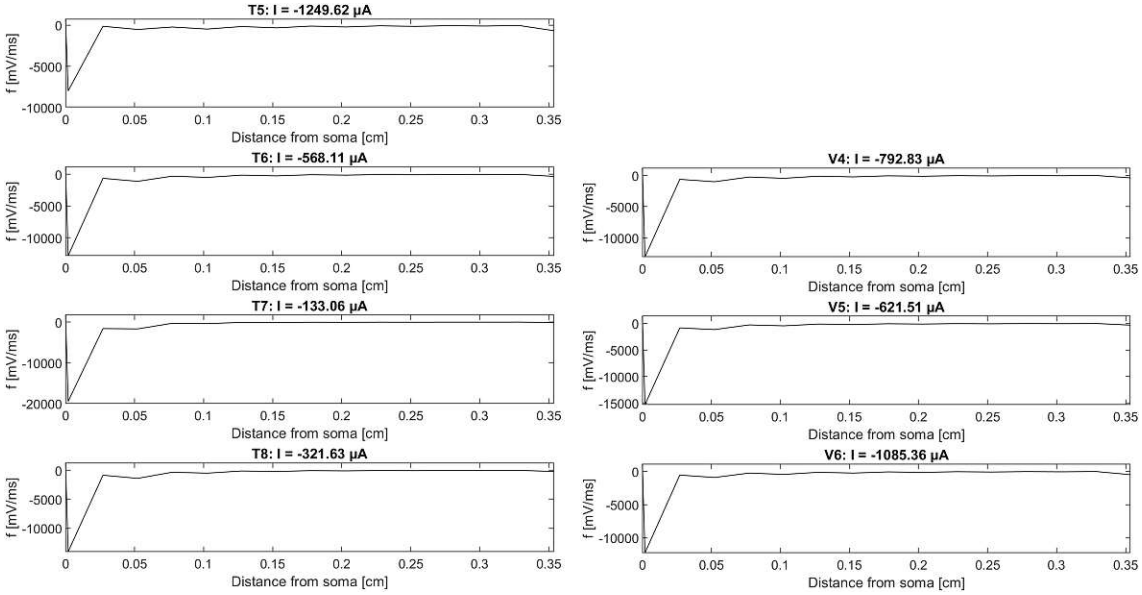

Figure 4.25: Activating function of degenerated Fiber 2 upon cathodic threshold stimulation. Each subplot represents another electrode, which was active during stimulation, while the others were inactivated.

4.4 Fiber 3

4.4.1 Physiological Fiber

The course of the third fiber is shown in Figure 3.2 together with the other fibers. Fiber 3 was stimulated with anodic and cathodic pulses for 0.1 ms. The threshold

Table 4.5: Threshold values for anodic and cathodic stimulation of Fiber 3. The pulse duration was set to 0.1 ms. The corresponding electrodes of the ST and the SV are listed next to each other.

Fiber 3	Scala Tympani		Fiber 3	Scala Vestibuli	
Electrode	Anodic Threshold [µA]	Cathodic Threshold [µA]	Electrode	Anodic Threshold [µA]	Cathodic Threshold [µA]
T9	70.96	-22.5	-	-	-
T10	44.25	-23.1	V7	44.85	-22.65
T11	99.56	-128.85	V8	71.56	-40.35
T12	131.71	-140.55	V9	176.72	-120.76

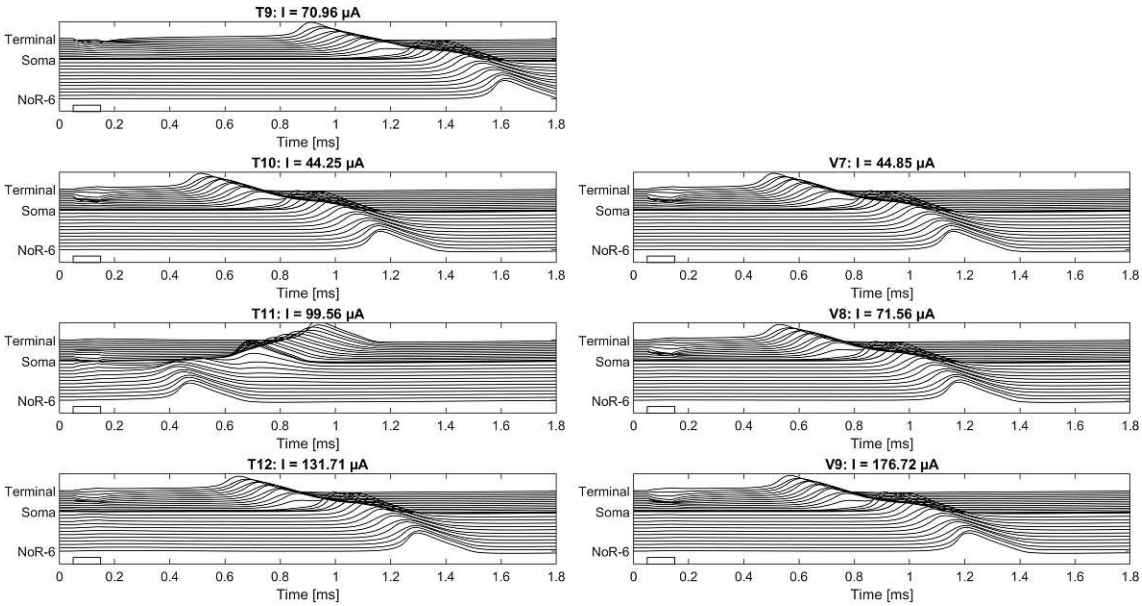

Figure 4.26: AP propagation along the fiber upon anodic threshold stimulation. Each subplot represents the excitation resulting from one specific electrode.

values are shown in Table 4.5. Based on these values, Figure 4.26 and Figure 4.27 were made. Figure 4.26 shows the AP propagation along the fiber upon anodic threshold stimulation, whereas Figure 4.27 shows the cathodic case.

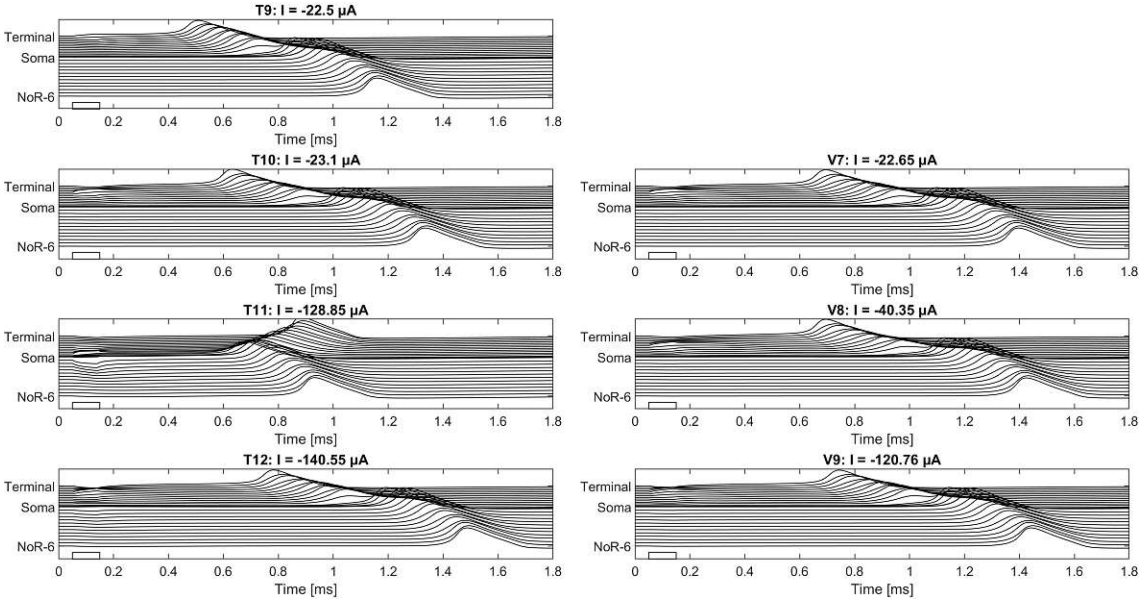

Figure 4.27: Cathodic threshold stimulation of Fiber 3. Different electrode positions of the ST and SV are compared by plotting the electrodes of equivalent position next to each other.

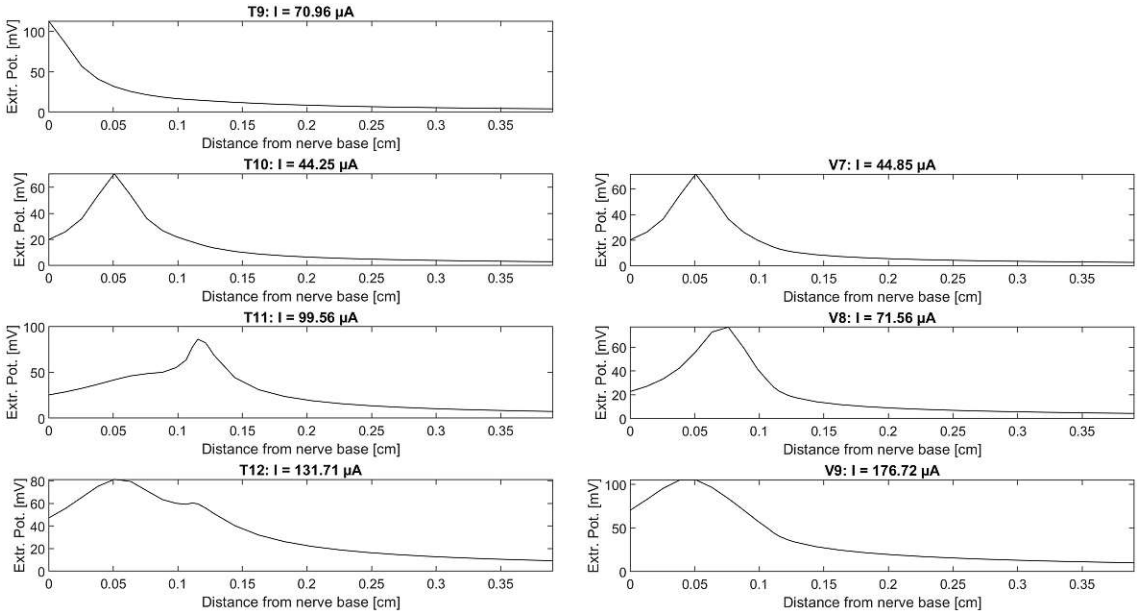

Figure 4.28: Extracellular potential resulting from anodic threshold stimulation of Fiber 3. The left subplots show the ST electrodes, the subplots shown on the right represnt the SV electrodes.

The extracellular potential and the activating function were also computed. The extracellular potential resulting from anodic stimulation with different electrodes is shown in Figure 4.28. The activating function is shown below in Figure 4.29.

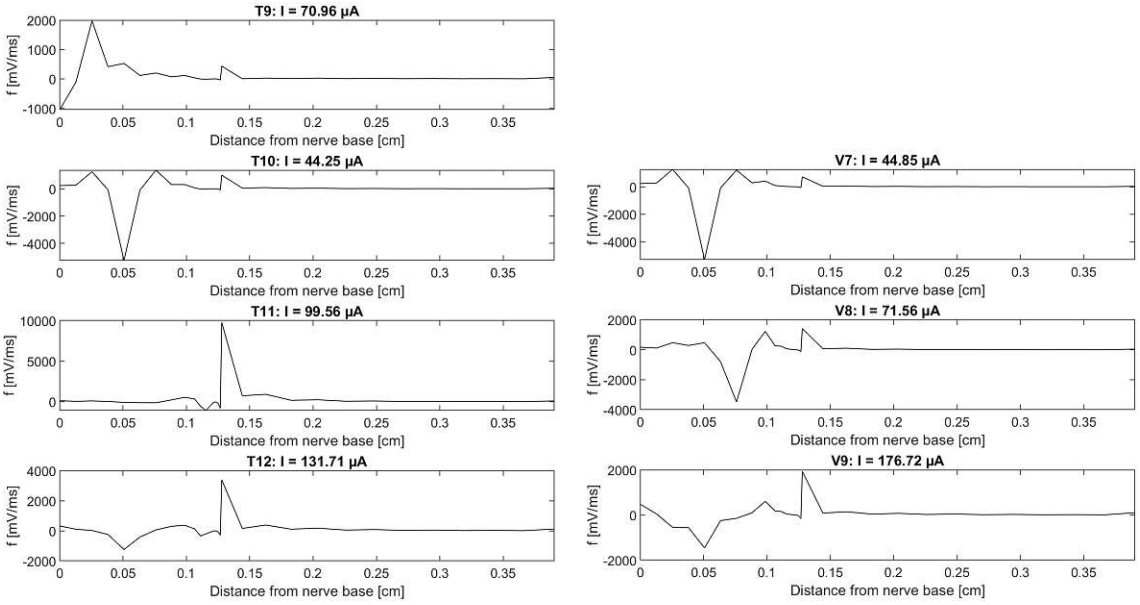

Figure 4.29: Activating function of Fiber 3, which was stimulated by anodic current pulses of different electrodes. Again, the subplots on the left side show the ST electrodes, the subplots on the right side show the SV electrodes.

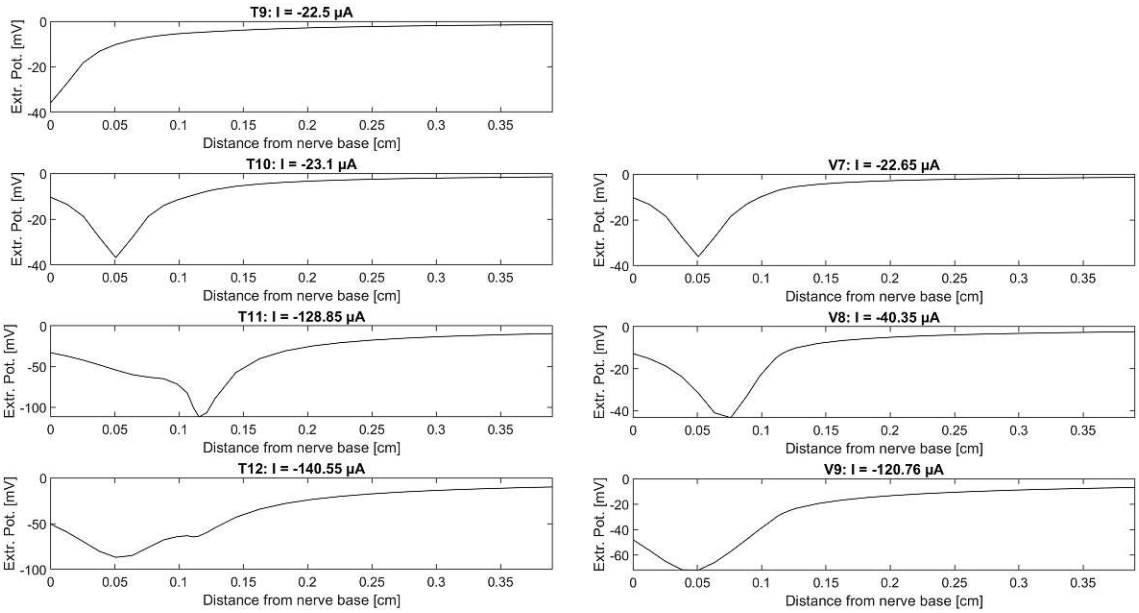

Figure 4.30: Extracellular potential upon cathodic stimulation of Fiber 3 by different electrodes, each represented by one subplot. The extracellular potential is based on equation 27.

For cathodic threshold stimulation, Figure 4.30 shows the extracellular potential and Figure 4.31 the activating function.

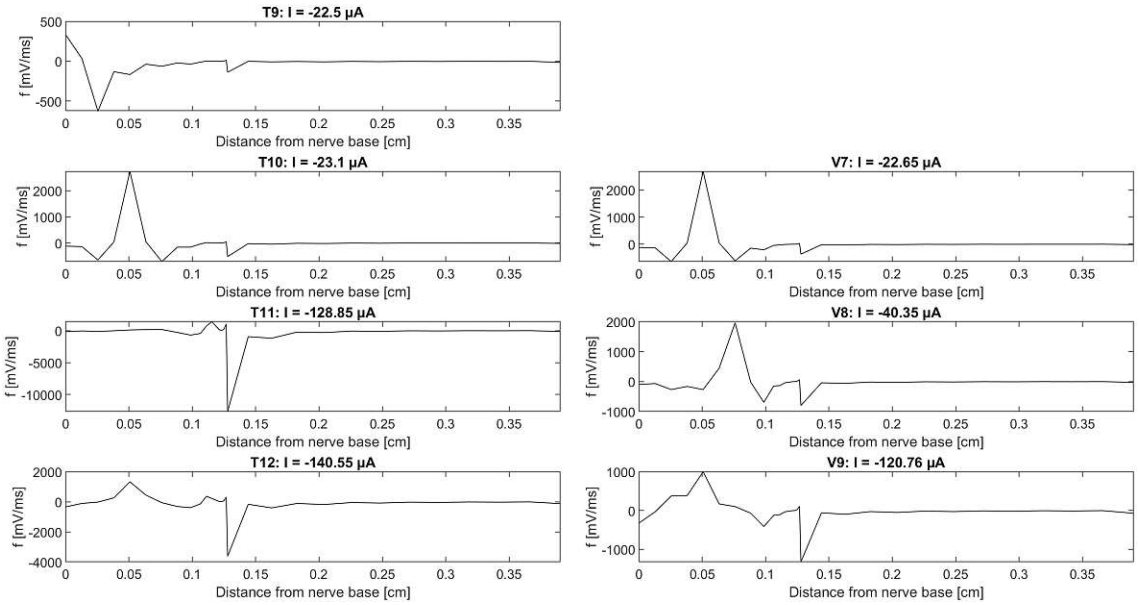

Figure 4.31: Activating function upon cathodic stimulation of Fiber 3 by different electrodes, each represented by one subplot. The subplots on the left side are the ST electrodes, whereas the subplots on the right side show the SV electrodes.

4.4.2 Degenerated Fiber

The degenerated Fiber 3 was simulated by cutting-off the dendrite. The threshold values for anodic and cathodic stimulation are shown in Table 4.6.

Table 4.6: Threshold values for anodic and cathodic stimulation of the degenerated Fiber 3. The pulse duration was set to 0.1 ms. The corresponding electrodes of the ST and the SV are listed next to each other.

Fiber 3	Scala Tympani		Fiber 3	Scala Vestibuli	
Electrode	Anodic Threshold [µA]	Cathodic Threshold [µA]	Electrode	Anodic Threshold [µA]	Cathodic Threshold [µA]
T9	631.11	-1265.03	-	-	-
T10	361.54	-572.26	V7	504.20	-808.83
T11	108.96	-179.67	V8	467.75	-735.77
T12	265.98	-424.34	V9	663.52	-1112.31

The APs elicited by anodic threshold stimulation propagate along the fiber, which is shown in Figure 4.32. The pulse duration was set to 0.1 ms.

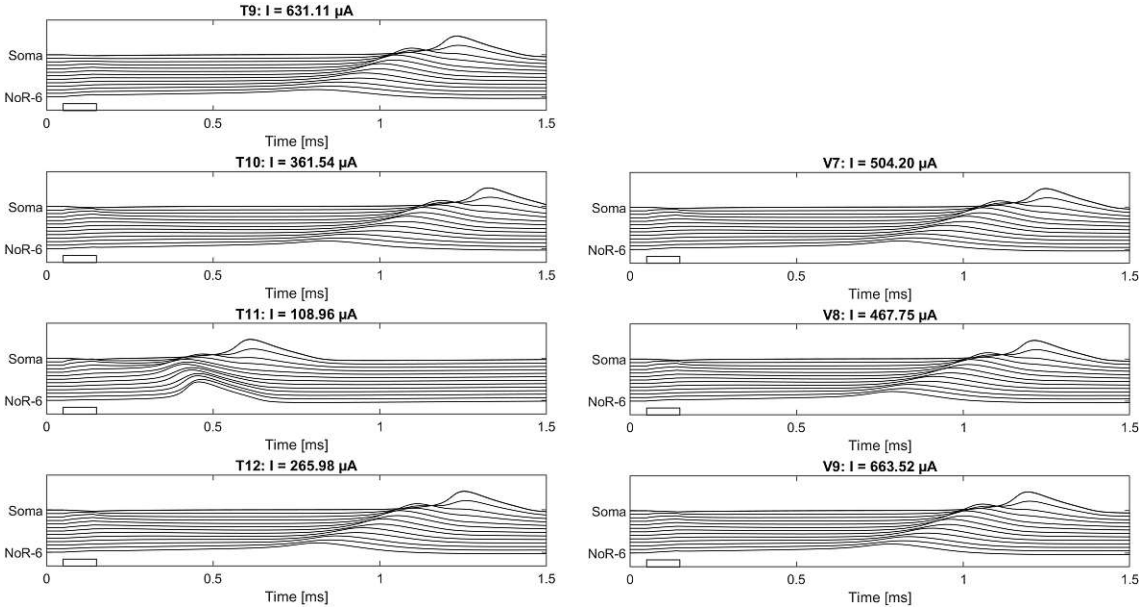

Figure 4.32: Anodic threshold stimulation of Fiber 3 without its dendrite to simulate degeneration of the fiber. Each subplot represents one electrode (left=ST, right = SV) and each line in each subplot corresponds to a compartment.

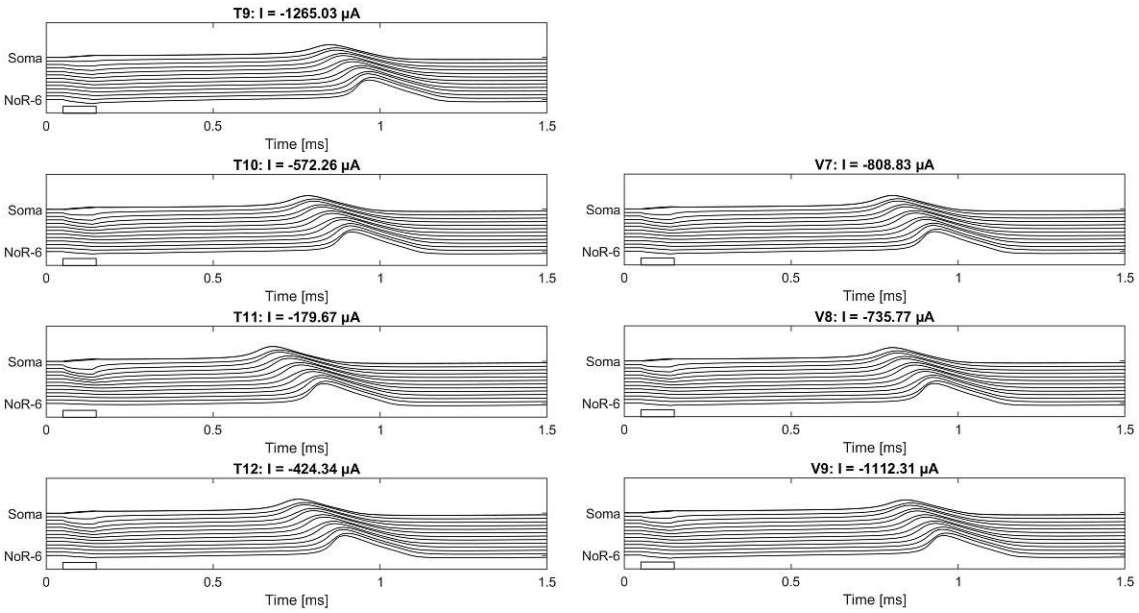

Figure 4.33: Cathodic threshold stimulation of Fiber 3 without its dendrite to simulate degeneration of the fiber. The AP propagates along the fiber: Each line represents one compartment of the fiber.

Figure 4.33 shows the APs propagating upon cathodic threshold stimulation of the degenerated Fiber 3. The extracellular potential and the activating function were again computed for the anodic and the cathodic case. Figure 4.34 shows the extracellular potential for the anodic case.

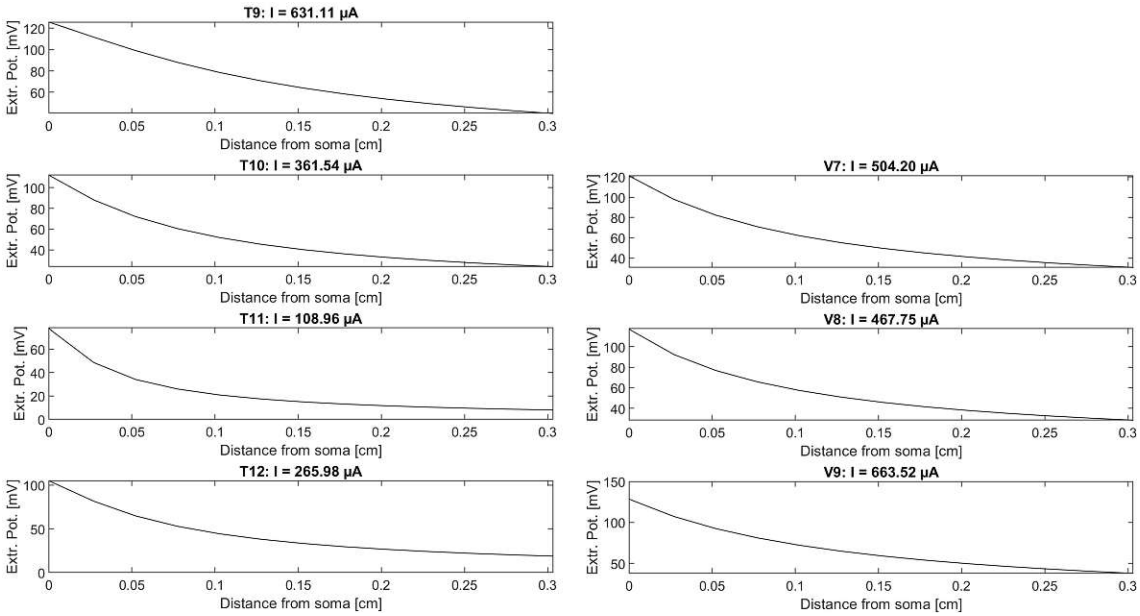

Figure 4.34: The degenerated Fiber 3 was stimulated by anodic current pulses taken from Table 4.6. The extracellular potential is shown.

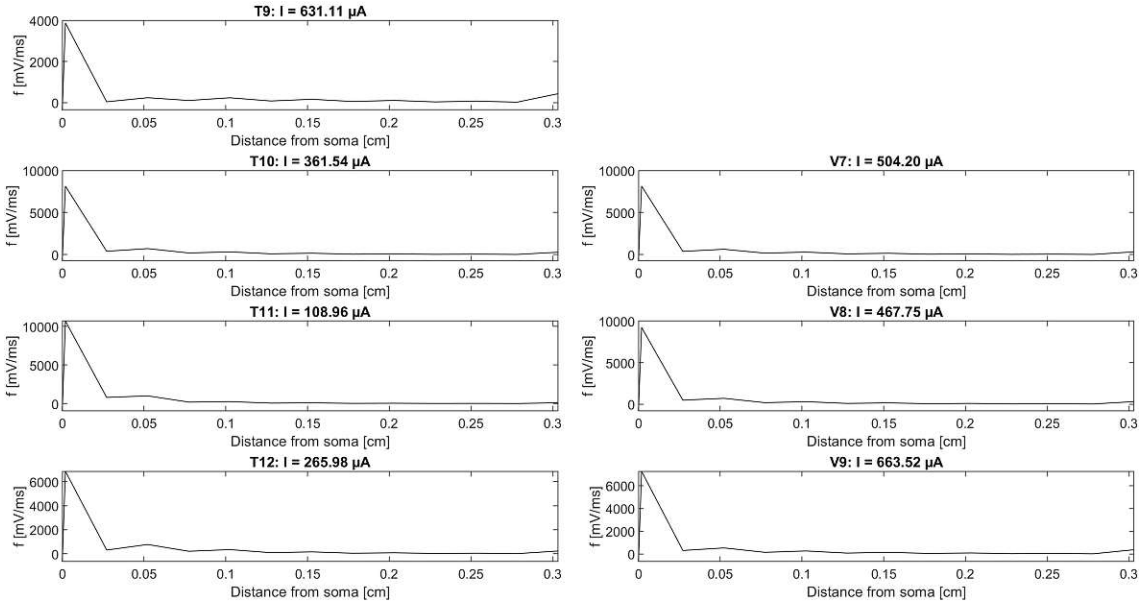

Figure 4.35: Activating function of degenerated Fiber 3 upon anodic threshold stimulation. Each subplot corresponds to another electrode (left = ST-electrodes, right = SV-electrodes).

Figure 4.35 shows the activating function of the degenerated Fiber 3 for anodic threshold stimulation. Figure 4.36 and Figure 4.37 show the extracellular potential and activating function for the cathodic case.

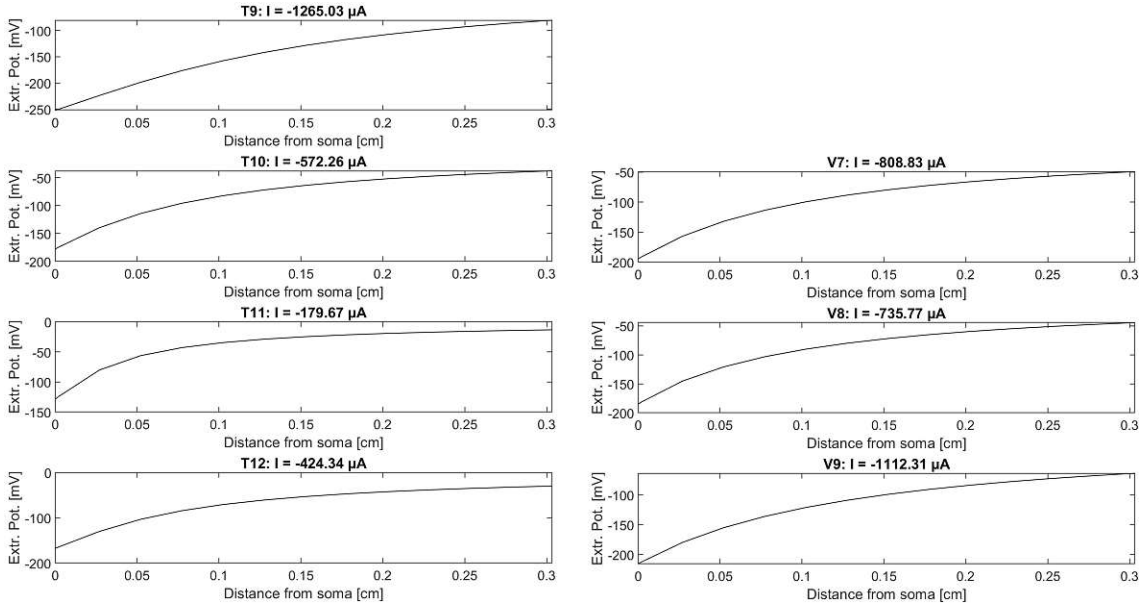

Figure 4.36: Extracellular potential resulting from cathodic stimulation of the degenerated Fiber 3. Again, the values were taken from Table 4.6.

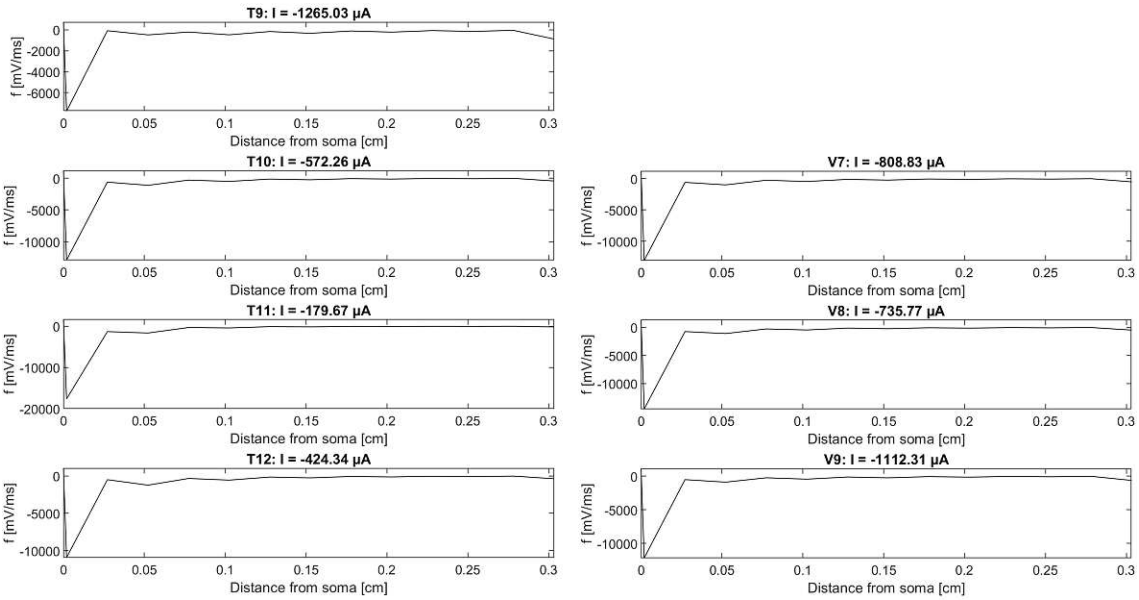

Figure 4.37: Activating function of degenerated Fiber 3 upon cathodic threshold stimulation. It can be seen as the second derivative of Figure 4.36.

4.5 Fiber 4

4.5.1 Physiological Fiber

The fourth and last fiber, which was analyzed, is Fiber 4. The threshold values for anodic and cathodic stimulation are shown in Table 4.7.

Table 4.7: Threshold values for anodic and cathodic stimulation of Fiber 4. The pulse duration was set to 0.1 ms. The corresponding electrodes of the ST and the SV are listed next to each other.

Fiber 4	Scala Tympani		Fiber 4	Scala Vestibuli	
Electrode	Anodic Threshold [µA]	Cathodic Threshold [µA]	Electrode	Anodic Threshold [µA]	Cathodic Threshold [µA]
T13	73.21	-22.35	-	-	-
T14	44.7	-22.8	V10	44.85	-22.65
T15	115.66	-110.26	V11	68.41	-36.45
T16	203.87	-204.62	V12	161.87	-125.26

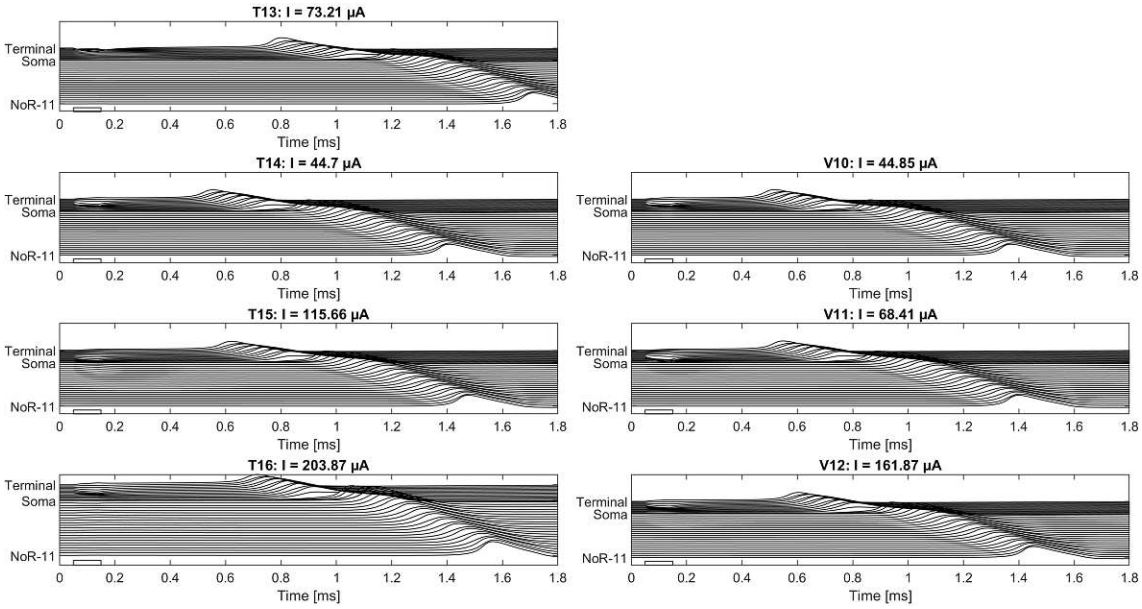

Figure 4.38: Anodic threshold stimulation of Fiber 4. In each subplot an AP propagates along the fiber, which is represented by the different compartments (=each line).

Figure 4.38 shows the AP propagation upon anodic threshold stimulation. Figure 4.39, which is shown below, also shows the AP propagation along the same Fiber 4, but for cathodic threshold stimulation.

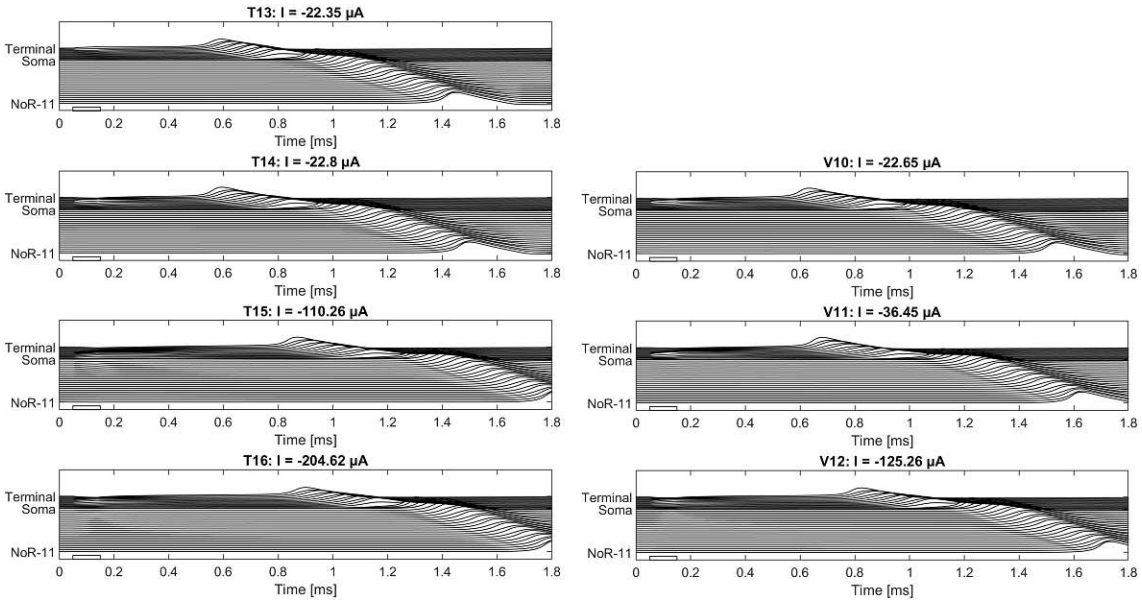

Figure 4.39: Cathodic threshold stimulation for Fiber 4. Each subplots represents one electrode and depicts the AP propagation along the fiber.

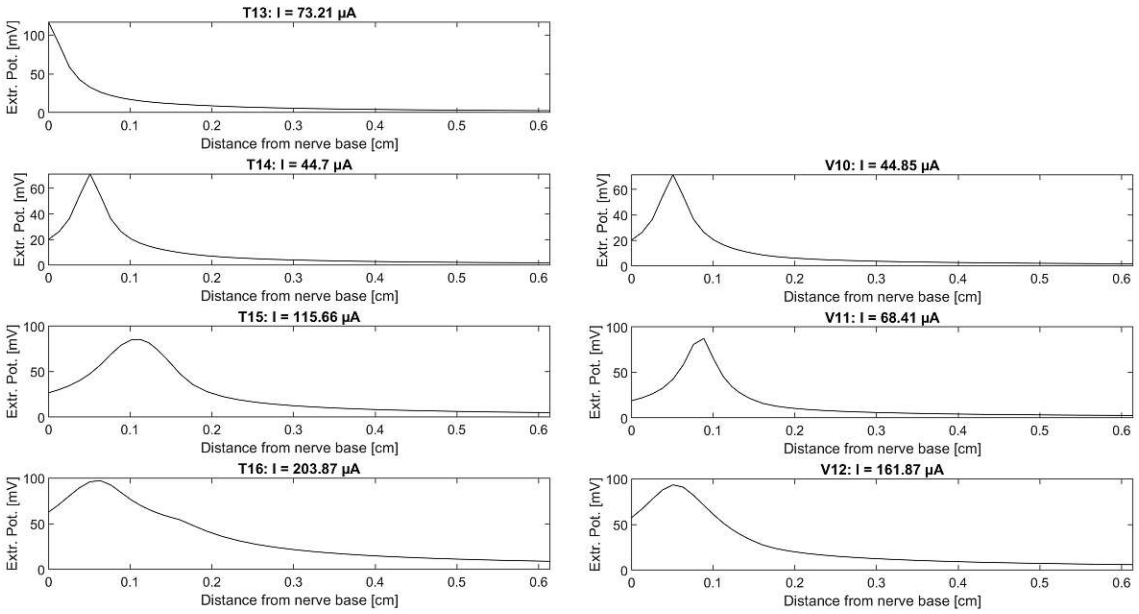

Figure 4.40: Extracellular potential upon anodic threshold stimulation of Fiber 4. The threshold values were taken from Table 4.7.

The extracellular potential and the activating function were also computed for anodic as well as for cathodic threshold stimulation. Figure 4.40 shows the extracellular potential and Figure 4.41 shows the activating function for anodic stimulation.

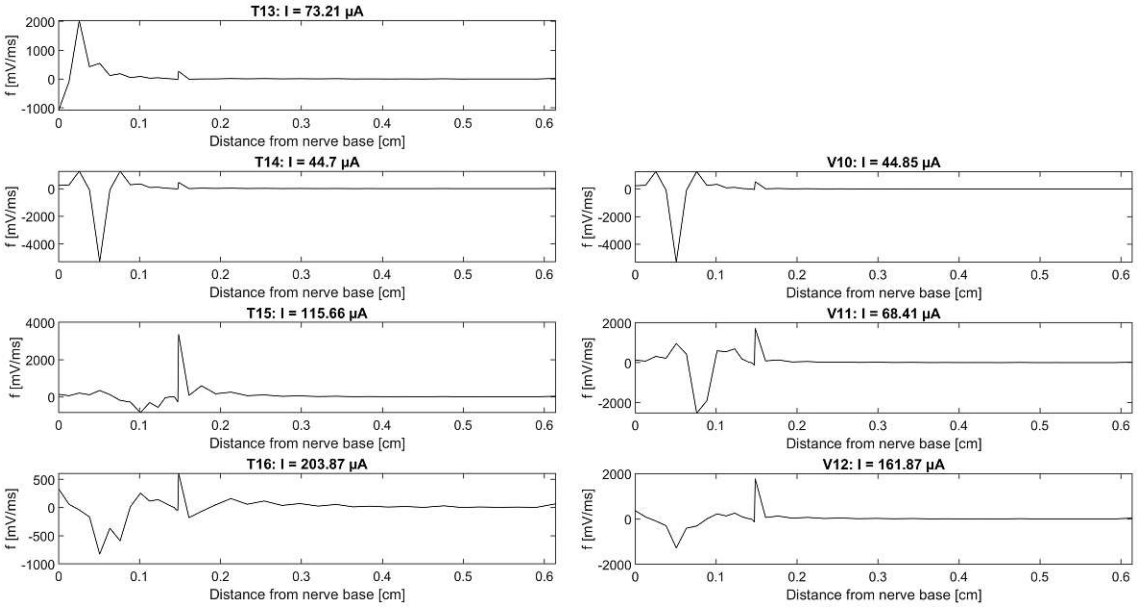

Figure 4.41: Activating function of Fiber 4 during anodic stimulation with different electrodes. Each subplot depicts the process initiated by a different electrode (left = ST-electrodes, right = SV-electrodes).

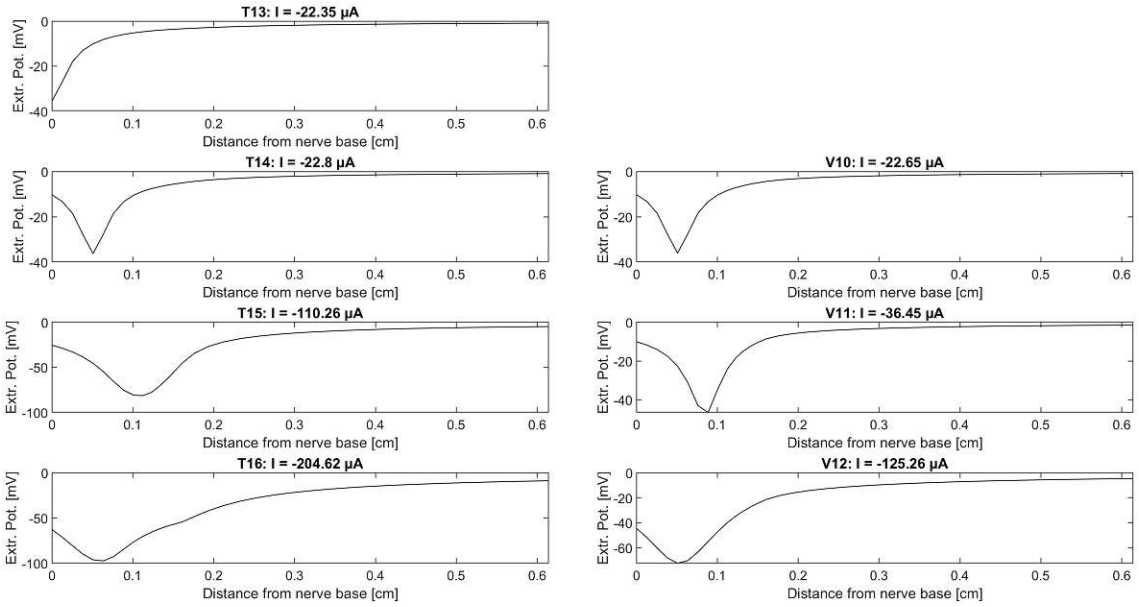

Figure 4.42: Extracellular potential upon cathodic threshold stimulation. The x-axis gives the distance from the nerve base, which is the compartment center of the terminal end of the dendrite of Fiber 4.

For the sake of completeness, the extracellular potential and the activating function were also computed for the cathodic case. Figure 4.42 depicts the extracellular potential for each electrode, and Figure 4.43 gives information about the activating function resulting from cathodic threshold stimulation of Fiber 4.

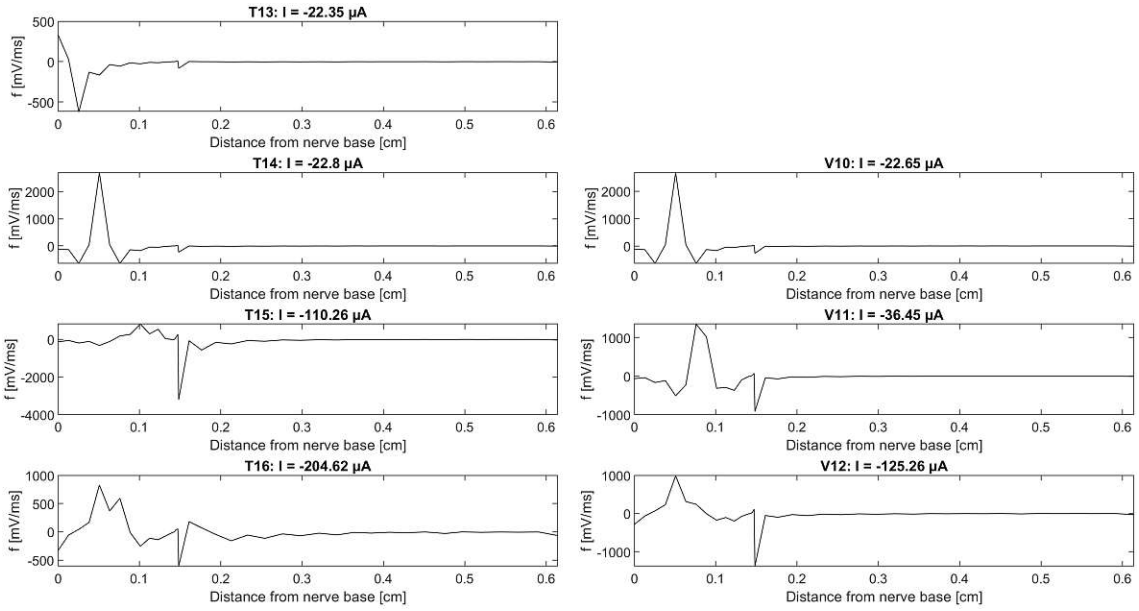

Figure 4.43: Activating function of Fiber 4 during cathodic threshold stimulation.

4.5.2 Degenerated Fiber

Cutting-off the dendrite of Fiber 4 offers the possibility to simulate a degenerated Fiber 4. This was done and the threshold values for the degenerated Fiber 4 for anodic and cathodic stimulation are shown below in Table 4.8 .

Table 4.8: Threshold values for anodic and cathodic stimulation of the degenerated Fiber 4. The pulse duration was set to 0.1 ms. The corresponding electrodes of the ST and the SV are listed next to each other.

Fiber 4	Scala Tympani		Fiber 4	Scala Vestibuli	
Electrode	Anodic Threshold [µA]	Cathodic Threshold [µA]	Electrode	Anodic Threshold [µA]	Cathodic Threshold [µA]
T13	1872.39	-1888.19	-	-	-
T14	745.07	-875.49	V10	791.73	-939.69
T15	199.62	-293.73	V11	428.39	-579.81
T16	724.57	-902.94	V12	906.64	-1071.41

The pulse duration was set to 0.1 ms, as with the other fibers before. The AP propagation for anodic threshold stimulation is shown in Figure 4.44 below. The values were taken from Table 4.8.

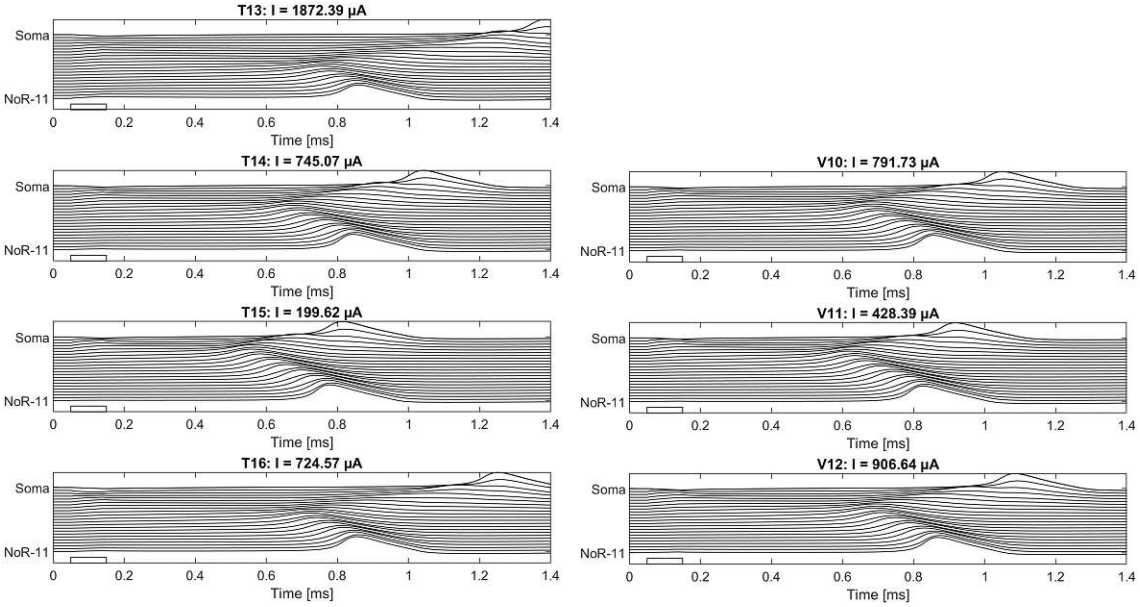

Figure 4.44: The degenerated Fiber 4 was stimulated by an anodic current pulse, which led to the propagation of an AP. Each subplots shows the stimulation process based on another electrode.

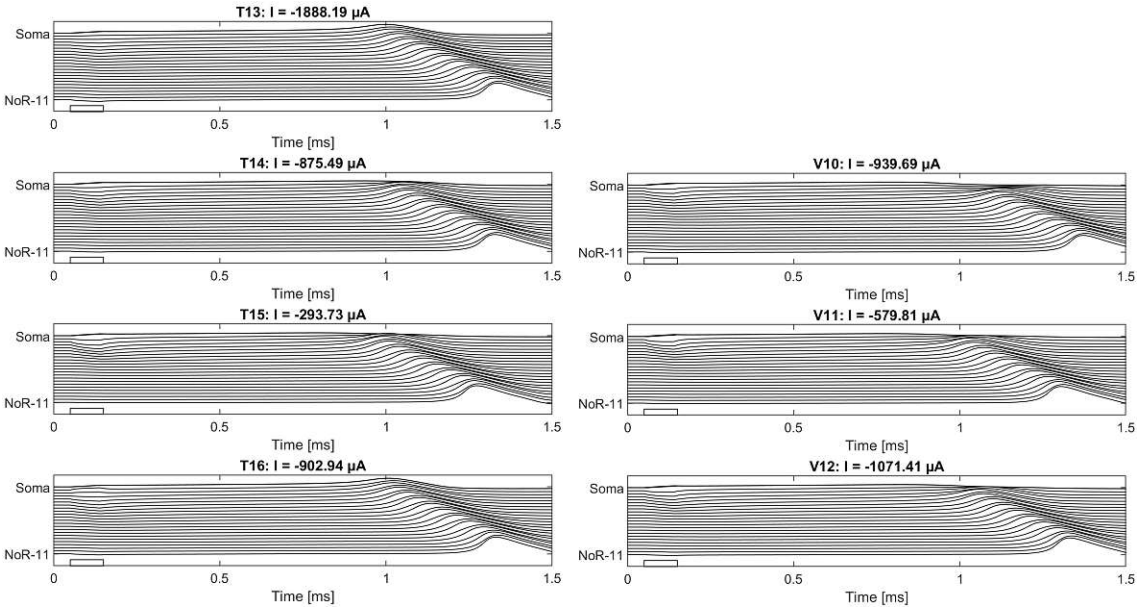

Figure 4.45: The degenerated Fiber 4 was also stimulated by a cathodic current pulse, which led to the propagation of an AP. Each subplots shows the stimulation process based on another electrode.

The cathodic threshold stimulation is shown in Figure 4.45. The extracellular potential and activating function were also calculated for anodic stimulation, depicted in Figure 4.46 respectively Figure 4.47.

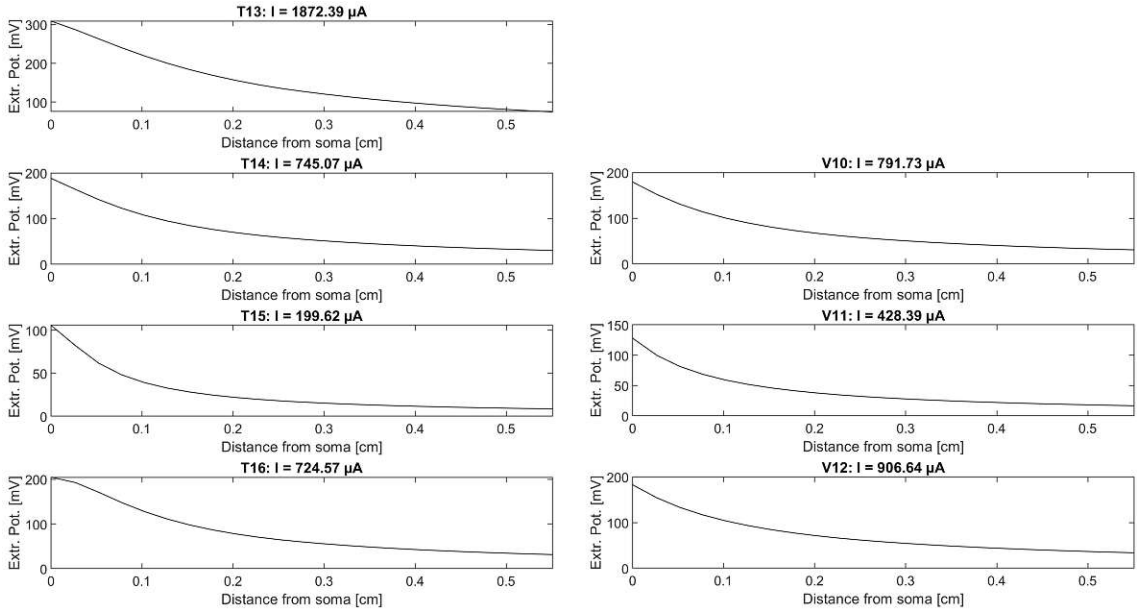

Figure 4.46: Extracellular potential along degenerated Fiber 4 upon anodic threshold stimulation. The x-axis gives the distance from the soma of Fiber 4.

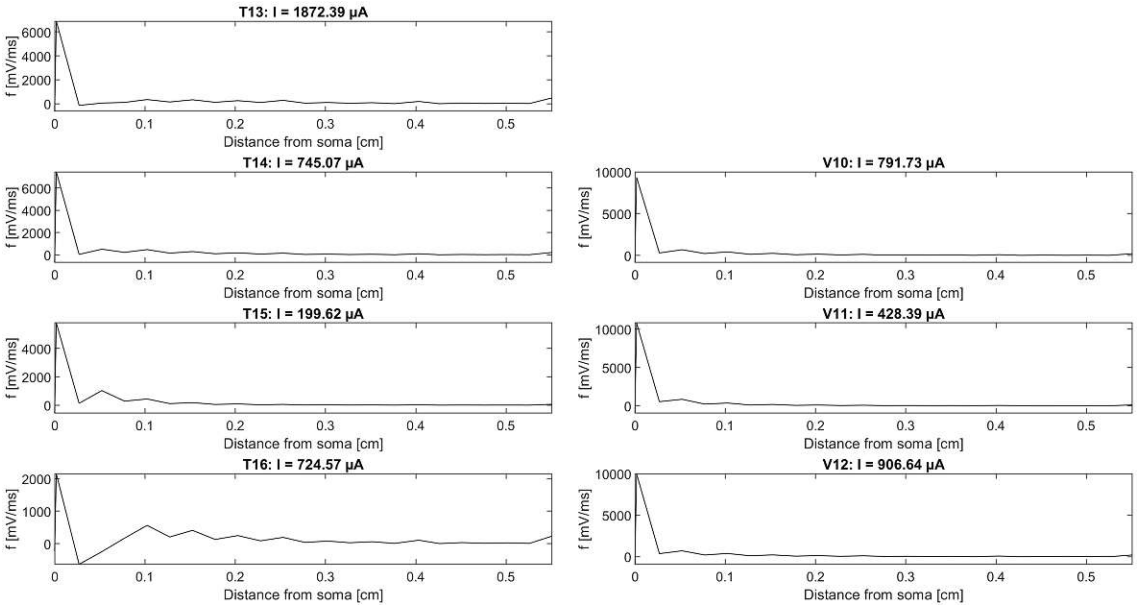

Figure 4.47: Activating function of degenerated Fiber 4 during anodic threshold stimulation.

The extracellular potential and the activating function were also analyzed for cathodic threshold stimulation. The results are shown in Figure 4.48 and Figure 4.49, on the next page.

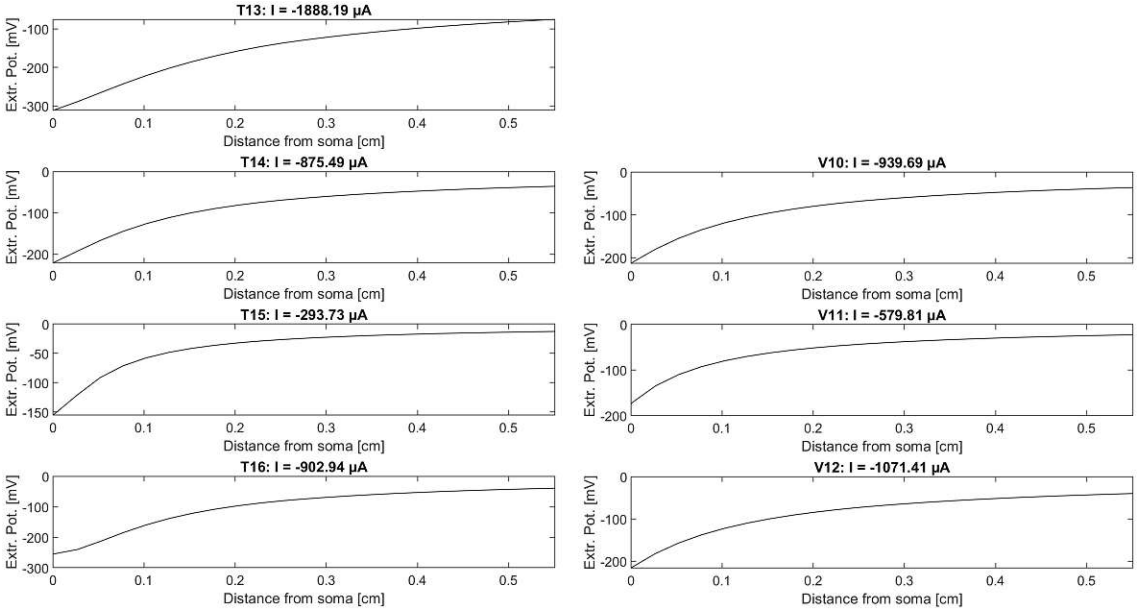

Figure 4.48: Cathodic threshold stimulation of degenerated Fiber 4. Depicted is the extracellular potential of each stimulating electrode.

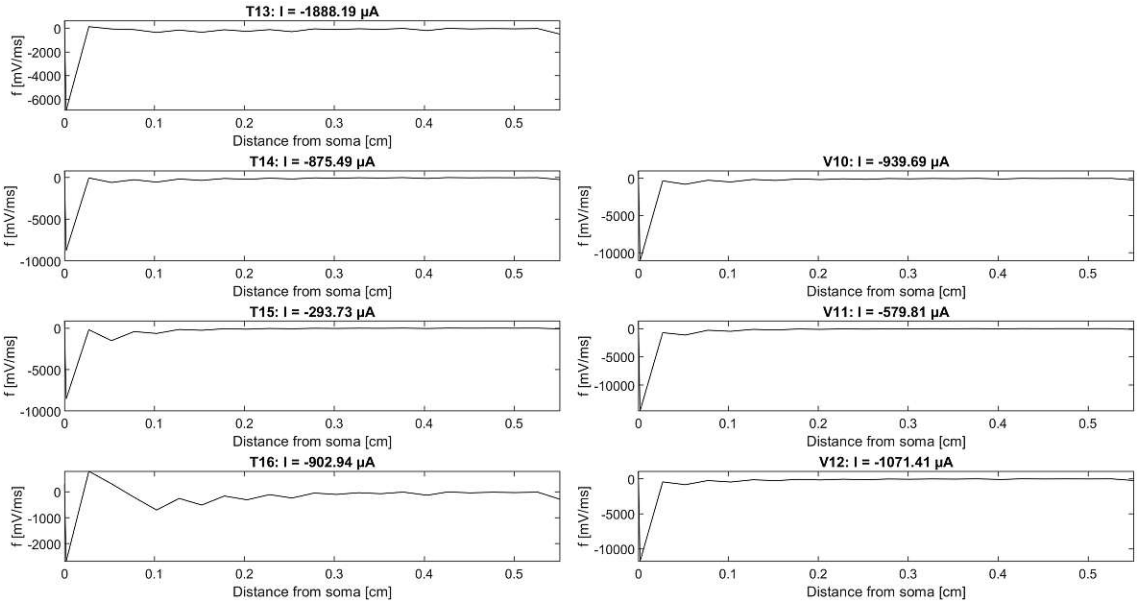

Figure 4.49: Activating function of degenerated Fiber 4 during cathodic threshold stimulation. Each subplot shows the situation based on another electrode: left = ST-electrodes; right = SV-electrodes.

5 Discussion

The simulation of ANF excitation with electrodes inserted in the ST and SV was successfully conducted. The program, where the Hodgkin-Huxley model was defined and where its equations were solved, works fine (see Appendix).

The aim of this thesis, as stated in chapter 1.4, was to analyze the ANF excitation with electrodes placed in the SV compared to electrode placement in the ST, which is considered the state-of-the-art method. (Lenarz, 2017) Based on threshold values, information on the plainness of fiber excitation is gained - casually spoken. The computed threshold values have an accuracy of ± 1 μA. As shown in Table 4.1, 4.3, 4.5, and 4.7, the terminal electrode and the mid-dendritic electrode (T1, T2, V1) have the lowest cathodic thresholds. Since the position T1 is only available for ST-electrode placement, a comparison to the SV is not possible. Interesting is the comparison between the mid-dendritic electrodes of Fiber 1-4, because for each fiber the mid-dendritic electrodes (T2/V1, T5/V4, T10/V7, and T14/V10) show similar behavior (see Figure 4.3, 4.15, 4.27, and 4.39). Moreover, the mid-dendritic position for the SV electrodes also shows a slightly lower cathodic threshold, indicating a more advantageous position compared to the mid-dendritic position of the ST. It is assumed that the curvature of the fiber (away from the SV) may be the reason for this observed behavior. The values of the activating function in the next NoR may support the SV-positioned electrode due to the curvature of the fiber. For a better understanding, it is helpful to think about the following situation: An electrode can be placed in the ST in that way that the equipotential lines (see Figure 3.4) lie along the fiber, respectively the path of the equipotential line is then congruent with the path of the fiber. Thus, the values of the activating function are zero, since it is the second derivative of the extracellular potential, which is the same along the fiber. In contrast, there does not exist a single position in the SV, where the equipotential lines of a SV-positioned electrode become congruent with the fiber path. This may be the reason for the advantageous excitation behavior of the SV placed electrode, e.g. V1, compared to the mid-dendritic electrode, e.g. T2, of the ST. This theory or assumption also gets fortified when looking at the perimodiolar electrodes (V2, T3, V5, T7, V8, T11, V11, T15). For the perimodiolar electrodes, the cathodic threshold is also lower for the electrodes placed in the SV. In contrast to the mid-dendritic position, where the difference between the ST and SV thresholds

is rather small and within the range of ± 1 μA, the cathodic threshold for the ST-placed electrode is higher by a factor of approximately 3 or 4. These findings may already be the breeding ground for theories, why the performance of SV-inserted electrodes is comparable or even better than the performance of ST-electrodes in clinical studies, such as (Trudel et al., 2018) or (Pasanisi et al., 2002). The last set of electrodes that can be compared for the physiological case are the central placed electrodes, which are the electrode positions, which were found by drawing the biggest possible inscribed-circle into the ST and SV and defining its center as electrode position. For the central electrodes, the SV-positioned electrodes are also advantageous, when comparing the cathodic threshold of the central ST and SV electrode. The reason here is that the distance to the fiber is smaller than for the ST positioned electrodes, meaning that the extracellular potential is higher for the SV-placed electrodes leading to eased excitation of the fiber.

Coming back to the terminal electrodes (T1, T5, T9, T13): It is unexpected that the anodic threshold is approximately twice as high as the anodic threshold for the mid-dendritic ST electrode (see Table 4.1, 4.3, 4.5, and 4.7), since the distance between electrode and fiber is the same for the mid-dendritic electrode and the fiber properties are also the same for the NoR and the terminal end, with the length of the compartment being the exception. An appropriate explanation for that observation has not been found yet. Another observation which has not been understood yet, is that the anodic threshold value is smaller than the cathodic (absolute) value for the perimodiolar and central electrodes of the ST of each fiber, with electrodes T4 and T15 being the exception. Another unanswered question arises when looking at Table 4.3, since V4 and V5 have the same cathodic threshold. The equivalent electrodes of the SV of the other fibers approximately differ by a factor 2, which is more plausible, since the distance of the perimodiolar electrode is larger than the distance of the mid-dendritic electrode to the fiber.

For one position in the ST, to be more precise for the mid-dendritic position of the ST, the behavior, when moving the mid-dendritic electrode by 125 µm to the center, was analyzed. T2 was initially located orthogonal to the second NoR of Fiber 1, but by moving the electrode, T2 becomes T2', meaning that T2' is located closest to the middle of the next internode. As shown in Table 4.1, the cathodic threshold for T2' was remarkably higher (nearly twice as high) than for T2. The anodic threshold; however, was only slightly higher. Thus, when inserting electrodes into a cavity it should be paid attention to position the electrodes as close to a NoR as possible in order to lower the current amplitude needed for excitation of the fiber.

The fibers were also simulated as degenerated fibers by cutting-off the dendrite. The aforementioned advantage of the SV-positioned electrodes due to the curvature of the fiber is now gone, since the dendrite is now missing. Thus, the shorter distance to the residual fiber of the ST-positioned electrodes compared to the SV-placed electrodes comes in handy. This can be seen in Table 4.2, 4.4, 4.6, and 4.8, because

for every fiber the SV electrodes have higher anodic and cathodic thresholds than the ST electrodes. However, the electrode T4 is the exception, since the anodic and cathodic threshold are higher than the anodic and cathodic threshold of V3. The distance to the soma is smaller for T4, which is why the question arises why the thresholds are still higher. It was tried to explain this by the curvature of Fiber 1, which might still be relevant for the soma of Fiber 1 compared to Fiber 2 and Fiber 3, but Fiber 4 has a similar path (only mirrored) like Fiber 1, but does not show the behavior observed for T4 and V3 for T16 and V12. Important to mention is that the excitation of the fiber is impeded in the degenerated case due to greater distances, and thus higher current amplitudes, compared to the physiological case, are required. Although higher currents were needed and used, it was not always possible to excite the soma of the fiber at threshold level, which is due to the high capacitive load of the soma (Rattay et al., 2001b) (see e.g. V10 degenerated in Figure 4.45). In addition, it should be mentioned that Fiber 2 and Fiber 3 had too short axons, which is why the AP propagates to the soma and not away from the soma. With increased currents this behavior could be corrected. Nevertheless, the AP should always propagate away from the soma, which is the case for Fiber 1 and Fiber 4, because they were initially modelled with longer axons. It was thought that it is not needed for Fiber 2 and 3, which held true for the physiological case, but later, when the degenerated case was simulated, it turned out that they should also have been modelled with longer axons. Nevertheless, it still can be said that the degenerated case was simulated successfully, since the behavior shown is still traceable. As shown in Table 4.2, 4.4, 4.6, and 4.8, the perimodiolar electrode has the lowest threshold for stimulation of the fiber due to the small distance to the soma respectively to the axon. The activating function of each fiber also shows that the degenerated fiber is most likely to be excited at the postsomatic region, since the activating function has a peak there.

5.1 Limitations

Although the outcomes gained can be classified as plausible and promising for further research, the model presented has limitations, since the model was implemented in a homogeneous medium with constant resistivity and time-constant extracellular potential. Furthermore, the number of compartments was restricted to one compartment per region, with the presomatic region being the exception, since it was segmented into three compartments to better model the transition of the AP to the soma. Also, the fiber paths were only estimated and approximated with lines, circles and arcs. Although attention was paid to define the paths as anatomically correct as possible, certain deviations cannot be excluded. Another deviation is the fact that the coordinates from the fibers had to be converted before calculation was possible. The program used for the definition of the fiber paths was *CorelDraw*, whose original

targets were not technical construction drawings. Therefore, the measurement tool for lengths and distances is not optimal, leading to inaccuracies during drawing of the fibers. Concerning the conversion issue of the coordinates, it must be said that there were two problems: The first problem was that Figure 3.1 was only available by copying it out of the paper (Rattay et al., 2001a), resulting in less good image quality. The second problem was that the image itself was in a certain scale indicated by the 1 mm mark in the left corner of the image. Thus, the conversion factor chosen was based on measuring the distance of that mark in *CorelDraw*, which, as already mentioned has certain inaccuracies concerning the measurement tool. Due to the rather bad image quality, the image was pixelated when zooming in, which resulted in blurred edges of the benchmark, to blurred edges of the ST and SV, which means that electrodes such as T3 may not be as close to the soma as possible. The last inaccuracy which was faced when using *CorelDraw*, respectively when the fiber paths and electrode positions were defined, was the coordinate system which was drawn. To be as accurate as possible, small steps in x and y directions were intended to be used. However, due to the resolution of the image and the line width of the lines of the coordinate system, a smaller step size than 10 μm was not possible. Thus, the measurement tool with its inaccuracies must be used for precise definition of a location or position between the lines of the coordinate system (e.g. center of electrode or compartment center). Nevertheless, these inaccuracies can be classified as systematic error, since it is assumed that they equally influence all electrodes and fibers.

Based on all these results and hypotheses, the following can be concluded (see chapter 6).

6 Conclusion and Outlook

Based on the results and their evaluation, it can be concluded that the SV is an adequate alternative for electrode insertion to the ST. The presented homogeneous extracellular medium model shows that the electrodes in the SV can excite the fiber more easily than electrodes in the ST for mid-dendritic and also perimodiolar located electrodes, since lower thresholds were observed for these SV electrodes. However, in case of degenerated fibers the ST might be more suited for electrode insertion due to a closer distance to the residual fiber. In case of an obstructed or ossified ST, the SV should be taken into account, but more research is needed to investigate the relation between curvature of the fiber and excitability of the fiber. Also, the model should be expanded to a non-homogeneous model to better simulate human tissue. For more precise results, the number of compartments should be increased, respectively it should be investigated, which number of compartments is sufficient for different simulation tasks.

To sum up, the SV is an adequate alternative for ST electrode placement, especially for mid-dendritic and perimodiolar electrode positions, but more research is needed to validate the outcomes of this thesis.

Appendix: Matlab Code

Main Code

```
1
2  %function [maxMax] = Master_Thesis_Code(stim) %for
       Finding Thresholds
3
4  %% ---------------------------- Master Thesis
       -----------------------------
5  % Simulation of auditory nerve fiber excitation with
       prostheses implanted
6  % in the scala vestibuli
7
8  % Author: Fred Bucek, BSc
9  % 1. Supervisor: Ao.Univ.-Prof.i.R.Privatdoz. Dipl.-Ing.
       Dr.sc.med. Dr.techn.
10 % Dr.rer.nat. Frank Rattay
11 % 2. Supervisor: Projektass.(FWF) Dipl.-Ing. Dr.techn.
       Paul Werginz
12
13 % Date: 30.06.23
14
15 close all
16 clear all
17 %% ---------------------------- Loading ...
       ------------------------------
18 % Load Files
19 % Electrode coordinates
20 S = load('El_coordinates.mat'); % loads variables from
       file "Einlesedatei für Matlab Code" [µm]
21 [El_coordinates] = deal(S.El_coordinates);
22
23 % Compartment centers
```

```
24 D = load('F1_compcent.mat'); % loads variables from file
   "Einlesedatei für Matlab Code" [µm]
25 [F1_compcent] = deal(D.F1_compcent); % converts struct
   into numeric matrix
26 L = load('F2_compcent.mat'); % loads variables from file
   "Einlesedatei für Matlab Code" [µm]
27 [F2_compcent] = deal(L.F2_compcent); % converts struct
   into numeric matrix
28 O = load('F3_compcent.mat'); % loads variables from file
   "Einlesedatei für Matlab Code" [µm]
29 [F3_compcent] = deal(O.F3_compcent); % converts struct
   into numeric matrix
30 U = load('F4_compcent.mat'); % loads variables from file
   "Einlesedatei für Matlab Code" [µm]
31 [F4_compcent] = deal(U.F4_compcent); % converts struct
   into numeric matrix
32
33 %% ---------------------- Step 1: Parameter Definition
   ----------------------
34 % Choose fibre and electrode
35 fibre = 'F1'; % Select Fibre: F1, F2, F3, F4
36 electrode = 'T1'; % Select electrode of Scala Tympani: T1
    - T16 + T2prime, or of Scala Vestibuli: V1 - V12
37 degenerated = 0;  % Cuts off the dendrite to simulate
   degenerated fibre, 1 = Yes, 0 = No
38 plotExAct = 1; % Plot Extracellular Potential and
   Activating Function? 1 = Yes, 0 = No
39 plotAP = 1; % Plot Action Potential in space and time 1 =
    Yes, 0 = No
40
41 % Temporal Parameters
42 start = 0; % Starting time of simulation [ms]
43 del = 5; % Delay of stimulus [ms] % 5
44 dur = 0.1; % Duration of stimulus [ms]
45 stop = 15; % Total duration of simulation [ms] %15
46 dt = 0.01; % Time steps [ms]
47 pretime = 0.05; % spare time before stimulus which is
   visible in plot %0.05
48 t = start:dt:stop; % time [ms]
49 time = start:dt:(stop-del+pretime); % time without
   initializing phase
50
51 % Electrode
52 Eldia = 200; % Electrode diameter [µm]
```

```
53 Iel = -100; %stim;  % Electrode current in [µA];  stim
      for threshold search
54
55 % Geometric Definition
56 % Lengths
57 lterm = 10; % length of unmyelinated terminal [µm]
58 lnode = 2.5; % length of node [µm]
59 lperiinter = 250; % length of peripheral internode [µm]
60 llastinter = 210; % length of last peripheral internode [
      µm]
61 lf4short = 231.7; % length of shorter internode in F4 [µm
      ]
62 lpresoma = 100; % length of presomatic region [µm]
63 lpostsoma = 5; % length of postsomatic region [µm]
64 lcentinter = 500; % length of central internodes [µm]
65
66 % Diameters
67 dperi = 1; % diameter of peripheral process (dendrite) [µ
      m]
68 dsoma = 20; % diameter of soma [µm]
69 dcent = 2*dperi; % diameter of central process (axon) [µm
      ]
70
71 % Myelin layers
72 mylayperi = 40; % number of peripheral myelin layers []
73 mylaycent = 80; % number of central myelin layers []
74 mylaysoma = 3; % number of myelin layers of soma []
75
76 % Electric Properties
77 % Medium
78 rhoe = 300; % Extracellular resistivity [Ohm*cm]
79 rhoi = 50; % intracellular/axial resistivity [Ohm cm]
80
81 % Capacities
82 cnode = 1; % capacity of nodes [µF/cm^2]
83 cperiinter = cnode/mylayperi; % capacity of peripheral
      internodes [µF/cm^2]
84 ccentinter = cnode/mylaycent; % capacity of central
      internodes [µF/cm^2]
85 csoma = cnode/mylaysoma; % capacity of soma [µF/cm^2]
86 cpre = 1; % capacity of presomatic region [µF/cm^2]
87 cpost = 1; % capacity of postsomatic region [µF/cm^2]
88
89 % Conductances for active compartments (terminal, nodes,
```

```
   pre-, postsomatic region)
densfac = 10; % density factor to simulate xx-fold
   channel density
gNa_HH10 = 120*densfac; % Sodium conductance [mS/cm^2]
gK_HH10 = 36*densfac; % Potassium conductance [mS/cm^2]
gL_HH10 = 0.3*densfac; % Leakage conductance [mS/cm^2]

% Conductances for soma
gNa_HH = 120; % Sodium conductance soma [mS/cm^2]
gK_HH = 36; % Potassium conductance soma [mS/cm^2]
gL_HH = 0.3; % Leakage conductance soma [mS/cm^2]

% Conductances for internodes (passive)
gperiinter = 1/mylayperi; % conductance of peripheral
   internodes [mS/cm^2]
gcentinter = 1/mylaycent; % conductance of central
   internodes [mS/cm^2]

% Hodgkin-Huxley Parameters
Vrest = -65; % Resting potential [mV]
V_Na = 115; % Sodium voltage [mV]
V_K = -12; % Potassium voltage [mV]
V_L = 10.6; % Leakage voltage [mV]

% Reversal Potential
E_Na = V_Na + Vrest; % [mV]
E_K = V_K + Vrest; % [mV]
E_L = V_L + Vrest; % [mV]

% Temperature
T = 29; % [Degree Celsius]
% Temperature Coefficient []
k = 3^(0.1*T-0.63); % for 6.3 degCelsius  k=1; for 29
   degC k = 12.11

%% ---------------------- Step 2: Initialize Vectors
   -----------------------
% Define matrix
% Fibre 1
for i = 1:length(F1_compcent)
    % Lengths
    if mod(i,2)== 0 % internodes

            % Capacities, Conductances
```

```
128             if i < 14
129                 lcomp(i,1) = lperiinter;
130                 ccomp(i,1) = cperiinter;
131                 gNacomp(i,1) = 0;
132                 gKcomp(i,1) = 0;
133                 gLcomp(i,1) = gperiinter;
134             elseif i==14
135                 ccomp(i,1) = csoma;
136                 gNacomp(i,1) = gNa_HH;
137                 gKcomp(i,1) = gK_HH;
138                 gLcomp(i,1) = gL_HH;
139             else
140                 lcomp(i,1) = lcentinter;
141                 ccomp(i,1) = ccentinter;
142                 gNacomp(i,1) = 0;
143                 gKcomp(i,1) = 0;
144                 gLcomp(i,1) = gcentinter;
145             end
146     else % nodes
147         lcomp(i,1) = lnode;
148         ccomp(i,1) = cnode;
149         gNacomp(i,1) = gNa_HH10;
150         gKcomp(i,1) = gK_HH10;
151         gLcomp(i,1) = gL_HH10;
152
153     end
154     % diameter
155     if i<14 % dendrite
156         dcomp(i,1) = dperi;
157     elseif i==14 % soma
158         dcomp(i,1) = dsoma;
159     else % axon
160         dcomp(i,1) = dcent;
161     end
162
163 end
164 %Special treatment for
165 lcomp(1,1) = lterm;          ccomp(11,1) = cpre;
       gNacomp(11,1) = gNa_HH10;
166 lcomp(10,1) = llastinter;    ccomp(12,1) = cpre;
       gNacomp(12,1) = gNa_HH10;
167 lcomp(11,1) = lpresoma/3;    ccomp(13,1) = cpre;
       gNacomp(13,1) = gNa_HH10;
168 lcomp(12,1) = lpresoma/3;    ccomp(15,1) = cpost;
```

```
   gNacomp(15,1) = gNa_HH10;
lcomp(13,1) = lpresoma/3;    gKcomp(11,1) = gK_HH10;
   gLcomp(11,1) = gL_HH10;
lcomp(14,1) = dsoma;         gKcomp(12,1) = gK_HH10;
   gLcomp(12,1) = gL_HH10;
lcomp(15,1) = lpostsoma;     gKcomp(13,1) = gK_HH10;
   gLcomp(13,1) = gL_HH10;
                             gKcomp(15,1) = gK_HH10;
                                gLcomp(15,1) = gL_HH10;

% Fibre 2
for i = 1:length(F2_compcent)
    % Lengths
    if mod(i,2)== 0 % internodes
            % Capacities, Conductances
            if i < 16
                lcomp(i,2) = lperiinter;
                ccomp(i,2) = cperiinter;
                gNacomp(i,2) = 0;
                gKcomp(i,2) = 0;
                gLcomp(i,2) = gperiinter;
            elseif i==16
                ccomp(i,2) = csoma;
                gNacomp(i,2) = gNa_HH;
                gKcomp(i,2) = gK_HH;
                gLcomp(i,2) = gL_HH;
            else
                lcomp(i,2) = lcentinter;
                ccomp(i,2) = ccentinter;
                gNacomp(i,2) = 0;
                gKcomp(i,2) = 0;
                gLcomp(i,2) = gcentinter;
            end
    else % nodes
        lcomp(i,2) = lnode;
        ccomp(i,2) = cnode;
        gNacomp(i,2) = gNa_HH10;
        gKcomp(i,2) = gK_HH10;
        gLcomp(i,2) = gL_HH10;

    end
    % diameter
    if i<16 % dendrite
        dcomp(i,2) = dperi;
```

```
208     elseif i==16 % soma
209         dcomp(i,2) = dsoma;
210     else % axon
211         dcomp(i,2) = dcent;
212     end
213
214 end
215 % Special treatment
216 lcomp(1,2) = lterm;          ccomp(13,2) = cpre;
       gNacomp(13,2) = gNa_HH10;
217 lcomp(12,2) = llastinter;    ccomp(14,2) = cpre;
       gNacomp(14,2) = gNa_HH10;
218 lcomp(13,2) = lpresoma/3;    ccomp(15,2) = cpre;
       gNacomp(15,2) = gNa_HH10;
219 lcomp(14,2) = lpresoma/3;    ccomp(17,2) = cpost;
       gNacomp(17,2) = gNa_HH10;
220 lcomp(15,2) = lpresoma/3;    gKcomp(13,2) = gK_HH10;
       gLcomp(13,2) = gL_HH10;
221 lcomp(16,2) = dsoma;         gKcomp(14,2) = gK_HH10;
       gLcomp(14,2) = gL_HH10;
222 lcomp(17,2) = lpostsoma;     gKcomp(15,2) = gK_HH10;
       gLcomp(15,2) = gL_HH10;
223                              gKcomp(17,2) = gK_HH10;
                                    gLcomp(17,2) = gL_HH10;
224
225 % Fibre 3
226 for i = 1:length(F3_compcent)
227     % Lengths
228     if mod(i,2)== 0 % internodes
229             % Capacities, Conductances
230             if i < 16
231                 lcomp(i,3) = lperiinter;
232                 ccomp(i,3) = cperiinter;
233                 gNacomp(i,3) = 0;
234                 gKcomp(i,3) = 0;
235                 gLcomp(i,3) = gperiinter;
236             elseif i==16
237                 ccomp(i,3) = csoma;
238                 gNacomp(i,3) = gNa_HH;
239                 gKcomp(i,3) = gK_HH;
240                 gLcomp(i,3) = gL_HH;
241             else
242                 lcomp(i,3) = lcentinter;
243                 ccomp(i,3) = ccentinter;
```

```
                gNacomp(i,3) = 0;
                gKcomp(i,3) = 0;
                gLcomp(i,3) = gcentinter;
            end
    else % nodes
        lcomp(i,3) = lnode;
        ccomp(i,3) = cnode;
        gNacomp(i,3) = gNa_HH10;
        gKcomp(i,3) = gK_HH10;
        gLcomp(i,3) = gL_HH10;

    end
    % diameter
    if i<16 % dendrite
        dcomp(i,3) = dperi;
    elseif i==16 % soma
        dcomp(i,3) = dsoma;
    else % axon
        dcomp(i,3) = dcent;
    end

end
% Special treatment
lcomp(1,3) = lterm;          ccomp(13,3) = cpre;
   gNacomp(13,3) = gNa_HH10;
lcomp(12,3) = llastinter;    ccomp(14,3) = cpre;
   gNacomp(14,3) = gNa_HH10;
lcomp(13,3) = lpresoma/3;    ccomp(15,3) = cpre;
   gNacomp(15,3) = gNa_HH10;
lcomp(14,3) = lpresoma/3;    ccomp(17,3) = cpost;
   gNacomp(17,3) = gNa_HH10;
lcomp(15,3) = lpresoma/3;    gKcomp(13,3) = gK_HH10;
   gLcomp(13,3) = gL_HH10;
lcomp(16,3) = dsoma;         gKcomp(14,3) = gK_HH10;
   gLcomp(14,3) = gL_HH10;
lcomp(17,3) = lpostsoma;     gKcomp(15,3) = gK_HH10;
   gLcomp(15,3) = gL_HH10;
                             gKcomp(17,3) = gK_HH10;
                                gLcomp(17,3) = gL_HH10;

% Fibre 4
for i = 1:length(F4_compcent)
% Lengths
    if mod(i,2)== 0 % internodes
```

```
280             % Capacities, Conductances
281             if i < 16
282                 lcomp(i,4) = lperiinter;
283                 ccomp(i,4) = cperiinter;
284                 gNacomp(i,4) = 0;
285                 gKcomp(i,4) = 0;
286                 gLcomp(i,4) = gperiinter;
287             elseif i==16
288                 ccomp(i,4) = csoma;
289                 gNacomp(i,4) = gNa_HH;
290                 gKcomp(i,4) = gK_HH;
291                 gLcomp(i,4) = gL_HH;
292             else
293                 lcomp(i,4) = lcentinter;
294                 ccomp(i,4) = ccentinter;
295                 gNacomp(i,4) = 0;
296                 gKcomp(i,4) = 0;
297                 gLcomp(i,4) = gcentinter;
298             end
299     else % nodes
300         lcomp(i,4) = lnode;
301         ccomp(i,4) = cnode;
302         gNacomp(i,4) = gNa_HH10;
303         gKcomp(i,4) = gK_HH10;
304         gLcomp(i,4) = gL_HH10;
305 
306     end
307     % diameter
308     if i<16 % dendrite
309         dcomp(i,4) = dperi;
310     elseif i==16 % soma
311         dcomp(i,4) = dsoma;
312     else % axon
313         dcomp(i,4) = dcent;
314     end
315 
316 end
317 
318 % Special treatment % soma has index 16 and short
      internode is last but one
319 lcomp(1,4) = lterm;      ccomp(13,4) = cpre;
      gNacomp(13,4) = gNa_HH10;
320 lcomp(10,4) = lf4short; ccomp(14,4) = cpre;
      gNacomp(14,4) = gNa_HH10;
```

```
lcomp(12,4) = llastinter; ccomp(15,4) = cpre;
   gNacomp(15,4) = gNa_HH10;
lcomp(13,4) = lpresoma/3; ccomp(17,4) = cpost;
   gNacomp(17,4) = gNa_HH10;
lcomp(14,4) = lpresoma/3; gKcomp(13,4) = gK_HH10;
   gLcomp(13,4) = gL_HH10;
lcomp(15,4) = lpresoma/3; gKcomp(14,4) = gK_HH10;
   gLcomp(14,4) = gL_HH10;
lcomp(16,4) = dsoma;      gKcomp(15,4) = gK_HH10;
   gLcomp(15,4) = gL_HH10;
lcomp(17,4) = lpostsoma;  gKcomp(17,4) = gK_HH10;
   gLcomp(17,4) = gL_HH10;


% Unit Overview
% lcomp in [µm] % dcomp in [µm] % ccomp in [µF/cm^2] %
   gNacomp, gKcomp, gLcomp in [mS/cm^2]

% Calculate axial resistances [kOhm]
R = ((2*rhoi*lcomp*1e-04)./(2*((dcomp/2)*1e-04).^2*pi))*1
   e-03; % [kOhm]

% Fibre 1
Rpretosoma1 = 1e-03*(1e-02*rhoi / (dperi*1e-06*pi)*log((
   dsoma/2+sqrt((dsoma/2)^2-(dperi/2)^2))/((dsoma/2-sqrt
   ((dsoma/2)^2-(dperi/2)^2)))));
Rpretosoma1 = Rpretosoma1/2;
Rsomatopost1 = 1e-03*(1e-02*rhoi / (dcent*1e-06*pi)*log((
   dsoma/2+sqrt((dsoma/2)^2-(dcent/2)^2))/((dsoma/2-sqrt
   ((dsoma/2)^2-(dcent/2)^2)))));
Rsomatopost1 = Rsomatopost1/2;
R(14,1) = NaN; % Soma of fibre 1 has index 14

% Fibre 2 geometry identical to fibre 1
Rpretosoma2 = Rpretosoma1;
Rsomatopost2 = Rsomatopost1;
R(16,2) = NaN; % Soma of fibre 2 has index 16

% Fibre 3 geometry identical to fibre 1
Rpretosoma3 = Rpretosoma1;
Rsomatopost3 = Rsomatopost1;
R(16,3) = NaN; % Soma of fibre 3 has index 16

% Fibre 4 geometry identical to fibre 1
```

```
353 Rpretosoma4 = Rpretosoma1;
354 Rsomatopost4 = Rsomatopost1;
355 R(16,4) = NaN; % Soma of fibre 4 has index 16
356
357 % Half resistance
358 Rhalf = R./2; %[kOhm]
359
360 % Calculate surface area
361 A = (2*(dcomp/2).*pi.*lcomp)*1e-08; % [cm^2]
362 % Fibre 1
363 Abuff = (dsoma/2-sqrt((dsoma/2)^2-(dperi/2)^2)); % [µm]
364 Abuff2 = (dsoma/2-sqrt((dsoma/2)^2-(dcent/2)^2)); % [µm]
365 Asoma = (4*(dsoma/2)^2.*pi-((dsoma*pi*Abuff)+(dsoma*pi*
       Abuff2)))*1e-08; % [cm^2]
366 A(14,1) = Asoma;
367 % Fibre 2 geometry is identical
368 A(16,2) = Asoma;
369 % Fibre 3 geometry is identical
370 A(16,3) = Asoma;
371 % Fibre 4 geometry is identical
372 A(16,4) = Asoma;
373
374 % Calculate Membrane Capacitance
375 C = ccomp.*A; % [µF]
376
377 % Set up matrices per fibre for calculation
378 switch fibre
379     case 'F1'
380         ncomp = length(F1_compcent);
381         R2 = Rhalf(1:length(F1_compcent),1);
382         R2_ = circshift(R2,1);
383         R2__ = circshift(R2,-1);
384         % Tridiagonal matrix (=axial resistance) for
              later Istim calculation
385         axres_dia = [-1/(R2(1)+R2(2));-1./(R2_(2:end-1)+
              R2(2:end-1))-1./(R2__(2:end-1)+R2(2:end-1))
              ;-1/(R2(end-1)+R2(end))]; % [1/V]
386         axres_offdia1 = 1./(circshift(R2(2:end),1)+R2(2:
              end));
387         axres_offdia2 = 1./(circshift(R2(1:end-1),-1)+R2
              (1:end-1));
388         % Special treatment due to soma
389         axres_dia(13) = -1./(R2(13)+R2(12))-1./(R2(13)+
              Rpretosoma1);
```

```
axres_dia(14) = -1./(R2(13)+Rpretosoma1)-1./(R2(15)+Rsomatopost1);
axres_dia(15) = -1./(R2(15)+Rsomatopost1)-1./(R2(15)+R2(16));
axres_offdia1(13) = 1./(Rpretosoma1+R2(13));
axres_offdia1(14) = 1./(Rsomatopost1+R2(15));
axres_offdia2(13) = 1./(R2(13)+Rpretosoma1);
axres_offdia2(14) = 1./(R2(15)+Rsomatopost1);
% Special treatment due to inhomogenous fibre
axres_offdia1(1) = 1./(R2(1)+R2(2));
axres_offdia2(36) = 1./(R2(36)+R2(37));
% Tridiagonal matrix
axres = diag(axres_dia,0)+diag(axres_offdia1,-1)+diag(axres_offdia2,1); % [mS]

% Split up capacitance matrix to get rid of 'NaN'
C = C(1:length(F1_compcent),1);
A = A(1:length(F1_compcent),1); % Get rid of NaN for later usage
% Inverse Matrix
invax_dia = [1+(dt/C(1))*(1/(R2(1)+R2(2))); ones(length(F1_compcent)-2,1)+(dt./C(2:end-1)).*(1./(R2_(2:end-1)+R2(2:end-1)) + 1./(R2__(2:end-1)+R2(2:end-1)));1+(dt/C(end)).*(1/(R2(end-1)+R2(end)))]; % []
invax_offdia1 = -(dt./C(2:end)).*(1./(circshift(R2(2:end),1)+R2(2:end))); %[]
invax_offdia2 = -(dt./C(1:end-1)).*(1./(circshift(R2(1:end-1),-1)+R2(1:end-1))); %[]
% Special treatment for soma
invax_dia(13) = 1+(dt./C(13)).*(1./(R2_(13)+R2(13))+ 1./(Rpretosoma1+R2(13)));
invax_dia(14) = 1+(dt./C(14)).*(1./(R2_(14)+Rpretosoma1)+ 1./(Rsomatopost1+R2__(14)));
invax_dia(15) = 1+(dt./C(15)).*(1./(R2(15)+Rsomatopost1)+ 1./(R2__(15)+R2(15)));
invax_offdia1(13) = -(dt./C(14)).*(1./(Rpretosoma1+R2(13)));
invax_offdia1(14) = -(dt./C(15)).*(1./(Rsomatopost1+R2(15)));
invax_offdia2(13) = -(dt./C(13)).*(1./(Rpretosoma1+R2(13)));
invax_offdia2(14) = -(dt./C(14)).*(1./(Rsomatopost1+R2(15)));
```

```
417         % Special treatment due to inhomogeneous fibre
418         invax_offdia1(1) = -(dt./C(2)).*(1./(R2(2)+R2(1))
               );
419         invax_offdia2(36) = -(dt./C(36)).*(1./(R2(36)+R2
               (37)));
420         % Inverse Matrix
421         invax = diag(invax_dia,0) + diag(invax_offdia1
               ,-1) + diag(invax_offdia2,1);
422
423         % Split up matrices for later usage
424         lcomp = lcomp(1:length(F1_compcent),1);
425         dcomp = dcomp(1:length(F1_compcent),1);
426         ccomp = ccomp(1:length(F1_compcent),1);
427         gNacomp = gNacomp(1:length(F1_compcent),1);
428         gKcomp = gKcomp(1:length(F1_compcent),1);
429         gLcomp = gLcomp(1:length(F1_compcent),1);
430
431     case 'F2'
432         ncomp = length(F2_compcent);
433         R2 = Rhalf(1:length(F2_compcent),2);
434         R2_ = circshift(R2,1);
435         R2__ = circshift(R2,-1);
436         axres_dia = [-1/(R2(1)+R2(2));-1./(R2_(2:end-1)+
               R2(2:end-1))-1./(R2__(2:end-1)+R2(2:end-1))
               ;-1/(R2(end-1)+R2(end))]; % [1/V]
437         axres_offdia1 = 1./(circshift(R2(2:end),1)+R2(2:
               end));
438         axres_offdia2 = 1./(circshift(R2(1:end-1),-1)+R2
               (1:end-1));
439         % Special treatment for soma
440         axres_dia(15) = -1./(R2(15)+R2(14))-1./(R2(15)+
               Rpretosoma2);
441         axres_dia(16) = -1./(R2(15)+Rpretosoma2)-1./(R2
               (17)+Rsomatopost2);
442         axres_dia(17) = -1./(R2(17)+Rsomatopost2)-1./(R2
               (17)+R2(18));
443         axres_offdia1(15) = 1./(Rpretosoma2+R2(15));
444         axres_offdia1(16) = 1./(Rsomatopost2+R2(17));
445         axres_offdia2(15) = 1./(R2(15)+Rpretosoma2);
446         axres_offdia2(16) = 1./(R2(17)+Rsomatopost2);
447         % Special treatment due to inhomogeneous fibre
448         axres_offdia1(1) = 1./(R2(1)+R2(2));
449         axres_offdia2(30) = 1./(R2(30)+R2(31));
450         % Tridiagonal matrix
```

```
451         axres = diag(axres_dia,0)+diag(axres_offdia1,-1)+
               diag(axres_offdia2,1); % [mS]
452
453         % Split up capacitance matrix to get rid of 'NaN'
454         C = C(1:length(F2_compcent),2);
455         A = A(1:length(F2_compcent),2); % Get rid of NaN
               for later usage
456         % Inverse Matrix
457         invax_dia = [1+(dt/C(1))*(1/(R2(1)+R2(2))); ones(
               length(F2_compcent)-2,1)+(dt./C(2:end-1))
               .*(1./(R2_(2:end-1)+R2(2:end-1)) + 1./(R2__(2:
               end-1)+R2(2:end-1)));1+(dt/C(end)).*(1/(R2(end
               -1)+R2(end)))]; % []
458         invax_offdia1 = -(dt./C(2:end)).*(1./(circshift(
               R2(2:end),1)+R2(2:end))); %[]
459         invax_offdia2 = -(dt./C(1:end-1)).*(1./(circshift
               (R2(1:end-1),-1)+R2(1:end-1))); %[]
460         % Special treatment for soma
461         invax_dia(15) = 1+(dt./C(15)).*(1./(R2(14)+R2(15)
               )+ 1./(Rpretosoma2+R2(15)));
462         invax_dia(16) = 1+(dt./C(16)).*(1./(R2(15)+
               Rpretosoma2)+ 1./(Rsomatopost2+R2(17)));
463         invax_dia(17) = 1+(dt./C(17)).*(1./(R2(17)+
               Rsomatopost2)+ 1./(R2(18)+R2(17)));
464         invax_offdia1(15) = -(dt./C(16)).*(1./(
               Rpretosoma2+R2(15)));
465         invax_offdia1(16) = -(dt./C(17)).*(1./(
               Rsomatopost2+R2(17)));
466         invax_offdia2(15) = -(dt./C(15)).*(1./(
               Rpretosoma2+R2(15)));
467         invax_offdia2(16) = -(dt./C(16)).*(1./(
               Rsomatopost2+R2(17)));
468         % Special treatment due to inhomogeneous fibre
469         invax_offdia1(1) = -(dt./C(2)).*(1./(R2(2)+R2(1))
               );
470         invax_offdia2(30) = -(dt./C(30)).*(1./(R2(30)+R2
               (31)));
471         % Inverse Matrix
472         invax = diag(invax_dia,0) + diag(invax_offdia1
               ,-1) + diag(invax_offdia2,1); %[]
473
474         % Split up matrices for later usage
475         lcomp = lcomp(1:length(F2_compcent),2);
476         dcomp = dcomp(1:length(F2_compcent),2);
```

```
477         ccomp = ccomp(1:length(F2_compcent),2);
478         gNacomp = gNacomp(1:length(F2_compcent),2);
479         gKcomp = gKcomp(1:length(F2_compcent),2);
480         gLcomp = gLcomp(1:length(F2_compcent),2);
481
482     case 'F3'
483         ncomp = length(F3_compcent);
484         R2 = Rhalf(1:length(F3_compcent),3);
485         R2_ = circshift(R2,1);
486         R2__ = circshift(R2,-1);
487         axres_dia = [-1/(R2(1)+R2(2));-1./(R2_(2:end-1)+
                R2(2:end-1))-1./(R2__(2:end-1)+R2(2:end-1))
                ;-1/(R2(end-1)+R2(end))]; % in [1/V]
488         axres_offdia1 = 1./(circshift(R2(2:end),1)+R2(2:
                end));
489         axres_offdia2 = 1./(circshift(R2(1:end-1),-1)+R2
                (1:end-1));
490         % Special treatment for soma
491         axres_dia(15) = -1./(R2(15)+R2(14))-1./(R2(15)+
                Rpretosoma3);
492         axres_dia(16) = -1./(R2(15)+Rpretosoma3)-1./(R2
                (17)+Rsomatopost3);
493         axres_dia(17) = -1./(R2(17)+Rsomatopost3)-1./(R2
                (17)+R2(18));
494         axres_offdia1(15) = 1./(Rpretosoma3+R2(15));
495         axres_offdia1(16) = 1./(Rsomatopost3+R2(17));
496         axres_offdia2(15) = 1./(R2(15)+Rpretosoma3);
497         axres_offdia2(16) = 1./(R2(17)+Rsomatopost3);
498         % Special treatment due to inhomogeneous fibre
499         axres_offdia1(1) = 1./(R2(1)+R2(2));
500         axres_offdia2(28) = 1./(R2(28)+R2(29));
501         % Tridiagonal matrix
502         axres = diag(axres_dia,0)+diag(axres_offdia1,-1)+
                diag(axres_offdia2,1); % [mS]
503
504         % Split up capacitance matrix to get rid of 'NaN'
505         C = C(1:length(F3_compcent),3);
506         A = A(1:length(F3_compcent),3); % Get rid of NaN
                for later usage
507         % Inverse Matrix
508         invax_dia = [1+(dt/C(1))*(1/(R2(1)+R2(2))); ones(
                length(F3_compcent)-2,1)+(dt./C(2:end-1))
                .*(1./(R2_(2:end-1)+R2(2:end-1)) + 1./(R2__(2:
                end-1)+R2(2:end-1)));1+(dt/C(end)).*(1/(R2(end
```

```
        -1)+R2(end)))]; % []
509     invax_offdia1 = -(dt./C(2:end)).*(1./(circshift(
        R2(2:end),1)+R2(2:end))); %[]
510     invax_offdia2 = -(dt./C(1:end-1)).*(1./(circshift
        (R2(1:end-1),-1)+R2(1:end-1))); %[]
511     % Special treatment for soma
512     invax_dia(15) = 1+(dt./C(15)).*(1./(R2(14)+R2(15)
        )+ 1./(Rpretosoma3+R2(15)));
513     invax_dia(16) = 1+(dt./C(16)).*(1./(R2(15)+
        Rpretosoma3)+ 1./(Rsomatopost3+R2(17)));
514     invax_dia(17) = 1+(dt./C(17)).*(1./(R2(17)+
        Rsomatopost3)+ 1./(R2(18)+R2(17)));
515     invax_offdia1(15) = -(dt./C(16)).*(1./(
        Rpretosoma3+R2(15))); %[]
516     invax_offdia1(16) = -(dt./C(17)).*(1./(
        Rsomatopost3+R2(17))); %[]
517     invax_offdia2(15) = -(dt./C(15)).*(1./(
        Rpretosoma3+R2(15))); %[]
518     invax_offdia2(16) = -(dt./C(16)).*(1./(
        Rsomatopost3+R2(17))); %[]
519     % Special treatment due to inhomogeneous fibre
520     invax_offdia1(1) = -(dt./C(2)).*(1./(R2(2)+R2(1))
        );
521     invax_offdia2(28) = -(dt./C(28)).*(1./(R2(28)+R2
        (29)));
522     % Inverse Matrix
523     invax = diag(invax_dia,0) + diag(invax_offdia1
        ,-1) + diag(invax_offdia2,1); %[]
524
525     % Split up matrices for later usage
526     lcomp = lcomp(1:length(F3_compcent),3);
527     dcomp = dcomp(1:length(F3_compcent),3);
528     ccomp = ccomp(1:length(F3_compcent),3);
529     gNacomp = gNacomp(1:length(F3_compcent),3);
530     gKcomp = gKcomp(1:length(F3_compcent),3);
531     gLcomp = gLcomp(1:length(F3_compcent),3);
532
533 case 'F4'
534     ncomp = length(F4_compcent);
535     R2 = Rhalf(1:length(F4_compcent),4);
536     R2_ = circshift(R2,1);
537     R2__ = circshift(R2,-1);
538     axres_dia = [-1/(R2(1)+R2(2));-1./(R2_(2:end-1)+
        R2(2:end-1))-1./(R2__(2:end-1)+R2(2:end-1))
```

```
   ;-1/(R2(end-1)+R2(end))]; % [1/V]
axres_offdia1 = 1./(circshift(R2(2:end),1)+R2(2:
   end));
axres_offdia2 = 1./(circshift(R2(1:end-1),-1)+R2
   (1:end-1));
% Special treatment for soma
axres_dia(15) = -1./(R2(15)+R2(14))-1./(R2(15)+
   Rpretosoma4);
axres_dia(16) = -1./(R2(15)+Rpretosoma4)-1./(R2
   (17)+Rsomatopost4);
axres_dia(17) = -1./(R2(17)+Rsomatopost4)-1./(R2
   (17)+R2(18));
axres_offdia1(15) = 1./(Rpretosoma4+R2(15));
axres_offdia1(16) = 1./(Rsomatopost4+R2(17));
axres_offdia2(15) = 1./(R2(15)+Rpretosoma4);
axres_offdia2(16) = 1./(R2(17)+Rsomatopost4);
% Special treatment due to inhomogeneous fibre
axres_offdia1(1) = 1./(R2(1)+R2(2));
axres_offdia2(38) = 1./(R2(38)+R2(39));
% Tridiagonal matrix
axres = diag(axres_dia,0)+diag(axres_offdia1,-1)+
   diag(axres_offdia2,1); % [mS]

% Split up capacitance matrix to get rid of 'NaN'
C = C(1:length(F4_compcent),4);
A = A(1:length(F4_compcent),4); % Get rid of NaN
   for later usage
% Inverse Matrix
invax_dia = [1+(dt/C(1))*(1/(R2(1)+R2(2))); ones(
   length(F4_compcent)-2,1)+(dt./C(2:end-1))
   .*(1./(R2_(2:end-1)+R2(2:end-1)) + 1./(R2__(2:
   end-1)+R2(2:end-1)));1+(dt/C(end)).*(1/(R2(end
   -1)+R2(end)))]; % []
invax_offdia1 = -(dt./C(2:end)).*(1./(circshift(
   R2(2:end),1)+R2(2:end))); %[]
invax_offdia2 = -(dt./C(1:end-1)).*(1./(circshift
   (R2(1:end-1),-1)+R2(1:end-1))); %[]
% Special treatment for soma
invax_dia(15) = 1+(dt./C(15)).*(1./(R2(14)+R2(15)
   )+ 1./(Rpretosoma4+R2(15)));
invax_dia(16) = 1+(dt./C(16)).*(1./(R2(15)+
   Rpretosoma4)+ 1./(Rsomatopost4+R2(17)));
invax_dia(17) = 1+(dt./C(17)).*(1./(R2(17)+
   Rsomatopost4)+ 1./(R2(18)+R2(17)));
```

```
566         invax_offdia1(15) = -(dt./C(16)).*(1./(
               Rpretosoma4+R2(15))); %[]
567         invax_offdia1(16) = -(dt./C(17)).*(1./(
               Rsomatopost4+R2(17))); %[]
568         invax_offdia2(15) = -(dt./C(15)).*(1./(
               Rpretosoma4+R2(15))); %[]
569         invax_offdia2(16) = -(dt./C(16)).*(1./(
               Rsomatopost4+R2(17))); %[]
570         % Special treatment due to inhomogeneous fibre
571         invax_offdia1(1) = -(dt./C(2)).*(1./(R2(2)+R2(1))
               );
572         invax_offdia2(38) = -(dt./C(38)).*(1./(R2(38)+R2
               (39)));
573         % Inverse Matrix
574         invax = diag(invax_dia,0) + diag(invax_offdia1
               ,-1) + diag(invax_offdia2,1); %[]
575
576         % Split up matrices for later usage
577         lcomp = lcomp(1:length(F4_compcent),4);
578         dcomp = dcomp(1:length(F4_compcent),4);
579         ccomp = ccomp(1:length(F4_compcent),4);
580         gNacomp = gNacomp(1:length(F4_compcent),4);
581         gKcomp = gKcomp(1:length(F4_compcent),4);
582         gLcomp = gLcomp(1:length(F4_compcent),4);
583
584     otherwise
585             disp('No fibre found')
586 end
587
588 %% ---------------------- Step 3: Extracellular Potential
       ------------------
589 % Calculate Extracellular Potential [mV]
590 switch fibre
591     case 'F1'
592
593         switch electrode
594             case 'T1'
595                 xy = zeros(size(F1_compcent));
596                 xy(:,1) = El_coordinates(1,1); % x-
                       coordinate  of electrode [µm]
597                 xy(:,2) = El_coordinates(1,2); % y-
                       coordinate of electrode [µm]
598
599                 diff = F1_compcent - xy; % vector between
```

```
                T1 and F1 compcenters [µm]
600             dist = 1e-04*sqrt((diff(:,1).^2+diff(:,2)
                .^2)); % length of each vector [cm]
601
602             Ve = 1e-03*(rhoe*Iel)./(4*pi*dist); %
                Extracellular Potential in [mV]
603
604         case 'T2'
605             xy = zeros(size(F1_compcent));
606             xy(:,1) = El_coordinates(2,1); % x-
                coordinate  of electrode [µm]
607             xy(:,2) = El_coordinates(2,2); % y-
                coordinate of electrode [µm]
608
609             diff = F1_compcent - xy; % vector between
                T2 and F1 compcenters [µm]
610             dist = 1e-04*sqrt((diff(:,1).^2+diff(:,2)
                .^2)); % length of each vector [cm]
611
612             Ve = 1e-03*(rhoe*Iel)./(4*pi*dist); %
                Extracellular Potential in [mV]
613
614         case 'T2prime'
615             xy = zeros(size(F1_compcent));
616             xy(:,1) = El_coordinates(17,1); % x-
                coordinate  of electrode [µm]
617             xy(:,2) = El_coordinates(17,2); % y-
                coordinate of electrode [µm]
618
619             diff = F1_compcent - xy; % vector between
                T2' and F1 compcenters [µm]
620             dist = 1e-04*sqrt((diff(:,1).^2+diff(:,2)
                .^2)); % length of each vector [cm]
621
622             Ve = 1e-03*(rhoe*Iel)./(4*pi*dist); %
                Extracellular Potential in [mV]
623
624         case 'T3'
625             xy = zeros(size(F1_compcent));
626             xy(:,1) = El_coordinates(3,1); % x-
                coordinate  of electrode [µm]
627             xy(:,2) = El_coordinates(3,2); % y-
                coordinate of electrode [µm]
628
```

```
629                 diff = F1_compcent - xy; % vector between
                        T3 and F1 compcenters [µm]
630                 dist = 1e-04*sqrt((diff(:,1).^2+diff(:,2)
                    .^2)); % length of each vector [cm]
631
632                 Ve = 1e-03*(rhoe*Iel)./(4*pi*dist); %
                    Extracellular Potential in [mV]
633
634             case 'T4'
635                 xy = zeros(size(F1_compcent));
636                 xy(:,1) = El_coordinates(4,1); % x-
                    coordinate  of electrode [µm]
637                 xy(:,2) = El_coordinates(4,2); % y-
                    coordinate of electrode [µm]
638
639                 diff = F1_compcent - xy; % vector between
                        T4 and F1 compcenters [µm]
640                 dist = 1e-04*sqrt((diff(:,1).^2+diff(:,2)
                    .^2)); % length of each vector [cm]
641
642                 Ve = 1e-03*(rhoe*Iel)./(4*pi*dist); %
                    Extracellular Potential in [mV]
643
644             case 'V1'
645                 xy = zeros(size(F1_compcent));
646                 xy(:,1) = El_coordinates(1,3); % x-
                    coordinate  of electrode [µm]
647                 xy(:,2) = El_coordinates(1,4); % y-
                    coordinate of electrode [µm]
648
649                 diff = F1_compcent - xy; % vector between
                        V1 and F1 compcenters [µm]
650                 dist = 1e-04*sqrt((diff(:,1).^2+diff(:,2)
                    .^2)); % length of each vector [cm]
651
652                 Ve = 1e-03*(rhoe*Iel)./(4*pi*dist); %
                    Extracellular Potential in [mV]
653
654             case 'V2'
655                 xy = zeros(size(F1_compcent));
656                 xy(:,1) = El_coordinates(2,3); % x-
                    coordinate  of electrode [µm]
657                 xy(:,2) = El_coordinates(2,4); % y-
                    coordinate of electrode [µm]
```

```
658
659                 diff = F1_compcent - xy; % vector between
                        V2 and F1 compcenters [µm]
660                 dist = 1e-04*sqrt((diff(:,1).^2+diff(:,2)
                        .^2)); % length of each vector [cm]
661
662                 Ve = 1e-03*(rhoe*Iel)./(4*pi*dist); %
                        Extracellular Potential in [mV]
663
664             case 'V3'
665                 xy = zeros(size(F1_compcent));
666                 xy(:,1) = El_coordinates(3,3); % x-
                        coordinate  of electrode [µm]
667                 xy(:,2) = El_coordinates(3,4); % y-
                        coordinate of electrode [µm]
668
669                 diff = F1_compcent - xy; % vector between
                        V3 and F1 compcenters [µm]
670                 dist = 1e-04*sqrt((diff(:,1).^2+diff(:,2)
                        .^2)); % length of each vector [cm]
671
672                 Ve = 1e-03*(rhoe*Iel)./(4*pi*dist); %
                        Extracellular Potential in [mV]
673             otherwise
674             disp('No fibre found')
675         end
676     case 'F2'
677         switch electrode
678             case 'T5'
679                 xy = zeros(size(F2_compcent));
680                 xy(:,1) = El_coordinates(5,1); % x-
                        coordinate  of electrode [µm]
681                 xy(:,2) = El_coordinates(5,2); % y-
                        coordinate of electrode [µm]
682
683                 diff = F2_compcent - xy; % vector between
                        T5 and F2 compcenters [µm]
684                 dist = 1e-04*sqrt((diff(:,1).^2+diff(:,2)
                        .^2)); % length of each vector [cm]
685
686                 Ve = 1e-03*(rhoe*Iel)./(4*pi*dist); %
                        Extracellular Potential in [mV]
687
688             case 'T6'
```

```
689                 xy = zeros(size(F2_compcent));
690                 xy(:,1) = El_coordinates(6,1); % x-
                        coordinate  of electrode [µm]
691                 xy(:,2) = El_coordinates(6,2); % y-
                        coordinate of electrode [µm]
692
693                 diff = F2_compcent - xy; % vector between
                         T6 and F2 compcenters [µm]
694                 dist = 1e-04*sqrt((diff(:,1).^2+diff(:,2)
                        .^2)); % length of each vector [cm]
695
696                 Ve = 1e-03*(rhoe*Iel)./(4*pi*dist); %
                        Extracellular Potential in [mV]
697
698             case 'T7'
699                 xy = zeros(size(F2_compcent));
700                 xy(:,1) = El_coordinates(7,1); % x-
                        coordinate  of electrode [µm]
701                 xy(:,2) = El_coordinates(7,2); % y-
                        coordinate of electrode [µm]
702
703                 diff = F2_compcent - xy; % vector between
                         T7 and F2 compcenters [µm]
704                 dist = 1e-04*sqrt((diff(:,1).^2+diff(:,2)
                        .^2)); % length of each vector [cm]
705
706                 Ve = 1e-03*(rhoe*Iel)./(4*pi*dist); %
                        Extracellular Potential in [mV]
707
708             case 'T8'
709                 xy = zeros(size(F2_compcent));
710                 xy(:,1) = El_coordinates(8,1); % x-
                        coordinate  of electrode [µm]
711                 xy(:,2) = El_coordinates(8,2); % y-
                        coordinate of electrode [µm]
712
713                 diff = F2_compcent - xy; % vector between
                         T8 and F2 compcenters [µm]
714                 dist = 1e-04*sqrt((diff(:,1).^2+diff(:,2)
                        .^2)); % length of each vector [cm]
715
716                 Ve = 1e-03*(rhoe*Iel)./(4*pi*dist); %
                        Extracellular Potential in [mV]
717
```

```
718             case 'V4'
719                 xy = zeros(size(F2_compcent));
720                 xy(:,1) = El_coordinates(5,3); % x-
                        coordinate  of electrode [µm]
721                 xy(:,2) = El_coordinates(5,4); % y-
                        coordinate of electrode [µm]
722
723                 diff = F2_compcent - xy; % vector between
                         V4 and F2 compcenters [µm]
724                 dist = 1e-04*sqrt((diff(:,1).^2+diff(:,2)
                        .^2)); % length of each vector [cm]
725
726                 Ve = 1e-03*(rhoe*Iel)./(4*pi*dist); %
                        Extracellular Potential in [mV]
727
728             case 'V5'
729                 xy = zeros(size(F2_compcent));
730                 xy(:,1) = El_coordinates(6,3); % x-
                        coordinate  of electrode [µm]
731                 xy(:,2) = El_coordinates(6,4); % y-
                        coordinate of electrode [µm]
732
733                 diff = F2_compcent - xy; % vector between
                         V5 and F2 compcenters [µm]
734                 dist = 1e-04*sqrt((diff(:,1).^2+diff(:,2)
                        .^2)); % length of each vector [cm]
735
736                 Ve = 1e-03*(rhoe*Iel)./(4*pi*dist); %
                        Extracellular Potential in [mV]
737
738             case 'V6'
739                 xy = zeros(size(F2_compcent));
740                 xy(:,1) = El_coordinates(7,3); % x-
                        coordinate  of electrode [µm]
741                 xy(:,2) = El_coordinates(7,4); % y-
                        coordinate of electrode [µm]
742
743                 diff = F2_compcent - xy; % vector between
                         V6 and F2 compcenters [µm]
744                 dist = 1e-04*sqrt((diff(:,1).^2+diff(:,2)
                        .^2)); % length of each vector [cm]
745
746                 Ve = 1e-03*(rhoe*Iel)./(4*pi*dist); %
                        Extracellular Potential in [mV]
```

```
747             otherwise
748             disp('No fibre found')
749         end
750
751     case 'F3'
752         switch electrode
753             case 'T9'
754                 xy = zeros(size(F3_compcent));
755                 xy(:,1) = El_coordinates(9,1); % x-
                        coordinate  of electrode [µm]
756                 xy(:,2) = El_coordinates(9,2); % y-
                        coordinate of electrode [µm]
757
758                 diff = F3_compcent - xy; % vector between
                         T9 and F3 compcenters [µm]
759                 dist = 1e-04*sqrt((diff(:,1).^2+diff(:,2)
                        .^2)); % length of each vector [cm]
760
761                 Ve = 1e-03*(rhoe*Iel)./(4*pi*dist); %
                        Extracellular Potential in [mV]
762
763             case 'T10'
764                 xy = zeros(size(F3_compcent));
765                 xy(:,1) = El_coordinates(10,1); % x-
                        coordinate  of electrode [µm]
766                 xy(:,2) = El_coordinates(10,2); % y-
                        coordinate of electrode [µm]
767
768                 diff = F3_compcent - xy; % vector between
                         T10 and F3 compcenters [µm]
769                 dist = 1e-04*sqrt((diff(:,1).^2+diff(:,2)
                        .^2)); % length of each vector [cm]
770
771                 Ve = 1e-03*(rhoe*Iel)./(4*pi*dist); %
                        Extracellular Potential in [mV]
772
773             case 'T11'
774                 xy = zeros(size(F3_compcent));
775                 xy(:,1) = El_coordinates(11,1); % x-
                        coordinate  of electrode [µm]
776                 xy(:,2) = El_coordinates(11,2); % y-
                        coordinate of electrode [µm]
777
778                 diff = F3_compcent - xy; % vector between
```

```
                T11 and F3 compcenters [µm]
779             dist = 1e-04*sqrt((diff(:,1).^2+diff(:,2)
                .^2)); % length of each vector [cm]
780
781             Ve = 1e-03*(rhoe*Iel)./(4*pi*dist); %
                Extracellular Potential in [mV]
782
783         case 'T12'
784             xy = zeros(size(F3_compcent));
785             xy(:,1) = El_coordinates(12,1); % x-
                coordinate  of electrode [µm]
786             xy(:,2) = El_coordinates(12,2); % y-
                coordinate of electrode [µm]
787
788             diff = F3_compcent - xy; % vector between
                T12 and F3 compcenters [µm]
789             dist = 1e-04*sqrt((diff(:,1).^2+diff(:,2)
                .^2)); % length of each vector [cm]
790
791             Ve = 1e-03*(rhoe*Iel)./(4*pi*dist); %
                Extracellular Potential in [mV]
792
793         case 'V7'
794             xy = zeros(size(F3_compcent));
795             xy(:,1) = El_coordinates(9,3); % x-
                coordinate  of electrode [µm]
796             xy(:,2) = El_coordinates(9,4); % y-
                coordinate of electrode [µm]
797
798             diff = F3_compcent - xy; % vector between
                V7 and F3 compcenters [µm]
799             dist = 1e-04*sqrt((diff(:,1).^2+diff(:,2)
                .^2)); % length of each vector [cm]
800
801             Ve = 1e-03*(rhoe*Iel)./(4*pi*dist); %
                Extracellular Potential in [mV]
802
803         case 'V8'
804             xy = zeros(size(F3_compcent));
805             xy(:,1) = El_coordinates(10,3); % x-
                coordinate  of electrode [µm]
806             xy(:,2) = El_coordinates(10,4); % y-
                coordinate of electrode [µm]
807
```

```
808                 diff = F3_compcent - xy; % vector between
                        V8 and F3 compcenters [µm]
809                 dist = 1e-04*sqrt((diff(:,1).^2+diff(:,2)
                        .^2)); % length of each vector [cm]
810
811                 Ve = 1e-03*(rhoe*Iel)./(4*pi*dist); %
                        Extracellular Potential in [mV]
812
813             case 'V9'
814                 xy = zeros(size(F3_compcent));
815                 xy(:,1) = El_coordinates(11,3); % x-
                        coordinate  of electrode [µm]
816                 xy(:,2) = El_coordinates(11,4); % y-
                        coordinate of electrode [µm]
817
818                 diff = F3_compcent - xy; % vector between
                        V9 and F3 compcenters [µm]
819                 dist = 1e-04*sqrt((diff(:,1).^2+diff(:,2)
                        .^2)); % length of each vector [cm]
820
821                 Ve = 1e-03*(rhoe*Iel)./(4*pi*dist); %
                        Extracellular Potential in [mV]
822             otherwise
823                 disp('No fibre found')
824         end
825     case 'F4'
826         switch electrode
827             case 'T13'
828                 xy = zeros(size(F4_compcent));
829                 xy(:,1) = El_coordinates(13,1); % x-
                        coordinate  of electrode [µm]
830                 xy(:,2) = El_coordinates(13,2); % y-
                        coordinate of electrode [µm]
831
832                 diff = F4_compcent - xy; % vector between
                        T13 and F4 compcenters [µm]
833                 dist = 1e-04*sqrt((diff(:,1).^2+diff(:,2)
                        .^2)); % length of each vector [cm]
834
835                 Ve = 1e-03*(rhoe*Iel)./(4*pi*dist); %
                        Extracellular Potential in [mV]
836
837             case 'T14'
838                 xy = zeros(size(F4_compcent));
```

```
839                 xy(:,1) = El_coordinates(14,1); % x-
                        coordinate  of electrode [µm]
840                 xy(:,2) = El_coordinates(14,2); % y-
                        coordinate of electrode [µm]
841
842                 diff = F4_compcent - xy; % vector between
                         T14 and F4 compcenters [µm]
843                 dist = 1e-04*sqrt((diff(:,1).^2+diff(:,2)
                        .^2)); % length of each vector [cm]
844
845                 Ve = 1e-03*(rhoe*Iel)./(4*pi*dist); %
                        Extracellular Potential in [mV]
846
847              case 'T15'
848                 xy = zeros(size(F4_compcent));
849                 xy(:,1) = El_coordinates(15,1); % x-
                        coordinate  of electrode [µm]
850                 xy(:,2) = El_coordinates(15,2); % y-
                        coordinate of electrode [µm]
851
852                 diff = F4_compcent - xy; % vector between
                         T15 and F4 compcenters [µm]
853                 dist = 1e-04*sqrt((diff(:,1).^2+diff(:,2)
                        .^2)); % length of each vector [cm]
854
855                 Ve = 1e-03*(rhoe*Iel)./(4*pi*dist); %
                        Extracellular Potential in [mV]
856
857              case 'T16'
858                 xy = zeros(size(F4_compcent));
859                 xy(:,1) = El_coordinates(16,1); % x-
                        coordinate  of electrode [µm]
860                 xy(:,2) = El_coordinates(16,2); % y-
                        coordinate of electrode [µm]
861
862                 diff = F4_compcent - xy; % vector between
                         T16 and F4 compcenters [µm]
863                 dist = 1e-04*sqrt((diff(:,1).^2+diff(:,2)
                        .^2)); % length of each vector [cm]
864
865                 Ve = 1e-03*(rhoe*Iel)./(4*pi*dist); %
                        Extracellular Potential in [mV]
866
867              case 'V10'
```

```
868                 xy = zeros(size(F4_compcent));
869                 xy(:,1) = El_coordinates(13,3); % x-
                        coordinate  of electrode [µm]
870                 xy(:,2) = El_coordinates(13,4); % y-
                        coordinate of electrode [µm]
871
872                 diff = F4_compcent - xy; % vector between
                         V10 and F4 compcenters [µm]
873                 dist = 1e-04*sqrt((diff(:,1).^2+diff(:,2)
                        .^2)); % length of each vector [cm]
874
875                 Ve = 1e-03*(rhoe*Iel)./(4*pi*dist); %
                        Extracellular Potential in [mV]
876
877              case 'V11'
878                 xy = zeros(size(F4_compcent));
879                 xy(:,1) = El_coordinates(14,3); % x-
                        coordinate  of electrode [µm]
880                 xy(:,2) = El_coordinates(14,4); % y-
                        coordinate of electrode [µm]
881
882                 diff = F4_compcent - xy; % vector between
                         V11 and F4 compcenters [µm]
883                 dist = 1e-04*sqrt((diff(:,1).^2+diff(:,2)
                        .^2)); % length of each vector [cm]
884
885                 Ve = 1e-03*(rhoe*Iel)./(4*pi*dist); %
                        Extracellular Potential in [mV]
886
887             case 'V12'
888                 xy = zeros(size(F4_compcent));
889                 xy(:,1) = El_coordinates(15,3); % x-
                        coordinate  of electrode [µm]
890                 xy(:,2) = El_coordinates(15,4); % y-
                        coordinate of electrode [µm]
891
892                 diff = F4_compcent - xy; % vector between
                         V12 and F4 compcenters [µm]
893                 dist = 1e-04*sqrt((diff(:,1).^2+diff(:,2)
                        .^2)); % length of each vector [cm]
894
895                 Ve = 1e-03*(rhoe*Iel)./(4*pi*dist); %
                        Extracellular Potential in [mV]
896             otherwise
```

```
897                 disp('No fibre found')
898
899         end
900
901 end
902
903 if degenerated == 1
904   switch fibre
905       case 'F1'
906             % Fibre 1
907             invax = invax(14:end,14:end);
908             % Adapt due to missing soma neighbor
909             invax(1,1) = invax(1,1) + -(dt./C(14)).*(1./(
                    Rpretosoma1+R2(13)));
910             % New main diagonal
911             invax_dia = diag(invax);
912             % Cut matrix
913             axres = axres(14:end,14:end);
914             % Adapt due to missing soma neighbor
915             axres(1,1) = axres(1,1) + 1./(Rpretosoma1+R2
                    (13));
916
917             % Cut remaining matrices
918             Ve = Ve(14:end);
919             A = A(14:end);
920             C = C(14:end);
921             F1_compcent = F1_compcent(14:end,:);
922             ncomp = length(F1_compcent);
923             lcomp = lcomp(14:end);
924             dcomp = dcomp(14:end);
925             ccomp = ccomp(14:end);
926             gNacomp = gNacomp(14:end);
927             gKcomp = gKcomp(14:end);
928             gLcomp = gLcomp(14:end);
929
930       case 'F2'
931           % Fibre 2
932             invax = invax(16:end,16:end);
933             % Adapt due to missing soma neighbor
934             invax(1,1) = invax(1,1) + -(dt./C(16)).*(1./(
                    Rpretosoma2+R2(15)));
935             % New main diagonal
936             invax_dia = diag(invax);
937             % Cut matrix
```

```
938             axres = axres(16:end,16:end);
939             % Adapt due to missing soma neighbor
940             axres(1,1) = axres(1,1) + 1./(Rpretosoma2+R2
                    (15));
941
942             % Cut remaining matrices
943             Ve = Ve(16:end);
944             A = A(16:end);
945             C = C(16:end);
946             F2_compcent = F2_compcent(16:end,:);
947             ncomp = length(F2_compcent);
948             lcomp = lcomp(16:end);
949             dcomp = dcomp(16:end);
950             ccomp = ccomp(16:end);
951             gNacomp = gNacomp(16:end);
952             gKcomp = gKcomp(16:end);
953             gLcomp = gLcomp(16:end);
954
955         case 'F3'
956             % Fibre 3
957             invax = invax(16:end,16:end);
958             % Adapt due to missing soma neighbor
959             invax(1,1) = invax(1,1) + -(dt./C(16)).*(1./(
                    Rpretosoma3+R2(15)));
960             % New main diagonal
961             invax_dia = diag(invax);
962             % Cut matrix
963             axres = axres(16:end,16:end);
964             % Adapt due to missing soma neighbor
965             axres(1,1) = axres(1,1) + 1./(Rpretosoma3+R2
                    (15));
966
967             % Cut remaining matrices
968             Ve = Ve(16:end);
969             A = A(16:end);
970             C = C(16:end);
971             F3_compcent = F3_compcent(16:end,:);
972             ncomp = length(F3_compcent);
973             lcomp = lcomp(16:end);
974             dcomp = dcomp(16:end);
975             ccomp = ccomp(16:end);
976             gNacomp = gNacomp(16:end);
977             gKcomp = gKcomp(16:end);
978             gLcomp = gLcomp(16:end);
```

```
979
980         case 'F4'
981               % Fibre 4
982               invax = invax(16:end,16:end);
983               % Adapt due to missing soma neighbor
984               invax(1,1) = invax(1,1) + -(dt./C(16)).*(1./(
                     Rpretosoma4+R2(15)));
985               % New main diagonal
986               invax_dia = diag(invax);
987               % Cut matrix
988               axres = axres(16:end,16:end);
989               % Adapt due to missing soma neighbor
990               axres(1,1) = axres(1,1) + 1./(Rpretosoma4+R2
                     (15));
991
992               % Cut remaining matrices
993               Ve = Ve(16:end);
994               A = A(16:end);
995               C = C(16:end);
996               F4_compcent = F4_compcent(16:end,:);
997               ncomp = length(F4_compcent);
998               lcomp = lcomp(16:end);
999               dcomp = dcomp(16:end);
1000              ccomp = ccomp(16:end);
1001              gNacomp = gNacomp(16:end);
1002              gKcomp = gKcomp(16:end);
1003              gLcomp = gLcomp(16:end);
1004
1005    end
1006 end
1007
1008 % Stimulus current
1009 iStim = axres*Ve./A; % [μA/cm^2]
1010
1011 % Activating function
1012 actfct = axres*Ve./C; % [mV/ms]
1013
1014
1015 %% -------------- Step 4: Solve Hodgkin-Huxley Model
       ----------------------
1016 % Membrane Potential
1017 V = zeros(ncomp,length(t));
1018 V(:,1) = Vrest;  % Initial membrane voltage [mV]
1019
```

```
% Membrane Potential without initializing phase
Vm = zeros(ncomp,length(time)); % [mV]
s=1;

% Additional BE Voltage
inclVadd = 1; % 1 == Yes, 0 == No
Vadd = 0.001; % [mV]

% Gating variables [1/ms]
% For m's
alphaM = solve_alpham(V(1),Vrest);
betaM = solve_betam(V(1), Vrest);
% For n's
alphaN = solve_alphan(V(1),Vrest);
betaN = solve_betan(V(1),Vrest);
% For h's
alphaH = solve_alphah(V(1),Vrest);
betaH = solve_betah(V(1),Vrest);

% Initialize gating variables for asymptotic values
m = zeros(ncomp,length(t));
n = zeros(ncomp,length(t));
h = zeros(ncomp,length(t));
% Initial values
m(:,1) = alphaM/(alphaM+betaM);
n(:,1) = alphaN/(alphaN+betaN);
h(:,1) = alphaH/(alphaH+betaH);
% m,n,h without initializing phase
mplot = zeros(ncomp,length(time));
nplot = zeros(ncomp,length(time));
hplot = zeros(ncomp,length(time));

% Solve ODE
for i = 1:length(t)
    % Align stimulus with time
    if i > del/dt && i ≤ (del+dur)/dt
        istim = iStim;
    else
       istim = 0; % [μA/cm^2]
    end

     % Calculate Conductances
     gNa(:,i) = gNacomp.*m(:,i).^3.*h(:,i); % [mS/cm^2]
     gK(:,i) = gKcomp.*n(:,i).^4; % [mS/cm^2]
```

```
1064        gL(:,i) = gLcomp; % [mS/cm^2]
1065
1066        % Ionic currents
1067        I_Na(:,i) = gNa(:,i).*(V(:,i)-E_Na); % [µA/cm^2]
1068        I_K(:,i) = gK(:,i).*(V(:,i)-E_K); % [µA/cm^2]
1069        I_L(:,i) = gL(:,i).*(V(:,i)-E_L); % [µA/cm^2]
1070
1071        Iion(:,i) = I_Na(:,i)+I_K(:,i)+I_L(:,i); % [µA/cm^2]
1072
1073        if inclVadd == 1 % Calculation with additional
               auxiliary currents
1074                         % for complete Backward Euler
1075
1076            I_Naadd(:,i) = gNacomp.*m(:,i).^3.*h(:,i).*(V(:,
                   i)+Vadd-E_Na); % [µA/cm^2]
1077            I_Kadd(:,i) = gKcomp.*n(:,i).^4.*(V(:,i)+Vadd-
                   E_K); % [µA/cm^2]
1078            I_Ladd(:,i) = gLcomp.*(V(:,i)+Vadd-E_L); %[µA/cm
                   ^2]
1079
1080            Iionadd(:,i) = (I_Naadd(:,i)-I_Na(:,i)+I_Kadd(:,
                   i)-I_K(:,i)+I_Ladd(:,i)-I_L(:,i))/Vadd; %[(µA
                   /cm^2)/mV]
1081
1082        else
1083            Iionadd(:,i) = 0;
1084
1085        end
1086
1087        % Calculate V
1088        % Vm,n(i+1)*(1-dt/c*axres) = Vm,n,i + dt/c[-Iion+
               Iionadd*Vm,n,i+icomp]
1089        %                 invax                          buff
1090        buff = V(:,i) + (dt./ccomp).*(-Iion(:,i)+Iionadd(:,i
               ).*V(:,i)+istim); %[mV]
1091        % Add auxiliary currents also to other side of
               equation (in main
1092        % diagonal)
1093        invax(1:1+length(invax):end) = invax_dia+Iionadd(:,i
               ).*(dt./ccomp);
1094
1095        % Solve for V
1096        V(:,i+1) = sparse(invax)\buff; % [mV]
1097
```

```
1098        if i > ((del/dt)-(pretime/dt))
1099
1100            Vm(:,s) = V(:,i);
1101            mplot(:,s) = m(:,i);
1102            nplot(:,s) = n(:,i);
1103            hplot(:,s) = h(:,i);
1104            s=s+1;
1105
1106        end
1107
1108        % Get next m,n,h values
1109        m(:,i+1) = (m(:,i)+k*dt*solve_alpham(V(:,i+1),Vrest)
               )./(1+k*dt*(solve_alpham(V(:,i+1),Vrest)+
               solve_betam(V(:,i+1),Vrest)));
1110        n(:,i+1) = (n(:,i)+k*dt*solve_alphan(V(:,i+1),Vrest)
               )./(1+k*dt*(solve_alphan(V(:,i+1),Vrest)+
               solve_betan(V(:,i+1),Vrest)));
1111        h(:,i+1) = (h(:,i)+k*dt*solve_alphah(V(:,i+1),Vrest)
               )./(1+k*dt*(solve_alphah(V(:,i+1),Vrest)+
               solve_betah(V(:,i+1),Vrest)));
1112
1113    end
1114    % Note: Code from line 713-774 calculates one iteration
           too much, but it is
1115    % needed to fill Vm completely
1116    % For the sake of completeness V is reduced to the right
           size
1117    V(:,end) = [];
1118
1119    %% ---------------------- Step 5: Plot Results
           -----------------------------
1120    % Plot Extracellular Potential
1121    % Calculate distance from nerve base (=unmyelinated
           terminal)
1122    switch fibre
1123        case 'F1'
1124            distnervebase = zeros(size(F1_compcent));
1125            for i = 1:length(F1_compcent)
1126                distnervebase(i,1) = F1_compcent(i,1)-
                       F1_compcent(1,1); % [µm]
1127                distnervebase(i,2) = F1_compcent(i,2)-
                       F1_compcent(1,2); % [µm]
1128            end
1129            fromnervebase = 1e-04*sqrt((distnervebase(:,1)
```

```
            .^2+distnervebase(:,2).^2)); % length of each
            vector [cm]

    case 'F2'
        distnervebase = zeros(size(F2_compcent));
        for i = 1:length(F2_compcent)
            distnervebase(i,1) = F2_compcent(i,1)-
               F2_compcent(1,1); % [µm]
            distnervebase(i,2) = F2_compcent(i,2)-
               F2_compcent(1,2); % [µm]
        end
        fromnervebase = 1e-04*sqrt((distnervebase(:,1)
            .^2+distnervebase(:,2).^2)); % length of each
            vector [cm]

    case 'F3'
        distnervebase = zeros(size(F3_compcent));
        for i = 1:length(F3_compcent)
            distnervebase(i,1) = F3_compcent(i,1)-
               F3_compcent(1,1); % [µm]
            distnervebase(i,2) = F3_compcent(i,2)-
               F3_compcent(1,2); % [µm]
        end
        fromnervebase = 1e-04*sqrt((distnervebase(:,1)
            .^2+distnervebase(:,2).^2)); % length of each
            vector [cm]
    case 'F4'
        distnervebase = zeros(size(F4_compcent));
        for i = 1:length(F4_compcent)
            distnervebase(i,1) = F4_compcent(i,1)-
               F4_compcent(1,1); % [µm]
            distnervebase(i,2) = F4_compcent(i,2)-
               F4_compcent(1,2); % [µm]
        end
        fromnervebase = 1e-04*sqrt((distnervebase(:,1)
            .^2+distnervebase(:,2).^2)); % length of each
            vector [cm]

end

% Plot Extracellular Potential and Activating Function
% vs. distance from unmyelinated terminal
if plotExAct == 1
    figure
```

```
1160      subplot(2,1,1)
1161      plot(fromnervebase,Ve,'k--') % fromnervebase
1162      xlim([min(fromnervebase) max(fromnervebase)]); %
            fromnervebase
1163      xlabel('Distance from nerve base [cm]');
1164      ylabel('Extracellular Potential [mV]');
1165      title('Extracellular Potential')
1166      subplot(2,1,2)
1167      plot(fromnervebase,actfct,'k--');
1168      xlim([min(fromnervebase) max(fromnervebase)]);
1169      xlabel('Distance from nerve base [cm]');
1170      ylabel('Activating Function [mV/ms]');
1171      title('Activating Function');
1172      sgtitle({ ...
1173          ['Fibre: ' num2str( fibre ) ] ...
1174          ['Electrode: ' num2str(electrode)]});
1175  end
1176
1177  % Length of whole fibre plus Vrest for y axis scaling
1178  scale = 7; % 7
1179  lfibre = sum(lcomp)-Vm(end,1)*scale;
1180
1181  % Define Offset
1182  for i=1:ncomp
1183
1184      if i == 1
1185          offset(i,1) = lfibre - lcomp(i)/2;
1186      else
1187          lcomp2 = lcomp./2;
1188          off = sum(lcomp2(1:i-1));
1189          offset(i,1) = offset(i-1,1)-((lcomp(i-1)+lcomp(i)
                )/2);
1190      end
1191
1192  end
1193  % Plot Vm with respect to fibre compartments
1194  if plotAP == 1
1195      figure
1196      subplot(1,2,1)
1197      hold on
1198      box off
1199      plot(time,Vm);
1200      rectangle('position',[pretime, -120, dur, 10],'
            Edgecolor',[0.7 0.7 0.7])
```

```
1201      xlim([min(time),time(201)]); % from 0 to 2 ms
1202      if degenerated == 1
1203          xlim([min(time), time(201)]); % from 0 to 2 ms
1204      end
1205      xlabel('Time [ms]');
1206      ylabel('Amplitude [mV]');
1207      title('Action Potential of each compartment')
1208
1209      subplot(1,2,2)
1210      plot(time,scale*Vm+offset,'k');
1211      yticks([0, 5534.8, 7106.62]) % F1:NoR11 1.2501,
            5536.35, 6872.11 %F2: NoR 7 0, 3472.29, 5024.67 %
            F3 NoR 6: % F4: NoR 11, 1.25,5480.6,7016.12
1212      yticklabels({'NoR 11', 'Soma', 'Terminal'});
1213      set(gca,'TickLabelInterpreter', 'tex')
1214      xlim([min(time), time(201)]); % from 0 to 1 = min(
            time), time(101) ms
1215      if degenerated == 1
1216          xlim([min(time), time(201)]); % from 0 to 2 ms
1217      end
1218      %ylim([-1000, 5500])
1219      rectangle('position',[pretime, -1000, dur, 500],'
            Edgecolor',[0.7 0.7 0.7])
1220      %ylabel('Location along fibre [μm]');
1221      xlabel('Time [ms]');
1222      title('Propagating Action Potential along the fibre')
1223      sgtitle({ ...
1224          ['Fibre: ' num2str( fibre ) ] ...
1225          ['Electrode: ' num2str(electrode)]});
1226  end
1227
1228
1229  % For Threshold Search
1230  Mamp = max(Vm,[],2); % gives max value of each row [mV]
1231  maxMax = max(Mamp);
1232
1233
1234  %Plot Results for Thesis
1235  % figure
1236  % subplot(4,2,1)
1237  % plot(time,15*T13_thresh+offset,'k');
1238  % yticks([-508.593, 5016.44]) %[-446.143, 4962.48,
        6459.48]
1239  % yticklabels({'NoR-11', 'Soma'});
```

```
% set(gca,'TickLabelInterpreter', 'tex')
% xlim([min(time),time(151)]); % from 0 to 1.8 ms %deg 1.4
% ylim([-1500, 6000])
% rectangle('position',[pretime, -1500, dur, 500],'Edgecolor',[0 0 0])
% %ylabel('Location along fibre [μm]');
% xlabel('Time [ms]');
% title('T13: I = -1888.19 μA');
% subplot(4,2,3)
% plot(time,15*T14_thresh+offset,'k');
% yticks([-508.593, 5016.44])
% yticklabels({'NoR-11', 'Soma'});
% set(gca,'TickLabelInterpreter', 'tex')
% xlim([min(time),time(151)]); % from 0 to 1 ms
% ylim([-1500, 6000])
% rectangle('position',[pretime, -1500, dur, 500],'Edgecolor',[0 0 0])
% %ylabel('Location along fibre [μm]');
% xlabel('Time [ms]');
% title('T14: I = -875.49 μA');
% subplot(4,2,5)
% plot(time,15*T15_thresh+offset,'k');
% yticks([-508.593, 5016.44]) %[-446.143, 4962.48, 6459.48]
% yticklabels({'NoR-11', 'Soma'});
% set(gca,'TickLabelInterpreter', 'tex')
% xlim([min(time),time(151)]); % from 0 to 1 ms
% ylim([-1500, 6000])
% rectangle('position',[pretime, -1500, dur, 500],'Edgecolor',[0 0 0])
% %ylabel('Location along fibre [μm]');
% xlabel('Time [ms]');
% title('T15: I = -293.73 μA');
% subplot(4,2,7)
% plot(time,15*T16_thresh+offset,'k');
% yticks([-508.593, 5016.44]) %[-446.143, 4962.48, 6459.48]
% yticklabels({'NoR-11', 'Soma'});
% set(gca,'TickLabelInterpreter', 'tex')
% xlim([min(time),time(151)]); % from 0 to 1 ms
% ylim([-1500, 6000])
% rectangle('position',[pretime, -1500, dur, 500],'Edgecolor',[0 0 0])
```

```
% %ylabel('Location along fibre [μm]');
% xlabel('Time [ms]');
% title('T16: I = -902.94 μA');
% subplot(4,2,4)
% plot(time,15*V10_thresh+offset,'k');
% yticks([-508.593, 5016.44]) %[-446.143, 4962.48,
   6459.48]
% yticklabels({'NoR-11', 'Soma'});
% set(gca,'TickLabelInterpreter', 'tex')
% xlim([min(time),time(151)]); % from 0 to 1 ms
% ylim([-1500, 6000])
% rectangle('position',[pretime, -1500, dur, 500],'
   Edgecolor',[0 0 0])
% %ylabel('Location along fibre [μm]');
% xlabel('Time [ms]');
% title('V10: I = -939.69 μA');
% subplot(4,2,6)
% plot(time,15*V11_thresh+offset,'k');
% yticks([-508.593, 5016.44]) %[-446.143, 4962.48,
   6459.48]
% yticklabels({'NoR-11', 'Soma'});
% set(gca,'TickLabelInterpreter', 'tex')
% xlim([min(time),time(151)]); % from 0 to 1 ms
% ylim([-1500, 6000])
% rectangle('position',[pretime, -1500, dur, 500],'
   Edgecolor',[0 0 0])
% %ylabel('Location along fibre [μm]');
% xlabel('Time [ms]');
% title('V11: I = -579.81 μA');
% subplot(4,2,8)
% plot(time,15*V12_thresh+offset,'k');
% yticks([-508.593, 5016.44]) %[-446.143, 4962.48,
   6459.48]
% yticklabels({'NoR-11', 'Soma'});
% set(gca,'TickLabelInterpreter', 'tex')
% xlim([min(time),time(151)]); % from 0 to 1 ms
% ylim([-1500, 6000])
% rectangle('position',[pretime, -1500, dur, 500],'
   Edgecolor',[0 0 0])
% %ylabel('Location along fibre [μm]');
% xlabel('Time [ms]');
% title('V12: I = -1071.41 μA');
%  sgtitle('Cathodic Threshold Stimulation');

```

```
%Extracellular Potential resp. Activating Function
% figure
% subplot(4,2,1)
% plot(fromnervebase,VeT13,'k');
% xlim([min(fromnervebase) max(fromnervebase)]); %
    fromnervebase
% xlabel('Distance from soma [cm]');
% ylabel('Extr. Pot. [mV]');
% title('T13: I = -1888.19 μA');
% subplot(4,2,3)
% plot(fromnervebase,VeT14,'k');
% xlim([min(fromnervebase) max(fromnervebase)]); %
    fromnervebase
% xlabel('Distance from soma [cm]');
% ylabel('Extr. Pot. [mV]');
% title('T14: I = -875.49 μA');
% subplot(4,2,5)
% plot(fromnervebase,VeT15,'k');
% xlim([min(fromnervebase) max(fromnervebase)]); %
    fromnervebase
% xlabel('Distance from soma [cm]');
% ylabel('Extr. Pot. [mV]');
% title('T15: I = -293.73 μA');
% subplot(4,2,7)
% plot(fromnervebase,VeT16,'k');
% xlim([min(fromnervebase) max(fromnervebase)]); %
    fromnervebase
% xlabel('Distance from soma [cm]');
% ylabel('Extr. Pot. [mV]');
% title('T16: I = -902.94 μA');
% subplot(4,2,4)
% plot(fromnervebase,VeV10,'k');
% xlim([min(fromnervebase) max(fromnervebase)]); %
    fromnervebase
% xlabel('Distance from soma [cm]');
% ylabel('Extr. Pot. [mV]');
% title('V10: I = -939.69 μA');
% subplot(4,2,6)
% plot(fromnervebase,VeV11,'k');
% xlim([min(fromnervebase) max(fromnervebase)]); %
    fromnervebase
% xlabel('Distance from soma [cm]');
% ylabel('Extr. Pot. [mV]');
% title('V11: I = -579.81 μA');
```

```
% subplot(4,2,8)
% plot(fromnervebase,VeV12,'k');
% xlim([min(fromnervebase) max(fromnervebase)]); %
    fromnervebase
% xlabel('Distance from soma [cm]');
% ylabel('Extr. Pot. [mV]');
% title('V12: I = -1071.41 μA');
% sgtitle('Extracellular Potential');

% figure
% subplot(4,2,1)
% plot(fromnervebase,actfctT13,'k');
% xlim([min(fromnervebase) max(fromnervebase)]); %
    fromnervebase
% xlabel('Distance from soma [cm]');
% ylabel('f [mV/ms]');
% title('T13: I = -1888.19 μA')
% subplot(4,2,3)
% plot(fromnervebase,actfctT14,'k');
% xlim([min(fromnervebase) max(fromnervebase)]); %
    fromnervebase
% xlabel('Distance from soma [cm]');
% ylabel('f [mV/ms]');
% title('T14: I = -875.49 μA');
% subplot(4,2,5)
% plot(fromnervebase,actfctT15,'k');
% xlim([min(fromnervebase) max(fromnervebase)]); %
    fromnervebase
% xlabel('Distance from soma [cm]');
% ylabel('f [mV/ms]');
% title('T15: I = -293.73 μA');
% subplot(4,2,7)
% plot(fromnervebase,actfctT16,'k');
% xlim([min(fromnervebase) max(fromnervebase)]); %
    fromnervebase
% xlabel('Distance from soma [cm]');
% ylabel('f [mV/ms]');
% title('T16: I = -902.94 μA');
% subplot(4,2,4)
% plot(fromnervebase,actfctV10,'k');
% xlim([min(fromnervebase) max(fromnervebase)]); %
    fromnervebase
% xlabel('Distance from soma [cm]');
% ylabel('f [mV/ms]');
```

```
% title('V10: I = -939.69 μA');
% subplot(4,2,6)
% plot(fromnervebase,actfctV11,'k');
% xlim([min(fromnervebase) max(fromnervebase)]); % fromnervebase
% xlabel('Distance from soma [cm]');
% ylabel('f [mV/ms]');
% title('V11: I = -579.81 μA');
% subplot(4,2,8)
% plot(fromnervebase,actfctV12,'k');
% xlim([min(fromnervebase) max(fromnervebase)]); % fromnervebase
% xlabel('Distance from soma [cm]');
% ylabel('f [mV/ms]');
% title('V12: I = -1071.41 μA');
% sgtitle('Activating Function');


%% -----------------Appendix: Functions for alphas and betas --------------
function alpha_m = solve_alpham(V, Vrest)
alpha_m = (2.5-0.1*(V-Vrest))./(exp(2.5-0.1*(V-Vrest))-1);
end
function beta_m = solve_betam(V,Vrest)
beta_m = 4*exp((Vrest-V)/18);
end
function alpha_n = solve_alphan(V,Vrest)
alpha_n = (1-0.1*(V-Vrest))./(10*(exp(1-0.1*(V-Vrest))-1));
end
function beta_n = solve_betan(V, Vrest)
beta_n = 0.125 *exp((Vrest-V)/80);
end
function alpha_h = solve_alphah(V,Vrest)
alpha_h = 0.07*exp((Vrest-V)/20);
end
function beta_h = solve_betah(V,Vrest)
beta_h=1./(exp(3-0.1*(V-Vrest))+1);
end

%end
```

Code to Find Thresholds

```
1      % Find Threshold
2  % Get: Minimum amplitude value of each compartment Action
       Potential = val
3
4  % Find Threshold
5  current = linspace(0, -1500,10000); %0, 1500 10000 [µA]
6  level = -40; % 20 for degenerated // defined as threshold
       . If membrane voltage > level => AP [mV]
7  success = 0;
8  L=0;
9  R=length(current);
10
11 while L≤R | success == 0
12        middle = floor((L+R)/2); % middle index
13        stim = current(middle);
14        amplitude(middle) = Master_Thesis_Code(stim); %
             call Function, returns maximum membrane voltage
15              if amplitude(middle)<level
16                 L = middle+1;
17              elseif amplitude(middle)>level
18                     stim = current(middle-1);
19                     amplitude(middle-1)=
                          Master_Thesis_Code(stim);
20                        if amplitude(middle-1) ≤ level
21                           success = 1;
22                           Ithreshold = current(middle);
23                        end
24                     R = middle-1;
25              else
26                     fprintf('---No threshold found')
27              end
28 end
```

Bibliography

Adrian, E. D. (1914). The all-or-none principle in nerve. *J. Physiol.*, 47(6):460–474.

Adunka, O., Kiefer, J., Unkelbach, M. H., Radeloff, A., and Gstoettner, W. (2005). Evaluating cochlear implant trauma to the scala vestibuli. *Clin. Otolaryngol.*, 30(2):121–127.

Armstrong, C. M. (2003). The Na/K pump, cl ion, and osmotic stabilization of cells. *Proc. Natl. Acad. Sci. U. S. A.*, 100(10):6257–6262.

Ashley, K. and Lui, F. (2023). Physiology, nerve. In *StatPearls*. StatPearls Publishing, Treasure Island (FL).

Azarfar, A., Calcini, N., Huang, C., Zeldenrust, F., and Celikel, T. (2018). Neural coding: A single neuron's perspective. *Neurosci. Biobehav. Rev.*, 94:238–247.

Barker, B., Young, G., Soubrane, C., Stephens, G., Stevens, E., and Patel, M. (2017). Chapter 2 - ion channels. In Conn, P. M., editor, *Conn's Translational Neuroscience*, pages 11–43. Academic Press, San Diego.

Berrettini, S., Forli, F., Neri, E., Segnini, G., and Franceschini, S. S. (2002). Scala vestibuli cochlear implantation in patients with partially ossified cochleas. *J. Laryngol. Otol.*, 116(11):946–950.

Biswas, B. N., Chatterjee, S., Mukherjee, S., and Pal, S. (2013). A discussion on euler method: A review. *Electronic Journal of Mathematical Analysis and Applications*, 1:294–317.

Carricondo, F. and Romero-Gómez, B. (2019). The cochlear spiral ganglion neurons: The auditory portion of the VIII nerve. *Anat. Rec. (Hoboken)*, 302(3):463–471.

Chen, I. and Lui, F. (2022). *Neuroanatomy, Neuron Action Potential*. StatPearls Publishing, Treasure Island (FL).

Crivellato, E. and Ribatti, D. (2007). Soul, mind, brain: Greek philosophy and the birth of neuroscience. *Brain Research Bulletin*, 71(4):327–336.

Daniels, D. L., Swartz, J. D., Harnsberger, H. R., Ulmer, J. L., Shaffer, K. A., and Mark, L. (1996). Anatomic moment. hearing, i: The cochlea. *AJNR Am. J. Neuroradiol.*, 17(7):1237–1241.

Debanne, D., Campanac, E., Bialowas, A., Carlier, E., and Alcaraz, G. (2011). Axon physiology. *Physiol. Rev.*, 91(2):555–602.

Eshraghi, A. A., Nazarian, R., Telischi, F. F., Rajguru, S. M., Truy, E., and Gupta, C. (2012). The cochlear implant: historical aspects and future prospects. *Anat. Rec. (Hoboken)*, 295(11):1967–1980.

Faller, A. and Schünke, M. (2016). *Der Körper des Menschen*. Thieme, Stuttgart, Germany, 17 edition.

Gantz, B. J., McCabe, B. F., and Tyler, R. S. (1988). Use of multichannel cochlear implants in obstructed and obliterated cochleas. *Otolaryngol. Head Neck Surg.*, 98(1):72–81.

Gfeller, K. and Lansing, C. R. (1991). Melodic, rhythmic, and timbral perception of adult cochlear implant users. *J. Speech Hear. Res.*, 34(4):916–920.

Gfeller, K. E., Olszewski, C., Turner, C., Gantz, B., and Oleson, J. (2006). Music perception with cochlear implants and residual hearing. *Audiol. Neurootol.*, 11 Suppl 1(Suppl. 1):12–15.

Gorman, B. M. and Flatla, D. R. (2017). A framework for speechreading acquisition tools. *Proceedings of the 2017 CHI Conference on Human Factors in Computing Systems*.

Guidelli, R. (2020). The common features of tetrameric ion channels and the role of electrostatic interactions. *Electrochemistry Communications*, 121:106866.

Gulya, A. J. and Steenerson, R. L. (1996). The scala vestibuli for cochlear implantation. an anatomic study. *Arch. Otolaryngol. Head. Neck Surg.*, 122(2):130–132.

Hans, P., Grant, A. J., Laitt, R. D., Ramsden, R. T., Kassner, A., and Jackson, A. (1999). Comparison of three-dimensional visualization techniques for depicting the scala vestibuli and scala tympani of the cochlea by using high-resolution MR imaging. *AJNR Am. J. Neuroradiol.*, 20(7):1197–1206.

Hodgkin, A. L. and Huxley, A. F. (1945). Resting and action potentials in single nerve fibres. *J. Physiol.*, 104(2):176–195.

Hodgkin, A. L. and Huxley, A. F. (1952a). The components of membrane conductance in the giant axon of loligo. *J. Physiol.*, 116(4):473–496.

Hodgkin, A. L. and Huxley, A. F. (1952b). A quantitative description of membrane current and its application to conduction and excitation in nerve. *J. Physiol.*, 117(4):500–544.

Hodgkin, A. L. and Katz, B. (1949). The effect of temperature on the electrical activity of the giant axon of the squid. *J. Physiol.*, 109(1-2):240–249.

Hoffmann, J. A. C., Warnecke, A., Timm, M. E., Kludt, E., Prenzler, N. K., Gärtner, L., Lenarz, T., and Salcher, R. B. (2022). Cochlear implantation in obliterated cochlea: A retrospective analysis and comparison between the IES stiff custom-made device and the split-array and regular electrodes. *J. Clin. Med.*, 11(20):6090.

Holzmeister, C., Andrianakis, A., Kiss, P., Moser, U., and Graupp, M. (2022). Scala vestibuli cochlear implant supported by 3D modeling of the inner ear. *Wien. Klin. Wochenschr.*, 134(5-6):243–248.

Hopkins, K. (2015). Chapter 27 - deafness in cochlear and auditory nerve disorders. In Aminoff, M. J., Boller, F., and Swaab, D. F., editors, *The Human Auditory System*, volume 129 of *Handbook of Clinical Neurology*, pages 479–494. Elsevier.

House, W. F. (1982). Surgical considerations in cochlear implantation. *Ann. Otol. Rhinol. Laryngol. Suppl.*, 91(2 Pt 3):15–20.

Johnson, M. G. and Chartier, S. (2017). Spike neural models (part i): The Hodgkin-Huxley model. *Quant. Methods Psychol.*, 13(2):105–119.

Kelley, M. W. (2006). Regulation of cell fate in the sensory epithelia of the inner ear. *Nat. Rev. Neurosci.*, 7(11):837–849.

Kiefer, J., Weber, A., Pfennigdorff, T., and von Ilberg, C. (2000). Scala vestibuli insertion in cochlear implantation: a valuable alternative for cases with obstructed scala tympani. *ORL J. Otorhinolaryngol. Relat. Spec.*, 62(5):251–256.

Lenarz, T. (2017). Cochlear implant - state of the art. *Laryngorhinootologie.*, 96(S 01):S123–S151.

Lin, K., Marrinan, M. S., Waltzman, S. B., and Roland, Jr, J. T. (2006). Multichannel cochlear implantation in the scala vestibuli. *Otol. Neurotol.*, 27(5):634–638.

Lin, Y.-S. (2009). Clinical outcomes of scala vestibuli cochlear implantation in children with partial labyrinthine ossification. *Acta Otolaryngol.*, 129(3):273–280.

Merla, C., Denzi, A., Paffi, A., Casciola, M., DInzeo, G., Apollonio, F., and Liberti, M. (2012). Novel passive element circuits for microdosimetry of nanosecond pulsed electric fields. *IEEE transactions on bio-medical engineering*, 59:2302–11.

Mistrík, P., Jolly, C., Sieber, D., and Hochmair, I. (2017). Challenging aspects of contemporary cochlear implant electrode array design. *World J. Otorhinolaryngol. Head Neck Surg.*, 3(4):192–199.

Nakao, M. and Gadsby, D. C. (1986). Voltage dependence of na translocation by the Na/K pump. *Nature*, 323(6089):628–630.

Navntoft, C. A., Landsberger, D. M., Barkat, T. R., and Marozeau, J. (2021). The perception of ramped pulse shapes in cochlear implant users. *Trends Hear.*, 25:23312165211061116.

Neher, E. and Sakmann, B. (1976). Single-channel currents recorded from membrane of denervated frog muscle fibres. *Nature*, 260(5554):799–802.

Nelson, M. and Rinzel, J. (1998). The Hodgkin—Huxley model. In *The Book of GENESIS*, pages 29–49. Springer New York, New York, NY.

O'Connell, B. P., Hunter, J. B., and Wanna, G. B. (2016). The importance of electrode location in cochlear implantation. *Laryngoscope Investig. Otolaryngol.*, 1(6):169–174.

Pasanisi, E., Bacciu, A., Vincenti, V., Guida, M., Barbot, A., Berghenti, M. T., and Bacciu, S. (2002). Multi-channel cochlear implant in cochlear ossification. *Acta Otorhinolaryngol. Ital.*, 22(3):127–134.

Peckham, P. H. and Knutson, J. S. (2005). Functional electrical stimulation for neuromuscular applications. *Annu. Rev. Biomed. Eng.*, 7(1):327–360.

Pfützner, H. (2011). *Angewandte Biophysik*. Springer, Vienna, Austria, 2 edition.

Potrusil, T., Wenger, C., Glueckert, R., Schrott-Fischer, A., and Rattay, F. (2012). Morphometric classification and spatial organization of spiral ganglion neurons in the human cochlea: consequences for single fiber response to electrical stimulation. *Neuroscience*, 214:120–135.

Prechtl, A. (1994). *Vorlesungen über die Grundlagen der Elektrotechnik*. Springer, Vienna, Austria.

Raghavan, M., Fee, D., and Barkhaus, P. E. (2019). Chapter 1 - generation and propagation of the action potential. In Levin, K. H. and Chauvel, P., editors, *Clinical Neurophysiology: Basis and Technical Aspects*, volume 160 of *Handbook of Clinical Neurology*, pages 3–22. Elsevier.

Rattay, F. (1986). Analysis of models for external stimulation of axons. *IEEE Trans. Biomed. Eng.*, 33(10):974–977.

Rattay, F. (1990). *Electrical nerve stimulation*. Springer, Vienna, Austria, 1990 edition.

Rattay, F., Bassereh, H., and Stiennon, I. (2018). Compartment models for the electrical stimulation of retinal bipolar cells. *PLoS One*, 13(12):e0209123.

Rattay, F., Greenberg, R. J., and Resatz, S. (2003). Neuron modeling. In Finn, W. E. and LoPresti, P. G., editors, *Handbook of Neuroprosthetic Methods*, pages 39–74. CRC Press LLC, Boca Raton.

Rattay, F., Leao, R. N., and Felix, H. (2001a). A model of the electrically excited human cochlear neuron. II. influence of the three-dimensional cochlear structure on neural excitability. *Hear. Res.*, 153(1-2):64–79.

Rattay, F., Lutter, P., and Felix, H. (2001b). A model of the electrically excited human cochlear neuron. i. contribution of neural substructures to the generation and propagation of spikes. *Hear. Res.*, 153(1-2):43–63.

Raufer, S., Idoff, C., Zosuls, A., Marino, G., Blanke, N., Bigio, I. J., O'Malley, J. T., Burgess, B. J., Nadol, J. B., Guinan, Jr, J. J., and Nakajima, H. H. (2020). Anatomy of the human osseous spiral lamina and cochlear partition bridge: Relevance for cochlear partition motion. *J. Assoc. Res. Otolaryngol.*, 21(2):171–182.

Richard, C., Fayad, J. N., Doherty, J., and Linthicum, Jr, F. H. (2012). Round window versus cochleostomy technique in cochlear implantation: histologic findings. *Otol. Neurotol.*, 33(7):1181–1187.

Rinia, A., Olphen, A., and Dunnebier, E. (2006). Cochlear implantation in obstructed cochleas: the effect of the degree of obstruction on the number of activated electrodes and the amount of postoperative speech perception. *Clinical Otolaryngology*, 31(4):280–286.

Schoen, I. and Fromherz, P. (2007). The mechanism of extracellular stimulation of nerve cells on an electrolyte-oxide-semiconductor capacitor. *Biophys. J.*, 92(3):1096–1111.

Sochacki, J. (2020). Extending power series methods for the Hodgkin-Huxley equations, including sensitive dependence. *CODEE J.*, 13(1):1–36.

Steenerson, R. L., Gary, L. B., and Wynens, M. S. (1990). Scala vestibuli cochlear implantation for labyrinthine ossification. *Am. J. Otol.*, 11(5):360–363.

Swenson, R. (2017). Chapter 8 - the vestibular system. In Conn, P. M., editor, *Conn's Translational Neuroscience*, pages 167–183. Academic Press, San Diego.

Szyfter, W., Karlik, M., Sekula, A., Harris, S., and Gawecki, W. (2019). Current indications for cochlear implantation in adults and children. *Otolaryngol. Pol.*, 73(3):1–5.

Tillman, T. S. and Cascio, M. (2003). Effects of membrane lipids on ion channel structure and function. *Cell Biochem. Biophys.*, 38(2):161–190.

Tokat, T., Catli, T., Bozkurt, E. B., and Olgun, L. (2022). Surgical methods and auditory outcomes of cochlear implantation in cochlear ossification. *J. Int. Adv. Otol.*, 18(1):51–56.

Trudel, M., Côté, M., Philippon, D., Simonyan, D., Villemure-Poliquin, N., and Bussières, R. (2018). Comparative impacts of scala vestibuli versus scala tympani cochlear implantation on auditory performances and programming parameters in partially ossified cochleae. *Otol. Neurotol.*, 39(6):700–706.

Yu, F. H. and Catterall, W. A. (2003). Overview of the voltage-gated sodium channel family. *Genome Biol.*, 4(3):207.